NTNU

Norwegian University of
Science and Technology

Detailed Design of a Thruster Solution for a Small Mass-Market Remotely Operated Underwater Vehicle

Johnny Quang Tuan Huynh

Project Description

Together with BluEye, NTNU is developing a maintenance-free ROV thruster. The master thesis will focus on the design of a thruster for a small mass-market remotely operated vehicle, and eventually development and testing of a prototype. In addition to testing, calculations are to be carried out in terms of performance and cost estimation.

Part of the master thesis should propose a thruster design compatible to the prototype P1 presented by BluEye. The prototype is currently equipped with a T200 thruster from Blue Robotics.

These demands for the prototype thruster are:

- A forward operation speed of 0.5 – 1.0 m/s
- Operation depth up to 100 meters
- Umbilical thickness of 2 millimeters
- Maximum weight of 2 kg per thruster
- Minimum bollard pull of 50 N
- Low-voltage DC power supply

Other than the operational restrictions, the solution should focus on low maintenance, high reliability, longevity and low cost. If time, a prototype of the thruster should be developed and tested, using the cavitation tunnel or other testing facilities available. Arrangements for reservation of the labs must be done in due time.

With all of the above, the thesis should contain:

- Motor selection
- Coating alternatives
- Propeller design
- Cost estimation

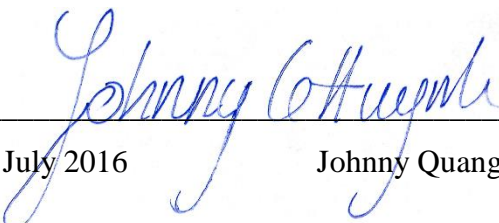_____
Martin Ludvigsen, Supervisor

II

Preface

This thesis is related to the mandatory master thesis in the 10th semester of the Master's Degree Programme at the Norwegian University of Science and Technology under the Department of Marine Technology. The content of the thesis involves design of a thruster-solution for a Remotely Operated Underwater Vehicle targeted for the consumer market.

The first chapter states the objective of the project, and the scope and limitations given by the project description. Chapter 2 concerns the motor system in terms of selection and reliability, while chapter 3 comprises propeller theory and computational estimation methods.

An overview of the existing design is presented in chapter 4. The design process is deduced in the following chapter, more specifically motor selection, determination of input parameters and optimization of a propeller with the use of OpenProp. The results of the objective are introduced in chapter 6 while chapter 7 discusses the results. The contents of chapter 8 conclude the thesis, and consider ways to improve the results and to better answer the scope of the project based on the discussions and the deductions throughout the report.

During the final semester, personal problems have demanded much of my attention. As such, I did not have the time to do everything I wanted to during the timespan of the semester. Some of these things are mentioned in chapter 7 and chapter 8. Even so, after working with this thesis, a greater understanding of motors and propeller design has been attained.

I would like to thank my supervisor Martin Ludvigsen for the opportunity to work with such an exciting project and for understanding of my situation. Additionally, I would like to thank Audun Scheide, Lars Mikkel Reiersen and Erik Kristian Frimanslund for insightful information.

_____

Trondheim, July 2016   Johnny Quang Tuan Huynh

IV

Abstract

This thesis addresses the design of a thruster-solution for a mass-market Remotely Operated Underwater Vehicle with respect to performance and cost while increasing reliability, efficiency and durability of the system.

With a relatively new and unexplored market, delivery of high quality is very important to make an impact with consumers. Factors such as performance, build quality and portability are important to be able to stay competitive in the market.

The objective is to design a thruster for the BluEye Explorer P1, a portable Remotely Operated Underwater Vehicle, with the existing thruster-solution as a guideline. Motor selection, protection of corrodible materials and propeller design are some of the problems encountered.

The required performance of a motor and propeller is dependent on the total drag force exerted on the system. By using the dimensions of the Remotely Operated Underwater Vehicle and its systems in combination with computational fluid dynamics analysis, necessary data is obtained to calculate the drag force on the body and the necessary power to operate the vessel.

Appropriate motor alternatives are chosen through a process of elimination assisted by a computational script based on extensive propeller series. Suitable propeller designs are optimized and analyzed, resulting in a low-voltage DC solution with an operation depth of up to 100 meters. Cost-wise, the thruster is estimated to be one third of the price of the existing motor and propeller; in-house production brings the price down drastically compared to outsourcing.

With the extensive propeller series and the aid of computational design programs such as OpenProp, the final product is ready to commence the production phase. Compared with the existing design, the thruster-solution is slightly bigger, but in return grants higher output.

Sammendrag

Denne avhandlingen tar for seg utformingen av en thruster-løsning for en masseprodusert fjernstyrt undervannsfarkost med hensyn til ytelse og pris, og samtidig øke påliteligheten, effektiviteten og levetiden til systemet.

Med et relativt nytt og uutforsket marked, er levering av høy kvalitet svært viktig for å gjøre inntrykk hos forbrukerne. Faktorer som ytelse, byggekvalitet og bærbarhet er nøkkelen for å kunne være konkurransedyktig i markedet.

Målet er å utforme en thruster for BluEye Explorer P1, en bærbar, fjernstyrt undervannsfarkost med den eksisterende thruster-løsningen som en retningslinje. Motorvalg, beskyttelse av ikke-korrosjonsbestandig materiale og propelldesign er noen av problemene man møter på.

Den nødvendige ytelsen av motor og propell er avhengig av den totale dragkraft som utøves på systemet. Ved hjelp av dimensjonene til den fjernstyrte undervannsfarkosten og dets systemer, i kombinasjon med numerisk fluiddynamikk analyse, er nødvendig data innsamlet for å beregne dragkraft på legemet, og den nødvendige kraften for å drive fartøyet.

Passende motoralternativer blir valgt gjennom en elimineringsprosess assistert av et beregningsskript basert på omfattende propellserier. Egnede propelldesign er optimalisert og analysert, hvilket resulterer i en lavspent DC løsning med en operasjonsdybde på opp til 100 meter. Kostnadsmessig er thrusteren anslått til å være en tredjedel av prisen på den eksisterende motoren og propellen; egenproduksjon bringer prisen ned drastisk i forhold til outsourcing.

Med den omfattende propellserien og ved hjelp av beregningsorientert designprogrammer som OpenProp, er det endelige produktet klart til å starte på produksjonsfasen. Sammenlignet med det eksisterende designet er thruster-løsningen litt større, men til gjengjeld gir den en høyere ytelse.

VIII

Contents

X

XII

List of Figures

XIV

List of Tables

XVI

Nomenclature

ABS	Acrylonitrile Butadiene Styrene
AC	Alternate Current
BL	Brushless
BLDC	Brushless Direct Current
CFD	Computational Fluid Dynamics
DC	Direct Current
emf	Electromotive Force
ESC	Electronic Speed Control
FBE	Fusion Bonded Epoxy
NACA	National Advisory Committee for Aeronautics
NTNU	Norwegian University of Science and Technology
PLA	Polylactic Acid
PM	Permanent Magnet
PMAC	Permanent Magnet Alternate Current
PMDC	Permanent Magnet Direct Current
RMF	Revolving Magnetic Field
ROV	Remotely Operated Underwater Vehicle
RPM	Revolutions Per Minute

XVIII

1 Introduction

1.1 Background

With a mass-market Remotely Operated Underwater Vehicle (ROV) under development, design of the system is an important aspect to create a solid fundament for an eventual testing phase. As with all systems, all parts must be optimized in such a way that the interaction between them is trouble-free. Furthermore, it is necessary that the ROV is constructed so it appeals to the intended consumer groups. In a constantly developing market, the demand for reliability and durability is an important attribute for the consumer. Ranging from cars to computers, high reliability is one of the decisive factors for users. When designing a propeller and a motor for use in a hostile environment such as the ocean, risk-preventing solutions must be contemplated; corrosion and other external influences may cause permanent damage to the system and eventually forcing it to fail. Moreover, it is important to ensure high system efficiency to provide great performance and an impression of high quality. Even though great quality is sought, the focus must not slip away from the fact that low cost is as important. Producing such a product for the mass-market, pricing must be coherent with the targeted consumer groups. If production costs and material expenses soars too high, the asking price will thusly be out of range, and the demand will drop. As such, a balance must be upheld between quality and cost.

1.2 Objective

The objective of this thesis is mainly to create a detailed design for an electric motor and propeller for a mass-market ROV with respect to performance and reduced risk, maintainability and cost while upholding reliability, efficiency and the lifespan of the system. Secondly, development of a prototype for testing and a production plan is to be assessed.

1.3 Scope and limitations

To enhance the overall quality, restrictions are set to increase reliability and durability. For instance, the motor utilized in the system must be electric with a low rate of maintenance. Thus, preferably it will be designed without a gearbox or a solution that include gears. Furthermore, protection of the motor is examined. Additionally, a low-voltage power supply is considered to prevent any electric-related injuries on the operators.

Physical attributes of the BluEye Explorer P1 must be taken into account in addition to the 2 mm thick umbilical. Thus, the thruster calculations must correspond to the size of the

ROV and other characteristics. The existing thruster solution, the T200 delivered by Blue Robotics, should be used as a guideline during the design.

The scope of the objective is limited to the design of the propeller, motor selection, coating and cost estimation. Any technical calculations of for instance speed controllers are not within the scope. Assumptions and restrictions are summarized in Table 1.

Table 1 – Assumptions and restrictions

Physical Attributes		
ROV Height	mm	350
ROV Length	mm	498
ROV Width	mm	180
Umbilical Thickness	mm	2
Maximum Thruster Weight	kg	2
Performance Criteria		
Maximum Operation Depth	m	100
Relative Forward Speed	m/s	0.5-1.0
Minimum Bollard Pull	N	50

2 Motor System

As the motor consists of metals, operating for several hours in seawater will eventually lead to failure caused by corrosion. By incorporating preventing measures or barriers, the probability of risk will be reduced, which in turn increase the reliability and longevity of the system. Furthermore, this will reduce the cost of such a solution, as the barriers will give a reduction in both maintenance and acquisition of spare parts for the consumer.

Moreover, external hazards such as collision with the seabed or coral reefs might damage both the propeller and the environment. Proactive barriers must be installed to prevent damage on the propeller in case of collisions. Reactive measurements should be defined if any failure of the system occurs, so that the user easily can perform maintenance to reestablish the system integrity.

2.1 Motors

When choosing an electric motor for the system, there are many possibilities. The electric motor, which converts electrical energy into mechanical energy, operates on three different physical principles; electrostatic, piezoelectric and the most commonly used, electromagnetic principle. Although the piezoelectric motor has some advantages compared to the other two motor types, it does not produce enough power to rotate the propeller. Electrostatic motors are highly efficient, and have a high power-to-weight ratio compared to conventional electromagnetic motors. Unfortunately, the research on electrostatic motors are progressing slowly, and as of now, there are no motors capable of generating the amount of power needed for the propeller with the given space limitation. Hence, an electromagnetic motor is the only suitable solution.

Electromagnetic motors can be driven by either AC or by DC. In marine engineering systems, AC is usually used, but for some applications in propulsion systems, this power may be converted to DC. Particularly for systems requiring continuously variable speed control, DC is preferred. Nevertheless, AC is used more frequently for the operation of electric motors.

Electromagnetic motors can be categorized into several groups of motors such as induction motors, permanent magnet (PM) motors and servomotors. Whether DC or AC drives it, PM motors exhibit higher efficiency than the others while being low cost.

4

2.1.1 Synchronous Motors

As the name suggest, a synchronous motor is capable of running at constant speed irrespective of the load acting on them. A typical motor consists of a stator and a rotor, which can be seen in Figure 1. They are respectively the stationary and the moving part of the system; the rotor spins inside a revolving magnetic field (RMF) created by the stator. The rotor, also called an armature, consists of an electromagnet formed by conducted coil. In addition, the rotor produces a constant magnetic field itself. The constant speed is achieved by interaction between the two magnetic fields.
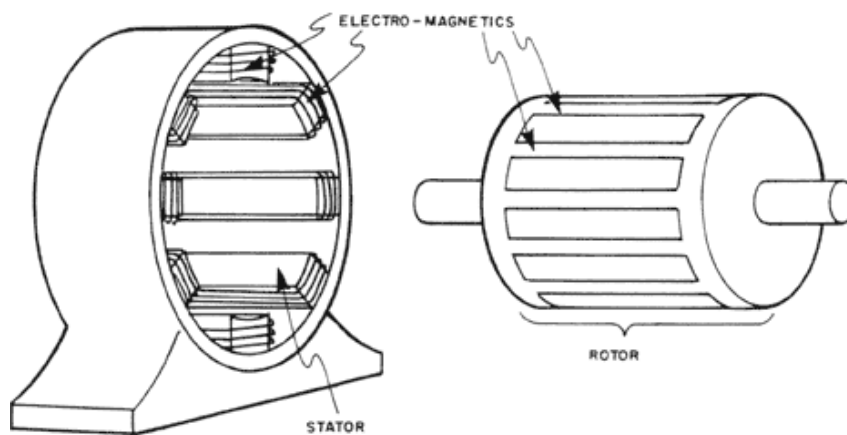
Figure 1 – Stator and rotor of a typical motor

In an AC synchronous motor, the stator is powered by a three-phase supply. The power will excite the windings in the stator in a rotating progression, which produces a rotating magnetic field that will rotate at synchronous speed. The armature consists of field coils that are connected in series to alternate polarity. It is important to note that for an AC synchronous motor, the number of rotor poles must equal the number of stator poles. Caused by the RMF, an electromotive force (emf) will be induced by the magnetic field. In turn, the emf will produce a current through the field coils in the rotor, which again produces magnetic force in the loop of coils. When the stator interacts with the rotor, the emf produces a magnetic field itself. This constant magnetic field locks itself onto the RMF. As can be seen from Figure 2, the opposite poles of RMF and armature will attract each other; the rotor will rotate at the same speed as the RMF, thus giving it synchronous speed.
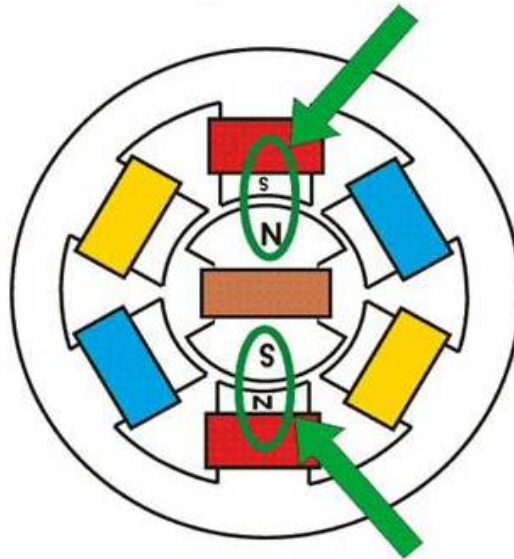
Figure 2 – Magnetic lock of a synchronous motor

From a motor's standpoint, the alternation of current is very important; the current direction must change in order for the armature to rotate. The reason for this is that the direction of the current is related to the direction of a conductor. This can be explained by Faraday's law; if a magnetic flux through a surface bounded by a conducting path changes, an emf equal in magnitude to the rate of change of the flux is induced in the wire. In our case, the rotor suspended inside the magnetic field is an electrical conductor. The excitation of the windings by AC produces the RMF in the stator. Caused by the rotation of the magnetic field, the magnetic flux is always changing. This induces an electric current inside the armature. The induced current will create its own magnetic field, more specifically the constant magnetic field discussed earlier. Another electromagnetic law, Lenz's law, states that "when a magnetic flux through a surface changes, the magnetic field due to any induced current produces a flux of its own – through the same surface and opposite in sign to the initial change in flux." (Tipler and Mosca, 2008). In other words, the constant magnetic field tries to stop the RMF. By doing so, the armature will rotate as well, trying to 'catch up' with the RMF in an effort to eliminate the difference in motion between them, which yields the magnetic lock mentioned previously.

In a synchronous AC motor, the speed of rotation is a function of input frequency *Hz*. This is caused by the fact that the armature will rotate at the same speed as the RMF produced by the stator windings; if the magnetic field is rotating at 500 RPM, the rotor will turn at 500 RPM. In addition, the speed of revolution is dependent on the number of poles. Rotating speed can be calculated from the following formula:

$$rpm = \frac{120 \cdot Hz}{Number\ of\ poles} \qquad\qquad \textbf{(2.1)}$$

From (2.1) it is seen that the increase in input frequency will simultaneously increase the rotational speed delivered to the propeller, which gives an easy way to control the speed of a motor.

2.1.2 Permanent Magnet Motors

By exchanging the coils in the rotor with magnets, a permanent magnet AC (PMAC) motor is obtained. The magnets are already magnetized and create their own persistent magnetic field. By using a permanent magnet, there will always be a magnetic field present and the PM displays magnetic behavior at all times. Thus, when the stators are powered by an AC source, an RMF is generated which in turn can interact with the rotor magnets.

Permanent magnet DC (PMDC) motors are similar to their PMAC counterpart. A significant difference is obviously the current flow. While AC will alternate the flow direction periodically, DC only flows in one direction. Batteries and fuel cells both produce DC; the positive and negative poles of a battery always stay, respectively, positive and negative, thus the electrons will always flow from the negative to the positive terminal. AC will reverse its direction of current periodically every half cycle.
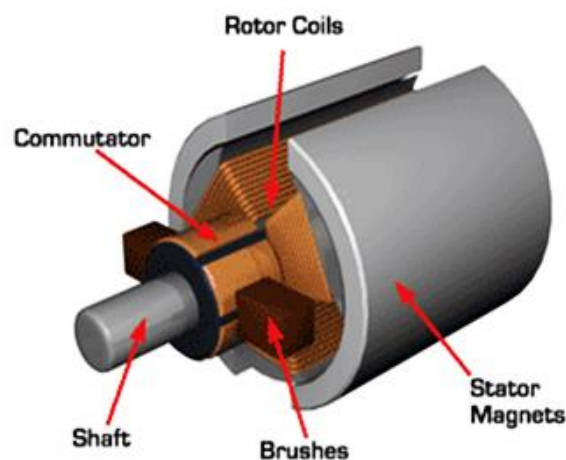
Figure 3 – Brushed DC motor

To be able to reverse the current, a PMDC motor must include a commutator. A commutator is an electrical switch that periodically changes the current direction. A typical PMDC motor set-up is shown in Figure 3. As can be seen from the figure, the permanent magnets are the stator, while the rotor consists of coils. Furthermore, the armature is connected to a commutator ring, which again is connected to brushes. The brushes are connected to a DC source. The DC power source supplies the rotor with electrical current. When the current flows through the coils, an emf is induced on it and the rotor will start to rotate. The stator consists of

paired magnets, thus the magnetic flux from the stator magnets will interact with the magnetic force in the coil. The magnetic force acts perpendicular to both the coil and the magnetic field, and produces a torque that spins the rotor. Figure 4 illustrates the armature rotating clockwise.
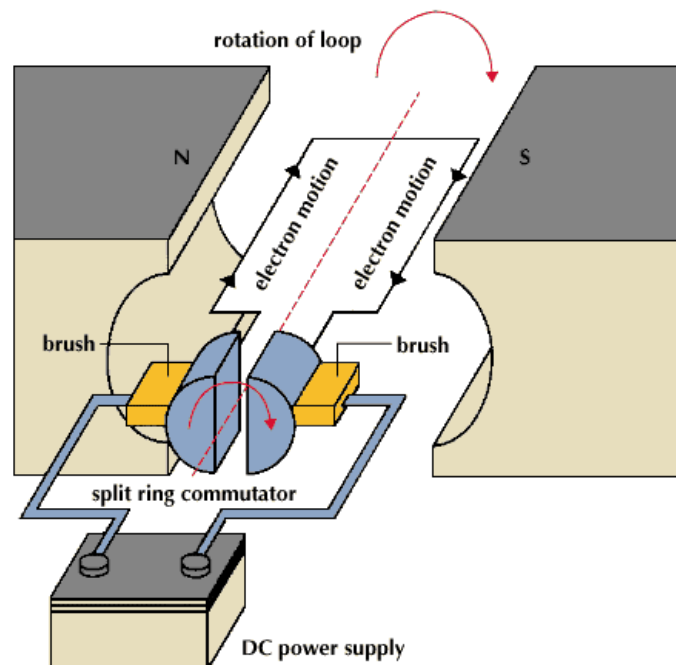
Figure 4 – Illustration of a brushed DC motor

As the slit in the commutator ring reaches the brushes, the coil will be positioned in the midpoint between the two magnetic poles. With a constant direct current, the coil will be held at rest at this point, caused by the magnetic flux and forces. The function of the commutator ring is to reverse the current. When the coil reaches the midpoint, one part of the commutator will get in contact with the other brush, causing the current to reverse the direction in the coil, which continues the rotating motion. As such, electrons will always flow from the left (negative) side to the right (positive) side of the DC supply, which completes the circuit.

A drawback with the brushed DC motor is the brushes; they wear out over time. In addition, they are in permanent physical contact with the commutators, which leads to sparking and wear on the commutators. Thus, regular maintenance and eventual replacement of parts are vital for these motor types. As such, for an operation that demand longevity and reliability, e.g. in an ROV, a brushed DC motor is not suitable.

To reduce the risk of motor failure, an alternative solution is a brushless DC (BLDC) motor. As the name suggest, brushless (BL) motors operate sans brushes. There are also design differences; BLDC motors has permanent magnets in the rotor and coils in the stator, opposite of how a brushed motor is constructed. Furthermore, since the rotor consists of permanent

magnets, it requires no power, yielding no commutator and no brushes. Instead, the stator is supplied by a DC power source. The stator consists of pairwise coils. To move the permanent magnet, sequential excitation of the pole pairs in the stator is necessary. Figure 5 shows an illustration of a three-phase BLDC motor. By exciting phase B, the rotor will try to align itself with the B-coils. By regulating, also called commutating, the current from B to C, the rotor will now try to align itself with the C-coils. Continuation of the commutating will force the rotor to spin in a clockwise direction. Thus, the alternation of current is not required as it is the permanent magnet and not the electromagnet that rotates. In addition to being more reliable, BL motors are also more efficient, less noisy and have a higher power-to-weight ratio compared to their counterpart. BLDC motors can be configured in two different ways, either with the rotor inside the stator or outside the stator, fittingly named inrunner and outrunner configurations.
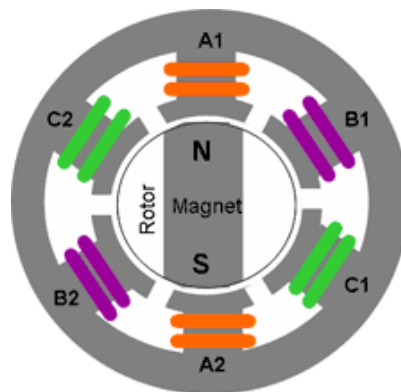
Figure 5 – Simple illustration of a brushless DC motor

The difference in physical configuration will also give different outputs. The inrunner will spin faster than an outrunner. On the other hand, it will provide less torque. By adding a gearbox, it is possible to increase the torque, but the gearbox will force a reduction in revolution speed. While the outrunner spins slower than the conventional inrunner, it eliminates the gearbox. Consequently, this eliminates the extra weight and complexity of the motor in addition to inefficiency and, most importantly, maintenance.

A negative effect of the outrunner configuration is something called cogging torque. At low speeds, the asymmetries in the magnetic field will cause a small but significant torque ripple. More specifically, when commutating the current out of one coil and into another coil, there is an associated torque ripple. Even though there exist ways to reduce cogging, the effect must be accounted for. Logically, cogging torque is dependent on the number of magnet poles in the rotor and coils in the stator. However, at higher speed, the moment of inertia will filter out the effect of cogging torque.

With a PMAC motor, cogging torque is not a factor. The smooth RMF that the AC excited stator produces, causes the PM to rotate without any symptoms of jerkiness. AC gives the opportunity to excite the motor with a higher voltage, yielding a higher power output compared to DC. On the other hand, an AC supply will require a bigger umbilical to transfer the necessary voltage, which will increase the total drag on the system, and thus equalize the differences. The main difference between a PMAC and a BLDC motor is the waveform of the commutation, being sinusoidal and trapezoidal, respectively.

The most suitable option is a BLDC motor with an outrunner configuration. In addition, it is highly efficient and entail low maintenance to function, providing longevity. Even though a brushed DC motor is cheaper than a BLDC motor, the operational costs for a brushed motor will accumulate a higher total cost than for a brushless motor.

2.2   Protection

As the ROV spends most of its time submerged, the motors will be exposed to seawater. One effect of motor submersion is corrosion. The coils and other types of metal in the motor will start to corrode. In addition, preventing spilling of fluids from the motor into the water is important. Despite the fact that the quantity of fluid is miniscule in an electrical motor, a spill near corals might affect the local marine habitat before the fluid dilutes.

To prevent corrosion on the metals inside the PM motor, coating should be applied. There are a lot of possible coating alternatives, many of them requiring application between each dive. This demands the user to go through a maintenance process after each dive, washing off the corrosion evoking seawater and spraying the inside of the motor with an insulating substance. In addition to being time-consuming, the disassembling and reassembling of the motor-solution increase the risk of motor failure caused by any mistakes or wear done by the user. Therefore, a more permanent solution must be found.

2.2.1 Epoxy Coating

By coating the stator and rotor in epoxy, a more permanent layer of polymers will cover the parts, refusing the seawater to get in contact with the motor. The magnetic forces and the electrical current will not be affected by the coating, thus it is possible to fully cover the stator and rotor with the compound. In the oil & gas industry, fusion bonded epoxy (FBE) coating is widely used to protect steel pipes and piping connections from the corrosive seawater. FBE comes in a dry powder form. To apply the coating to the surface, the powder is heated up, melted, and transformed into liquid form. By cross-linking, the liquid FBE becomes a solid coating.

The FBE coating is used on industrial materials, thus it might be expensive to obtain in small quantities such as for our purpose. Fortunately, there are other feasible epoxies. While they may not provide the longevity of FBE, they are cheaper. An important feature of epoxy is that it will deteriorate by exposure to UV, thus application is limited to within the core. When choosing an epoxy type to use as coating, an aspect is the durability of the epoxy when it comes to wear. As the rotor and the shaft spins, galling may occur. Testing for the specific motor may be necessary to decide how many operating hours it takes until the epoxy rubs off caused by friction or in other ways.

2.2.2 Superhydrophobic Solutions

In the past couple of years, development of superhydrophobic solutions introduces another viable option for coating. Hydrophobicity is the physical property of repelling water. Thus, when the compound is applied to a surface, water droplets will roll off the surface. One such product is the Ultra-Ever Dry, which, since 2014, has been tested by Nissan for application on their cars, with a goal to develop self-cleaning cars (Ultratech International, n.d.). While the superhydrophobic keeps the coated object dry, it implicitly also protects the object from corrosion. The product consists of a top coat and a bottom coat. The manufacturer states that the top coat will endure for a little over a year before reapplying is required. Although the bottom coat will still be intact and functional, the durability of the bottom coating has not yet been tested. They also state that abrasive environments should be avoided, but that testing in the specific surrounding should be undertaken. Another aspect of such products is that whilst they are splash proofed, they might not be suitable for extensive submerged operations. Not enough testing has been done on superhydrophobic composites, but with more research, it might be a favorable coating option in the future.

Even though the motor is coated with epoxy, the continuous exposure to seawater and interaction with moving parts will eventually wear out the protecting surface. By enclosing the motor and shaft all the way out to the propeller with a corrosive resistant and non-degradable material, e.g. plastic, there is a significant higher probability to prevent the seawater from interacting with the motor and shaft in the first place. In case of failure of this barrier, other barriers, such as the coating and the bearings, will prevent corrosion on the metals utilized in the motor. As important is that the capsule will be able to withstand the pressure at the operating water depths to avoid implosion.

2.2.3 Nozzle

By installing a nozzle, the incidence rate of propeller collision with any foreign object, such as coral reefs, is reduced. This prevents damage on both the propeller and the environment. Additionally, a nozzle will increase the propeller's efficiency by assisting the propeller with the acceleration of water.

Operating in seawater, the propeller and nozzle should be designed with a corrosion resistant material. Even though it is possible to wash off the seawater with freshwater after each dive, the exposure will eventually erode the ducted propeller. A plastic material hard enough to withstand the force and pressure of the water flow would be a viable option. Alternatively, a propeller can be made out of stainless steel. Lower grade stainless steel will be subject to corrosion in the chloride environment, hence only high-grade steel is suitable. In the marine industry, low-carbon steel 316L is the most generally used stainless steel worldwide because of its increased resistance against corrosion, especially pitting and crevice corrosion. The 316L alloy will be a suitable option for the propeller shaft and the propeller. As of July 2015, the price of the alloy ranges between $3000 and $4000 per tonne depending on fabrication method (MEPS LTD, 2015). With a downward trend the last year, it might be possible to obtain stainless steel at an even lower price if the trend continues. However, acquiring stainless steel in less quantity might increase the cost of material. Comparison with the alternative hard plastic should be performed in respect of both price and durability, in addition to efficiency.

While there exist cheaper motors, e.g. brushed motors, PM motors are the most reliable. In addition, they are almost free of maintenance. Adding epoxy coating in the motor core will further extend the durability of the motor, preventing exposure to seawater. By encapsulating the motor, in addition to the appliance of bearings to the shaft opening, several protective barriers are created around the motor core.

An open propeller is susceptible to damage from the environment, whether it is by collision or cavitation. By including a nozzle, physical protection of the propeller against the surroundings is established. However, adding a nozzle will influence the cavitation risk negatively or positively depending on whether the nozzle is accelerating or decelerating the water.

There are several feasible options that will increase the reliability and durability of the system. To be able to decide the final design of the motor and propeller, thorough testing must be performed to conclude with a detailed overview of materials; even though epoxy will provide a durable coating, there are different types of epoxies with different abilities, which must be tested for the intended use. Research and testing on superhydrophobic solutions as a

12

replacement for epoxy coating should be carried out. An optimization process must be conducted to achieve the best correlation between propeller and nozzle characteristics to prevent corrosion while maintaining efficiency. Furthermore, a study of cost in contrast to durability is an important aspect of the design.

Even though preventive measurements have been assessed, it is important to consider reactive procedures in case the system should fail; if the propeller breaks, there should exist an easy way to replace it without further harming the surrounding components.

2.2.4 Bearings

To reduce mechanical friction on a shaft, bearings are applied to support the shaft in its rotational movement. Although the mechanical friction now is reduced, the new friction between shaft and bearing will negatively affect the lifespan of the shaft, reduce the torque and rotational speed, and create noise. Lubrication, usually oil based, is applied to the bearings to prevent the aforementioned wear. Additionally, the lubrication is used to prevent rust on the bearings. Over the years, new bearing types have been invented and improved.

For our intended use, a particular bearing type excludes the use of lubrication, more specifically ball-bearings. Figure 6 shows a ball-bearing, with inner and outer races between balls, which rolls with the rotation of the inner race. By producing ball-bearings in plastic, the need for any lubrication is redundant, thus there are no fluids to spill. On top of that, by using plastic, corrosion will not occur. Although the races will be made of plastic, the balls are usually made of stainless steel. Another alternative is to opt for balls made of glass, which will remove any risk of corrosion.

Figure 6 – Plastic ball-bearing

Metal ball-bearings will allow for higher speed and loads, but the lubricants are often washed out of the sealed bearings and corrosion is a big problem. If a spray or coating is applied on the bearings, it will eventually wear off caused by the moving parts, which entails plastic bearings. Other types of bearings are also produced in plastic, and might be viable options. However, the rolling-element bearings have the best overall performance. Furthermore, the bearings maintain a watertight barrier that prevents water ingress into the motor.

3 Propeller Theory

3.1 Simple Momentum Theory

The propeller behavior can easily be explained with momentum theory. It is important to understand the theory and reasoning behind how the characteristics are defined. The simplest way to explain the behavior of a propeller is with change in momentum and kinetic energy, hence the name. It should be noted that this method is not applicable to propeller design or analysis. On the other hand, it is useful to estimate the average velocity induced by the propeller and calculate theoretical maximum efficiency.

First, assume that the propeller can be regarded as a disk that accelerates without adding tangential velocities to the flow behind the propeller. While regarded as a disk, the number of propeller blades is therefore infinite. Secondly, presume that the inflow on the propeller disk is uniform over the radius. Thus, there is a correlation between thrust and efficiency; the propeller thrust in infinite media is given by the change in momentum from a point far ahead to infinitely behind a propeller (Steen, 2007).
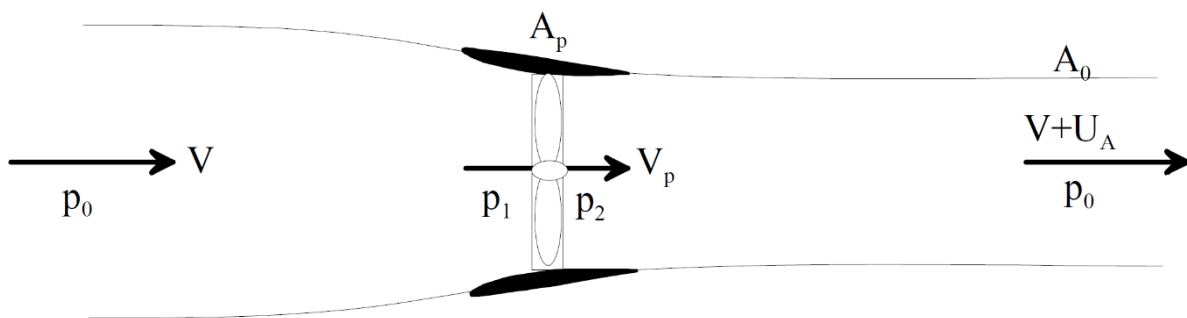
Figure 7 – Simple momentum theory applied to ducted propeller

Using the change in momentum as an expression for the thrust:

$$T = \rho \cdot Q \cdot U_A \qquad \qquad \textbf{(3.1)}$$

where

$Q = A_P \cdot V_P$ = Volume flow through propeller disk

V_P = Velocity through propeller disk

A_P = Area of propeller disk

U_A = Added velocity in flow behind propeller

Additional nomenclature for the momentum theory is shown in Figure 7.

The pressure jump over the propeller disk gives the thrust. By applying Bernoulli's equation, expressions for pressure in front of and behind the propeller are obtained:

$$\Delta p_1 = \frac{1}{2}\rho\left[V_p{}^2 - V^2\right] \tag{3.2}$$

$$\Delta p_2 = \frac{1}{2}\rho\left[(V + U_A)^2 - V_p{}^2\right] \tag{3.3}$$

which gives the propeller thrust:

$$T_p = A_p(\Delta p_1 + \Delta p_2) = \rho A_p\left(V + \frac{1}{2}U_A\right)\cdot U_A \tag{3.4}$$

where an expression for the volume flow is:

$$Q = A_p\left(V + \frac{U_A}{2}\right) \tag{3.5}$$

and the velocity through the propeller disk:

$$V_p = V + \frac{U_A}{2} \tag{3.6}$$

It should be noted that the propeller induced velocity through the propeller disk is half the velocity far behind the propeller.

3.1.1 Ducted Propellers

As a propeller rotates, the blades will produce high pressure areas behind them and low pressure areas in front. This pressure differential provides the excessive thrust to move the vessel in the fluid. However, at the tip of each blade, losses will occur as water escapes from the high pressure side of the blade to the low pressure side. A nozzle around the propeller will hinder the escaping water by restricting water flow to the propeller tips. The nozzle is designed as a funnel; the entrance diameter is bigger than the trailing throat. As the water density is constant, the mass flow rate must be constant. As the area becomes smaller, the mass must compensate with a higher velocity at the trailing end, thus accelerating throughout the nozzle. More water is moved by the ducted propeller, yielding more thrust at the same input power. The mentioned nozzle will lower the pressure contribution on the propeller, increasing the inflow velocity and the efficiency. On the other hand, lowering the pressure in the propeller disc will increase the risk of cavitation. Increasing the pressure through the propeller disc will reduce the inflow velocity, but in turn reduce the cavitation risk.

Cavitation occurs when water is vaporized at low temperature due to very low pressure. In seawater, small nuclei filled with gas or water vapor are present. When the pressure in a nucleus drops below vapor pressure, a bubble of water vapor is created. With continued low pressure, the bubble will grow and merge with other bubbles, creating a cavity. This condition is called cavitation. After a while, the bubbles may start to implode, causing strong local shockwaves in the fluid, which inflicts damage on the propeller. Furthermore, the presence of cavitation increases the profile drag strongly.

To avoid cavitation, the design of the propeller must be taken into account. While a bigger propeller blade area will reduce the risk of cavitation, it will increase the resistance of the profile, hence reducing the propeller efficiency. Adding an accelerating nozzle will increase the efficiency and accelerate the water flow through the propeller, but will increase the risk of cavitation. The final thruster design must be a balanced solution between propeller characteristics and nozzle effects.

Ducted propellers have the ability to increase or decrease the flow through the propeller disk, dependent on its shape. As noticed from the expressions derived earlier in this section, induced velocity from an eventual duct is not taken into account. By introducing duct-induced velocity δ, the velocity can be determined:

$$V_p = V + \frac{U_A}{2} + \delta \qquad\qquad (3.7)$$

The requirement of continuity gives the following velocity through the disk:

$$V_p = \frac{A_0}{A_p}(V + U_A) \qquad\qquad (3.8)$$

Hence, with a duct, this can be expressed as:

$$\frac{\delta}{V} = \frac{A_0}{A_p} + \frac{U_A}{V}\left(\frac{A_0}{A_p} - \frac{1}{2}\right) - 1 \qquad\qquad (3.9)$$

For a fixed propeller loading, or a given U_A/V, the flow δ through the duct increases with A_0. Using the change in momentum, the total thrust is acquired:

$$T_0 = T_p + T_d = \rho A_p\left(V + \frac{U_A}{2} + \delta\right) \cdot U_A \qquad\qquad (3.10)$$

The duct thrust T_d is due to a lift force created by circulation around the duct profile; the lift force is mainly directed towards the center of the duct, but due to oblique inflow, there exist a component in the forward direction, which gives T_d.

The efficiency of the propeller system can be written as:

$$\eta = \frac{T_0 \cdot V}{P} = \frac{(T_p + T_d)}{P} = \frac{2}{2 + \frac{U_A}{V}} \tag{3.11}$$

where P is the absorbed power which follows from the rate of change in kinetic energy:

$$P = \frac{1}{2}\rho A_p \left[V + \frac{U_A}{2} + \delta\right]\{(V + U_A)^2 - V^2\} \tag{3.12}$$

The propeller thrust can be expressed as a dimensionless coefficient:

$$C_{TP} = \frac{T_p}{\frac{1}{2}\rho V^2 A_p} \tag{3.13}$$

Thus, the induced velocity of the duct is:

$$\frac{U_A}{V} = \sqrt{1 + C_{TP}} - 1 \tag{3.14}$$

and the efficiency is reduced to:

$$\eta = \frac{2}{1 + \sqrt{1 + \tau * C_{TP}}} \tag{3.15}$$

where the duct loading coefficient τ is:

$$\tau = \frac{T_p}{T_0} = \frac{1 + \frac{U_A}{2V}}{1 + \frac{U_A}{2V} + \frac{\delta}{V}} \tag{3.16}$$

Approximating the induced velocity δ to be $U_A/2$, the duct loading coefficient becomes:

$$\tau = \frac{1 + \sqrt{1 + C_{TP}}}{2\sqrt{1 + C_{TP}}} \tag{3.17}$$
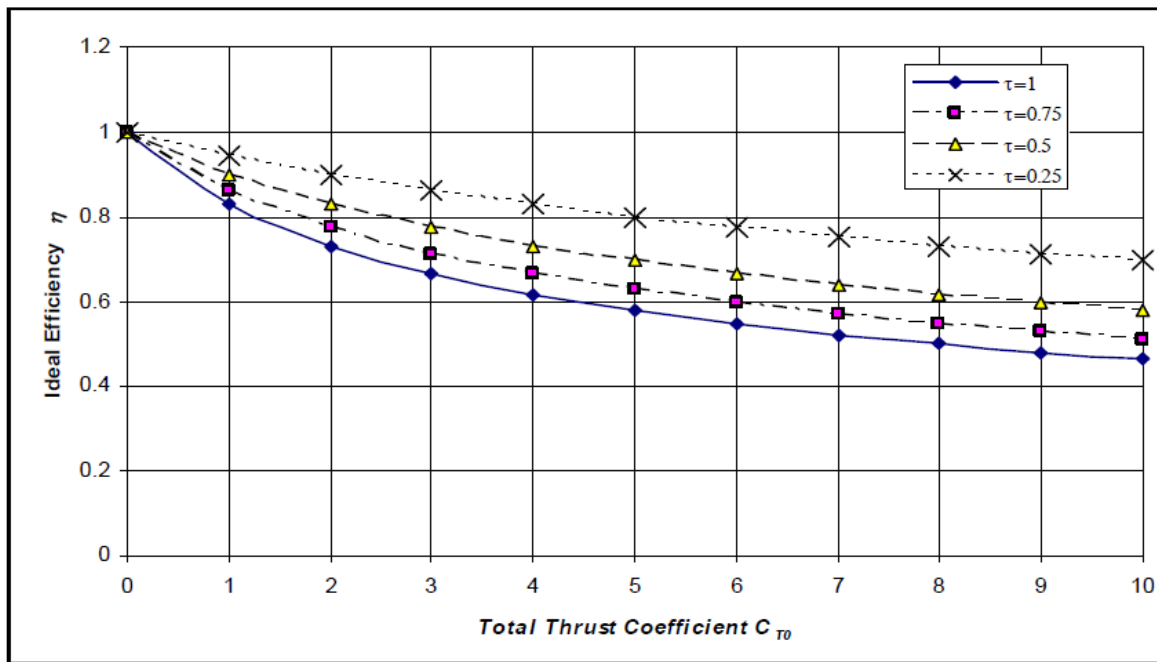
Figure 8 – Ideal efficiency for different values of the duct induced velocity. The induced velocity ratio τ is shown as a function of the total thrust loading coefficient. τ=1 corresponds to an open propeller or a neutral duct

From Figure 8, the highest efficiency for a given propeller loading is obtained with a high induced velocity δ, corresponding to a small A_P/A_0-ratio. In addition, higher duct loading coefficient τ gives a lower efficiency. Figure 9 shows τ as function of the propeller thrust coefficient C_{TP}. It is observed that for low propeller loads, a loading coefficient close to one is the optimum, which means that an open propeller is a better choice, while for higher loads, the optimum duct loading is approaching 0.5, which is a common approximation for ducted propellers. It is noted that due to the nozzle action, the inflow velocity of the impeller can be either less or greater than that of an open propeller under equal conditions, which explains the three types of nozzles introduced in this section. A duct loading coefficient equal to 1 indicates no force acting on the nozzle, and the flow pattern is comparable to a conventional propeller. With decreasing values of τ, the nozzle produces positive thrust which increases the inflow velocity on the impeller, and an improvement in the ideal efficiency is found. For the opposite scenario, a negative thrust, or drag force, acts on the nozzle, which decreases the inflow velocity and the ideal efficiency is lower.
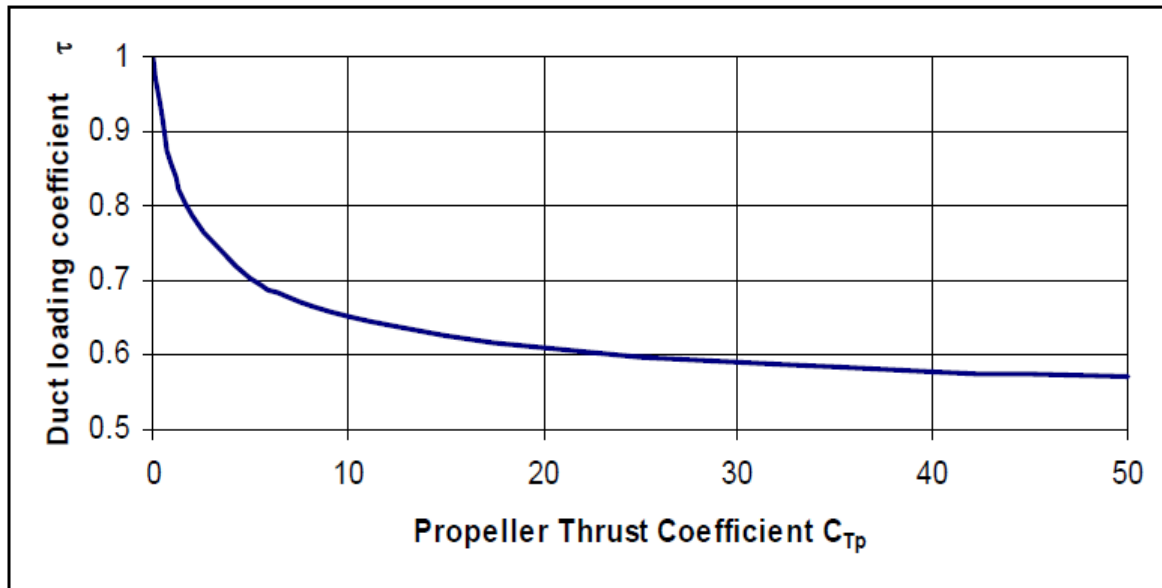
Figure 9 – Optimum duct loading coefficient. Presented as a function of propeller thrust loading coefficient

The nozzle with accelerating flow is used extensively in cases where the propeller is heavily loaded or where the propeller is limited in terms of diameter and dimensions. The accelerating nozzle provides a means of increasing the efficiency of said heavily loaded propellers. The acceleration of flow will make the ducted propeller more prone to cavitation compared to an open propeller with the same cavitation number and thrust loading. In the case of decelerating nozzles, the nozzle is used to increase the static pressure at the impeller, which reduces the risk of cavitation. On the other hand, the duct will provide a negative thrust, so the efficiency is generally lower than for open propellers. Thus, decelerating ducts are only applied to reduce cavitation.

The theory assessed in this section does not give any data about the danger of flow separation on the nozzle; if flow separation occurs, the drag of the nozzle will increase sharply. This may happen if the duct is heavily loaded and will lead to a decrease of system efficiency, and a highly irregular flow will be created in the workspace of the propeller. Hence, it is critical to avoid flow separation on the nozzle surface. Furthermore, even though the nozzle will affect the flow, the addition of the duct will also lead to friction force, which will act to reduce the total net thrust of the propeller.

The frictional efficiency of the duct can be defined as:

$$\eta_F = \frac{T_0 - D_F}{T_0} = 1 - \frac{\pi D L_F}{A_P} \cdot \frac{C_{Df}}{C_{T0}} \qquad \textbf{(3.18)}$$

where

$$C_{Df} = \frac{D_f}{\frac{1}{2}\rho V^2 \pi D L_f} = \text{frictional coefficient for the duct}$$

L_F = length of the duct

D_F = frictional drag force of the duct

D = propeller diameter

The total efficiency is thus:

$$\eta_{tot} = \eta_F \cdot \eta \qquad \textbf{(3.19)}$$

It should be noted that the duct friction drag is only important for the efficiency at low thrust loading coefficients. Furthermore, it should be noted that the calculations in Figure 8 has not considered friction drag. By including friction, an open propeller is more efficient for low thrust loadings.

3.2 Propeller series

To estimate a few important parameters for the design and choice of a propeller, a dimensional analysis can be done.

The goal of the analysis is to define certain coefficients, which are useful for presenting performance data for propellers. As given in (Steen, 2007), data such as torque, propeller thrust, revolutions and the forward speed can be expressed dimensionless as:

$$K_T = \frac{T}{\rho n^2 D^4} = \frac{T}{\rho (nD)^2 D^2} \tag{3.20}$$

$$K_Q = \frac{Q}{\rho n^2 D^5} = \frac{Q}{\rho (nD)^2 D^2 D} \tag{3.21}$$

$$J_A = \frac{V_A}{nD} \tag{3.22}$$

where

K_T = thrust coefficient

K_Q = torque coefficient

J_A = advance ratio for the propeller

V_A = velocity of advance (m/s)

n = number of revolutions (rev/s)

D = propeller diameter (m)

The advance ratio is the ratio between the diameter of the propeller and the distance the propeller moves forward through the fluid during one revolution. K_T and K_Q can be measured from a given *J*-value and a given propeller geometry with an open water test, by holding *n* constant and varying V_A from zero to the velocity which gives zero thrust. Further, the propeller thrust and torque are calculated.

3.2.1 Efficiency

The power supplied to the propeller is given as:

$$P_D = 2\pi n Q \tag{3.23}$$

The useful power output can be expressed as:

$$P_T = T \cdot V_A \tag{3.24}$$

Therefore, the propeller efficiency is given by:

$$\eta_{prop} = \frac{P_T}{P_D} = \frac{TV_A}{2\pi nQ} = \frac{J_A K_T}{2\pi K_Q} \tag{3.25}$$

At this point in the design process, to get a quick estimate of approximate values, results from already conducted open water tests where parameters such as blade area, blade number and pitch ratios are systematically varied can be used. A variation like this will give a propeller series, which in turn gives a simple method for determination of propeller diameter and propeller efficiency.

3.2.2 Wageningen B-series

The most comprehensive series that has been tested is the Wageningen B-Screw Series. It includes over 20 blade area-blade number configurations, and is probably the most widely used propeller series. Test results and analysis are further explained in (Oosterveld and Oossanen, 1975).

With this series the values for K_T and K_Q are estimated with the following relations:

$$K_T = f_1\left(J, \frac{P}{D}, \frac{A_E}{A_O}, Z, R_N, \frac{t}{c}\right) \tag{3.26}$$

$$K_Q = f_2\left(J, \frac{P}{D}, \frac{A_E}{A_O}, Z, R_N, \frac{t}{c}\right) \tag{3.27}$$

where

P/D = pitch ratio

A_E/A_O = blade-area ratio

Z = blade number

t/c = thickness of the blade profile at characteristic radius

3.2.3 Limitations

The propeller series comprises models with blade numbers ranging from 2 to 7, blade-area ratios between 0.30 and 1.05, and pitch ratios in the range 0.5 to 1.4.

A problem connected to testing of propellers is that the results are exposed to scale effects. For instance, the effect of Reynolds number variation is significant, varying with the dependence of the drag and lift coefficients C_D and C_L. Reynolds number for propeller characteristics is defined as:

$$R_N = \frac{c(x_0)}{v} \sqrt{V_A^2 + (x_0 \pi n D)^2} \qquad (3.28)$$

where

c(x) = chord length

v = fluid viscosity

x_0 = the equivalent radius, the radius where the propeller efficiency $\eta_{prop} = \eta(x_0)$

Correction of such scale effects will be discussed later.

3.2.4 Propeller Geometry

In propeller theory, design and analysis, the propeller must be described as accurately as possible using a limited number of parameters, opposed to a complex, three-dimensional, physical model. Figure 10 shows the main propeller dimensions used in propeller theory.
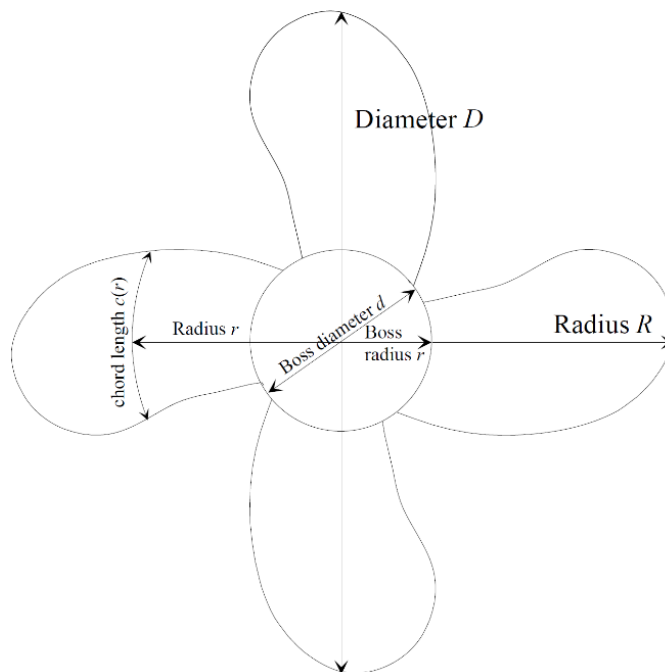
Figure 10 – Propeller dimensions

3.2.5 Propeller Pitch and Blade Area

Pitch is defined as the axial distance the propeller will move during one revolution if the propeller is considered as a nut on a screw. Usually, the pitch/diameter-ratio is used to state the pitch of a propeller. There is also the possibility to use the pitch angle θ to express pitch:

$$P = 2\pi r tan(\theta) \tag{3.29}$$

In general, the pitch at 70% of the radius is utilized as reference when deciding pitch P. The blade-area ratio, expressed as the Expanded Blade Area Ratio (EAR), is defined as:

$$EAR = \frac{A}{\pi R^2} \tag{3.30}$$

where A is the expanded blade area:

$$A = Z \int c(r)dr \tag{3.31}$$

The integral spans from the circumference of the boss, r_b, out to radius R. The chord length $c(r)$ is defined as the length of the circle segment and not a straight line across the blade since the fluid flows over the blade in an approximate circular arc. Often, the dimensionless radius x = r/R is used as the variable. Hence, the expanded blade area is rewritten as:

$$A = Z \int Rc(x)dx \tag{3.32}$$

For x = r/R = 0.70, the reference point for pitch P, the expanded blade area can be found for different radii R, blade number and chord length.

3.2.6 Polynomials and Scale Effects

In the B-series, thrust and torque coefficients K_T and K_Q are expressed as polynomials in the advance ratio J, the pitch ratio P/D, the blade-area ratio A_E/A_Q, and the blade number Z. In addition, the effect of the thickness of the blade profile is accounted for in the polynomials.

By using Lerbs method, the effect of Reynolds number variation is calculated and accounted for in the polynomials. At a specific value of the advance ratio, the lift and drag coefficients C_L and C_D and the corresponding angle of attack for the blade section are deduced from the K_T- and K_Q-values from the open water test. The Reynolds number effects are only considered to influence the drag of the equivalent profile, specifically the minimum value of the drag coefficient, $C_{D,min}$. With Lerbs method, Oosterveld and Oossanen obtained the lift and drag coefficients expressed as a function of blade number, blade-area ratio, pitch ratio and angle

of attack by regression analysis. For specific combinations of the variables mentioned, K_T and K_Q polynomials were developed.

The polynomials are chosen to be expressed with $R_N = 2x10^6$ from the fact that the corresponding $C_{D,min}$-values is an average of all model $C_{D,min}$-values. The regression polynomials are shown in Appendix A. For Reynolds numbers greater than $2 \cdot 10^6$ the propeller characteristics should be corrected. Additional polynomials for Reynolds numbers equal to $2 \cdot 10^7$, $2 \cdot 10^8$ and $2 \cdot 10^9$ are shown in Appendix A.1. Although, given the fact that the ROV will be streamlined and operate in relative low velocities, turbulent flow is not seen as a concern during this design process.

3.3 Computational Estimation Method

The propeller characteristics can now be calculated by hand with the given equations and approach, but the coefficients in Appendix A makes it possible to create a computational script to calculate K_T and K_Q, which in turn gives thrust and torque of the propeller by rewriting (3.20) and (3.21).

3.3.1 MATLAB

With the polynomial coefficients, a MATLAB function is created to calculate torque and thrust based on Wageningen B-series. The function requires propeller characteristics such as blade number, EAR, revolution speed, diameter and pitch ratio *P/D* in addition to mentioned coefficients. By calculating the advance number J_A with (3.22) for a range of revolutions, it is further possible to compute K_T and K_Q. Moreover, thrust and torque can be calculated from the coefficients. The results are presented in a table for all revolutions in the inputted range. Additionally, plots are created to graphically display the results. Furthermore, the efficiency for each case is also calculated, and the pitch angle for the given propeller characteristics is represented in degrees. Thus, for any given case of propeller dimensions within the limitations of the B-series, the performance of the propeller can be calculated with this script.

The complete script can be seen in Appendix B.

3.3.2 Comparison with the T200

As of now, the ROV prototype is using the T200 thruster from Blue Robotics, thus the actual propeller dimensions can be compared with the computational analysis of the constructed script to check if it provides realistic results. By using the specifications from the T200 thruster as input in the function, it is easy to compare the results with the data provided by the manufacturer. Significant characteristics of the T200 are listed below:

Table 2 – T200 significant characteristics

Propeller diameter	mm	76
Propeller radius	mm	38
Blade number	Z	3
Rotational speed min.	rev/s	5
Rotational speed max.	rev/s	63

The results of the computation are somewhat similar to the T200, but without a defined blade area ratio, it is difficult to simulate similar characteristics. In addition, the effect of a nozzle is not considered with the B-series, and calculations has to be done to properly implement a nozzle in the thruster-system.

Anyhow, according to the empirical widespread results from the B-series, the T200 does not provide enough thrust to overcome the total drag of the vehicle and umbilical. The performance data given by the manufacturer states that the maximum forward thrust of the T200 thruster is 5.1 kgf or 50 N. With two thrusters providing forward thrust, this equals to a meagre 100 N while the requirement is at least 126 N to move the ROV with a velocity of 1 m/s with a 100 meter long umbilical.

3.3.3 Ducted Propeller Series

As for the Wageningen B-series, sets of tests have been performed for ducted propellers over the years. Although less extensive than the B-series, calculations and testing on the Wageningen Ka-propeller series have been substantial enough to create regression polynomials and coefficients, which can be used to calculate thrust and torque for a ducted propeller.

The screws of the Ka-series have relatively wide blade tips, which make them less susceptible to blade tip cavitation. Furthermore, investigations performed by MARIN in the Netherlands have led to a uniform pitch and flat face sections for the design of these series. These investigations showed that this type of screw has no drawbacks with respect to efficiency and cavitation. One of these nozzles is the Nozzle No. 19A, which is designated for applications that require heavy propeller loads. The shape of the nozzle, from a structural point of view, is very simple. Thus, it is also easier to fabricate opposed to more complicated shapes. The inner side of the nozzle has an axial cylindrical form, while the outside of the profile is straight with a relatively thick trailing edge. The profile of duct 19A is shown in Figure 11.

Open water tests were performed with the nozzle in combination with the Ka-4.70 series. Testing of nozzles in combination with the B-series were also performed, but mathematical representation of the test data is unfortunately not available. With the screw used in Ka-4.70, there are some extra limitations opposed to calculations with the B-series. It is stated that the ducted Ka-4.70 is a 4-bladed propeller, with a blade-area ratio of 0.70, which fittingly can be seen from the model name. As for the B-series, regression coefficients have been established. These can be seen in Appendix A.2. To calculate thrust and torque, these coefficients are used in the following polynomials:

$$K_T = \sum_{x,y} A(x,y) \cdot \left(\frac{P}{D}\right)^x \cdot J^y \qquad (3.33)$$

$$K_Q = \sum_{x,y} B(x,y) \cdot \left(\frac{P}{D}\right)^x \cdot J^y \qquad (3.34)$$

$$K_{TN} = \sum_{x,y} C(x,y) \cdot \left(\frac{P}{D}\right)^x \cdot J^y \qquad (3.35)$$

where

K_T is the total thrust coefficient

K_Q is the torque coefficient

K_{TN} is the nozzle thrust coefficient

MARIN 19A

MARIN's Nozzle No. 19A

L/D = 0.5

STRAIGHT LINE

d/L=3.78

AXIAL | CYLINDRIC

CLEARANCE C

d/L=5.57

8.49

Y

L

D/2+C+Xᵢ — D/2 — D/2+C+Xᵤ

ORDINATES FOR NOZZLE PROFILE 19ᵃ

Y/L	0	1.25	2.50	5.0	7.5	10	15	20	25	30	40	50	60	70	80	90	95	100
X_i/L	18.25	14.66	12.80	10.87	8.00	6.34	3.87	2.17	1.10	0.48	CIRCULAR CYLINDRIC			0.29	0.82	1.45	1.86	2.36
X_u/L	—	20.72	21.07	20.80	STRAIGHT LINE													±6.36
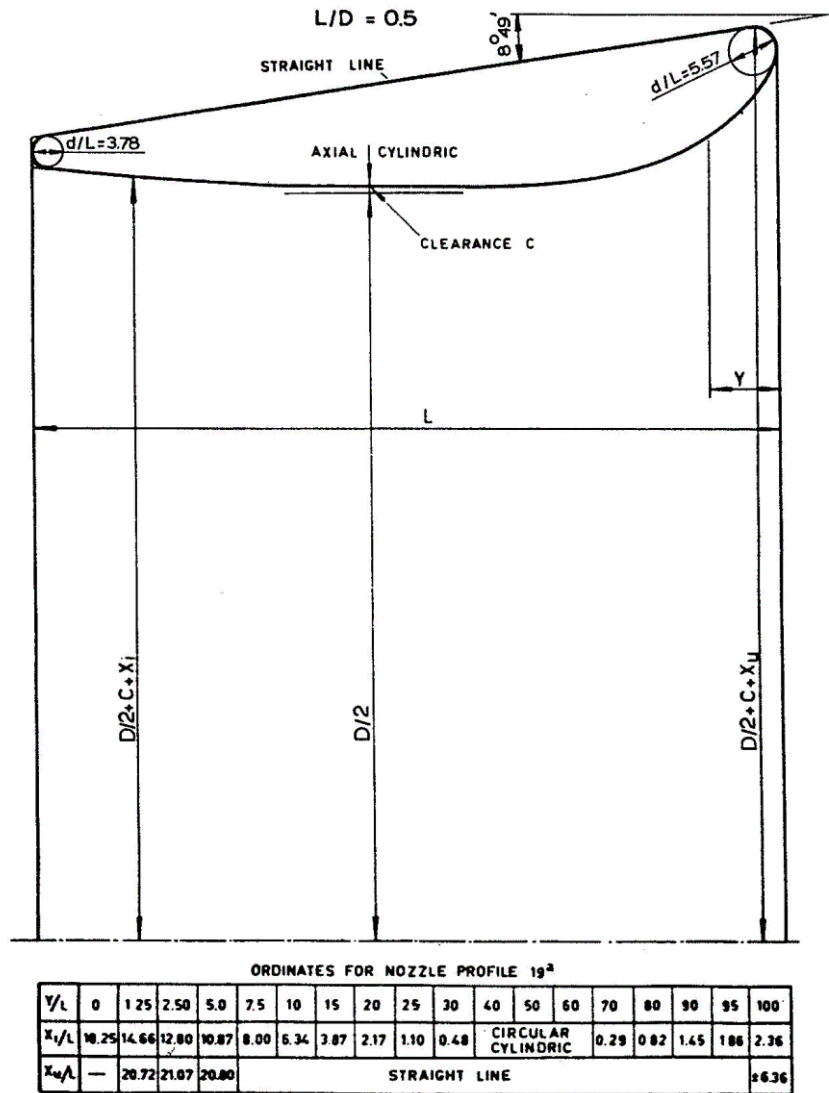
Figure 11 – Profile of MARIN's Nozzle No. 19A and its ordinates

3.3.3.1 Bollard Pull

An important factor for selection of a propeller in our case is bollard pull. Bollard pull is the pull force a vessel can produce at zero forward speed. Based on regression analysis of 95 bollard pull model tests from MARINTEK, the dataset reveals that there is surprisingly little difference between total propulsion thrust and bollard pull force. More specifically, the bollard pull force is typically around 97% of the total thrust. A comparison of the static bollard pull can be made with the aid of Figure 12 and Figure 13.
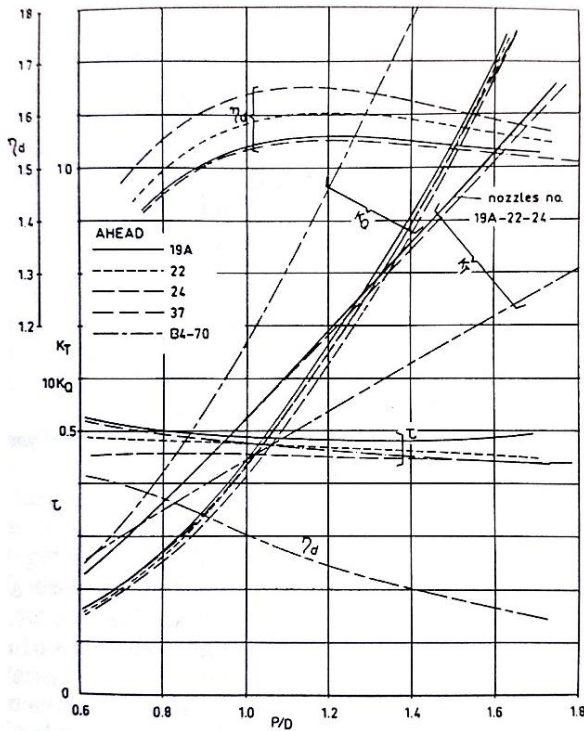
Figure 12 – Characteristics of different propulsion devices. Given for forward static bollard condition
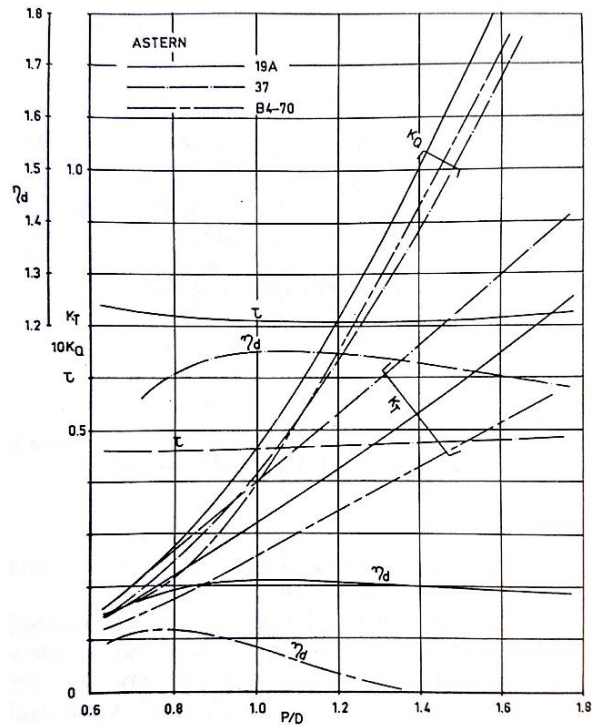
Figure 13 – Characteristics of different propulsion devices. Given at astern static bollard condition

In the diagrams, the total thrust coefficient K_T, the torque coefficient K_Q, the duct loading coefficient τ, and the efficiency coefficient η_d of the propulsion devices are given on the base of the pitch ratio P/D. Included in the diagrams are also Nozzles Nos. 22, 24 and 37. The efficiency coefficient is given as:

$$\eta_d = \frac{(K_T/\pi)^{3/2}}{K_Q} \tag{3.36}$$

This efficiency coefficient can be used as a direct measure for effectiveness of different propulsion devices at the static condition, i.e. bollard pull condition. The different devices must be of the same diameter, and same power input must be considered. However, if there are any restrictions on the revolutionary speed on any of the devices, this coefficient cannot be used. It can be seen from Figure 12 and Figure 13 that the efficiency η_d is much higher for ducted propellers than for an open propeller. Furthermore, it can be seen that the effect of nozzle length on η_d is small; a slight increase of the factor can be found with increasing length-diameter ratio.

More importantly, at astern static bollard pull it can be seen that the efficiency for Nozzle No. 37 is much higher than for Nozzle No. 19A. This is explained by the fact that duct

19A usually suffers from flow separation when operating astern. Nevertheless, the efficiency factor for the 19A is still higher than for the B-4.70.

The difference between the ducted propellers are in reality small. While Nozzle No. 19A provides about 2 percent higher efficiency than Nozzle No. 37, duct 37 presents a better solution when astern operation is of interest.

Not surprisingly, the results of the computational analysis for the two series yields a higher efficiency for the ducted propeller than the conventional propeller at larger propeller loads. The open water tests and the propeller series, along with the computational script, provides a good estimation method for the early design of a propeller. These are used in chapter 5, where the design process is discussed.

3.4　Lifting Line Theory

The simple momentum theory disregards the fact that the propeller has a finite number of blades and that the screw induces tangential velocities. There were only considered axial velocities, and assumed that the induced axial velocity, U_A, was uniformly distributed over the propeller disk. With the complete momentum theory, also called lifting line theory, the aforementioned aspects are introduced. Previously, using simple momentum theory, the propeller was considered a disk with infinite number of blades. While with lifting line theory, a propeller blade is represented by a lifting line, with trailing vorticities (Steen, 2014).

Assume that U_A varies with the radius and that there is a tangential induced velocity U_T which varies with the radius. When evaluating tangential velocities, the fact that the propeller absorbs torque which causes a change in momentum has to be considered. More specifically, a circular motioned momentum in the water at different radii. Behind the propeller, this angular momentum is induced as tangential velocity U_T. As such, there is a corresponding torque dQ.

The induced tangential velocity U_T is due to circulation. According to Biot Savart's law, this can be written as:

$$U_T(r) = \frac{\Gamma(r)}{2\pi r} \Rightarrow \Gamma(r) = 2\pi U_T r \qquad \textbf{(3.37)}$$

By applying Kutta-Joukowski's theorem, the torque at a given radius r is:

$$dQ = \rho \cdot \Gamma \cdot V_p \cdot r \cdot dr \qquad \textbf{(3.38)}$$

By inserting (3.37), (3.38) can be rewritten:

$$dQ = \rho \cdot 2\pi \cdot r \cdot U_T \cdot V_P \cdot r \cdot dr \tag{3.39}$$

where V_P is the axial velocity through the propeller disk as stated in (3.6).

Bernoulli's equation can be utilized on the flow just in front and just behind the propeller disk. The axial velocity V_P behind and in front of the propeller disk is equal, thus V_P is excluded from the expression for differential pressure. This leads to the following pressure jump over the disk:

$$\Delta p = \frac{\rho}{2}[(2\pi r n)^2 - (2\pi r n - U_T)^2] \tag{3.40}$$

$$\Delta p = \rho\left(2\pi r n - \frac{1}{2}U_T\right)U_T \tag{3.41}$$

The pressure jump Δp over the segment dr of radius r results in the propeller thrust dT:

$$dT = 2\pi r \Delta p dr = \rho 2\pi\left[2\pi r n - \frac{1}{2}U_T\right]U_T r dr \tag{3.42}$$

$$dT = \rho\Gamma\left(2\pi r n - \frac{1}{2}U_T\right)dr \tag{3.43}$$

Equation (3.43) can also be derived using Kutta Joukowski's theorem by assuming that the tangential induced velocity at the propeller disk is half the induced velocity infinitely behind the propeller.

With the change in momentum in axial direction and axial velocity V_P, the equation for dT can be expressed as:

$$dT = \rho 2\pi r V_P U_A \, dr \tag{3.44}$$

Implementing (3.43) in equation (3.44) above, circulation Γ can be expressed as:

$$dT = \rho\Gamma\left(2\pi r n - \frac{1}{2}U_T\right)dr = \rho 2\pi r V_P U_A \, dr \tag{3.45}$$

$$\Gamma = \frac{2\pi r V_P U_A}{2\pi r n - \frac{1}{2}U_T} \tag{3.46}$$

Applying (3.37) in (3.46):

$$2\pi U_T r = \frac{2\pi r V_P U_A}{2\pi rn - \frac{1}{2}U_T} \tag{3.47}$$

$$\frac{U_T}{U_A} = \frac{V_P}{2\pi rn - \frac{1}{2}U_T} = tan\beta_i \tag{3.48}$$

(3.48) is an expression for the hydrodynamic angle of pitch of a blade section at a given radius.

Assume that the pressure steps in front of, behind and over the disc are Δp_1, Δp_2 and Δp respectively. These can be written as:

$$\Delta p_1 = \frac{\rho}{2}\left[V_P{}^2 - V^2\right] \tag{3.49}$$

$$\Delta p_2 = \frac{\rho}{2}\left[\left(V_P{}^2 + kU_T{}^2\right) - \left((V + U_A)^2 + U_T{}^2\right)\right] \tag{3.50}$$

$$\Delta p = \Delta p_1 - \Delta p_2 = \rho\left[V + \left\{1 - (1 - k)\left(\frac{U_T}{U_A}\right)^2\right\}\frac{U_A}{2}\right]U_A \tag{3.51}$$

Now, by assuming that the change in angular momentum manifests itself straight behind the propeller so that the constant k≈1, the thrust and velocity through the propeller disk becomes:

$$dT = 2r\pi\Delta p dr = \rho 2\pi r V_P U_A\, dr = \rho 2\pi r\left[V + \frac{U_A}{2}\right]U_A\, dr \tag{3.52}$$

where:

$$V_p = V + \frac{U_A}{2} \tag{3.53}$$

Equation (3.53) shows that the resulting induced velocity is normal to the inflow direction of the section.

Up to this point, it has not been considered that the propeller blade or blade sections are exposed to resistance due to lift and friction. The frictional drag will reduce the thrust and increase the torque. The torque contribution is significant while the reduction in lift is in the order of 3 to 4 percent.

The drag dD is included by using the following expression:

$$dD = \frac{\rho}{2}V_\infty{}^2 \cdot c \cdot C_D dr \tag{3.54}$$

where:

c = chord length

C_D = drag coefficient (0.006 – 0.008)

The drag or resistance coefficient is given by:

$$C_D = 2C_F \left(1 + 2\frac{t_{max}}{c}\right) \tag{3.55}$$

Where the frictional coefficient C_F is approximated by the ITTC 1957 curve:

$$C_F = \frac{0.075}{[\log(R_n) - 2]^2} \tag{3.56}$$

$$R_n = \frac{V_\infty c}{V} \tag{3.57}$$

The inflow velocity of the propeller:

$$V_\infty = \sqrt{\left(V(r) + \frac{U_A}{2}\right)^2 + \left(2\pi rn - \frac{1}{2}U_T\right)^2} \tag{3.58}$$

Given that the circulation Γ is a function of the radius, T and Q can be calculated for any given value of velocity $V(r)$, as shown below:

$$V(r) = V\left(1 - w(r)\right) \tag{3.59}$$

where

w(r) = mean wake at given radius

To calculate the induced velocities, the distribution of circulation is needed. A suitable circulation distribution is given by the expression:

$$\Gamma(r) = k\left[\sin\left(\pi \frac{r - r_{boss}}{R - r_{boss}}\right) - a \sin\left(2\pi \frac{r - r_{boss}}{R - r_{boss}}\right)\right]^m \tag{3.60}$$

where

k = constant

m = constant

The constants a, k and m will determine the type of circulation during a calculation. The constant k is altered until desired thrust or power is obtained. a defines the point of maximal circulation. For maximal circulation midway between the propeller tip and hub, $a = 0$ is chosen. The maximum point is moving towards the propeller tip with increasing values of a. Normally, the value of a will be in the region $0.10 - 0.20$. The constant m regulates the fullness of the curve, increasing with decreasing m-values. An approximately elliptical distribution is obtained with $m = 0.5$. For a decrease in loading against the hub and propeller tip, m-values in proximity to $m = 1$ can be chosen. Then a distribution similar to a sinus curve is attained. Furthermore, by applying smaller m values for the inner part than for the outer part, the loading is directed more at the hub, thus unloading the propeller tip.

3.4.1 Finite number of blades

Up to this point it has been assumed that the screw has an infinite number of blades. For a given circulation, the effect of a reduction in number of blades will be an increase in the induced velocity over the blade in comparison to a propeller with infinite number of blades. The effect of blade number can be taken into account using the following methods:

- Prandtl's Method (for a first approximation, and for slender blades)
- Goldstein Method (for simple calculations)
- Induction Factors (for more accurate applications)
- Lifting Surface Methods (for up to date applications)

The basis of the approach specified by Prandtl, Goldstein and Induction Factors is that the induced velocities are larger close to each blade than the value computed with complete momentum theory. In other words, for a finite number of blades, the induced velocities are larger compared to the lifting line theory presented earlier. How much larger these velocities are, depends on the propeller loading and, logically, the number of blades. It is possible to perform a direct calculation of the local induced velocity by using Biot-Savart's law in combination with the trailing vortices, but this is quite complicated. With the aforementioned methods, the calculation is simplified. Furthermore, the grade of simplicity is what separates the approaches; Prandtl and Glodstein are the two easiest methods to use, while Induction Factors and Lifting Surface Methods are usually utilized for calculations that are more detailed, where the latter is often used by computational software.

3.4.2 Thrust and Torque

By using circulation, diameter, rotational speed and velocities, the thrust and torque of the propeller can be calculated.

According to Kutta Joukowski, the lift of a foil placed in a flow with velocity V_0 over a width dy is given by:

$$dL = \rho V_0 \Gamma dy \tag{3.61}$$

Applying this to the propeller, the ideal thrust and torque from all blades over a segment dr of the radius are obtained:

$$dT_i = \rho \Gamma(\mathrm{r}) \left(2\pi \mathrm{rn} - \frac{\mathrm{U_T}}{2} \right) dr \tag{3.62}$$

$$dQ_i = \rho \Gamma(r) \left(V(r) + \frac{1}{2} U_A \right) r dr \tag{3.63}$$

The speed $V(r)$ is given by:

$$V(r) = [1 - w(r)]V_0 \tag{3.64}$$

where w(r) = mean effective wake at a given radius.

This entails that the resulting force dL_i attacks with an angle β_i relative to dT_i. These forces are given by:

$$dL_i = \left(dT_i^2 + dK_i^2 \right)^{0.5} \tag{3.65}$$

$$\tan \beta_i = \frac{V(r) + \frac{1}{2} U_A}{2\pi r n - \frac{1}{2} U_T} \tag{3.66}$$

The profile drag dD is parallel with the resulting inflow velocity and will reduce the total thrust. The reduction in thrust from profile drag at radius r can be expressed as:

$$dT_D = \frac{1}{2} \rho V_\infty(r)^2 c(r) C_D(r) z \sin\beta_i dr \tag{3.67}$$

Where the resulting velocity V_∞ is:

$$V_\infty(r) = \sqrt{\left(V(r) + \frac{1}{2}U_A\right)^2 + \left(2\pi rn - \frac{1}{2}U_T\right)^2} \qquad \textbf{(3.68)}$$

The profile drag d*D* will also affect the total torque; the torque increases with the profile drag. The added contribution is given by:

$$dQ_D = \frac{1}{2}\rho V_\infty(r)^2 c(r) C_D(r) zr\cos\beta_i dr \qquad \textbf{(3.69)}$$

Using (3.62), (3.63), (3.67) and (3.69), the final thrust and torque are represented as:

$$T = \int (dT_i - dT_D) \qquad \textbf{(3.70)}$$

$$Q = \int (dQ_i + dQ_D) \qquad \textbf{(3.71)}$$

Figure 14 shows a velocity diagram where the resulting velocity V_∞ on a section of the blade consists of the axial velocity and the tangential velocity as shown in (3.68). The figure also depicts how the Kutta Joukowski's theorem provides a tangential force and thrust on a section of the propeller blade.
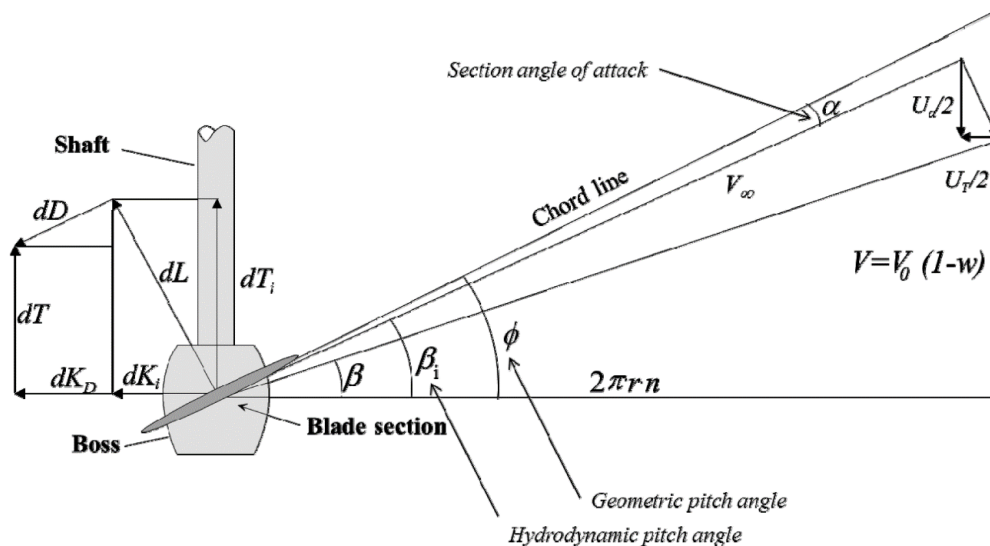
Figure 14 – Velocities and force components at a radial section of a propeller blade

4   BluEye Explorer P1

The BluEye Explorer P1 is an underwater drone designed by BluEye Robotics. Still in the testing phase, the aim is to make underwater exploration possible for everyone (Robotics, n.d.). Its small size and low weight makes it possible to explore the sea with a portable drone. To be able to design a thruster, data from the current prototype is reviewed to find the best solution. The specifications are shown in Table 3 and the prototype is depicted in Figure 15.
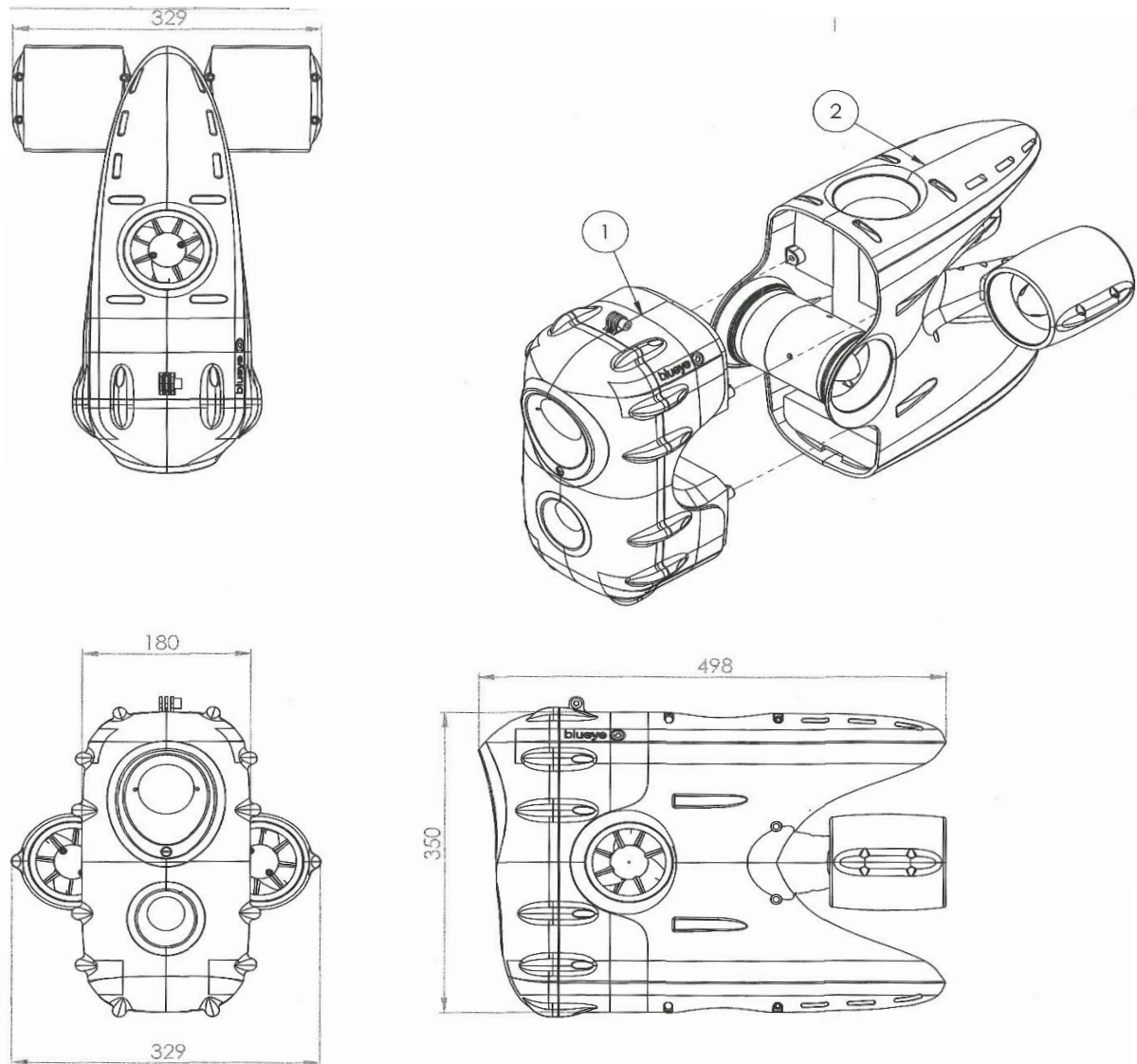
Figure 15 – BluEye Explorer P1

In the specifications, there are two values given for the width; one excluding the thrusters and one including the thrusters. Figure 15 shows the difference between the two. Notice that the thrusters are placed outside of the main body. Hence, any influence from the body on the fluid will not affect the incoming flow on the thrusters. If the thrusters were placed behind the ROV, separation of the fluid might cause changes in the inflow, but with a smooth

40

surface with no edges, placing them on the sides will not cause these changes. The uniform inflow and the small size prevents risk of both cavitation and vibrations. Thus, skew on the blade profile is not necessary, and a symmetric profile is suitable (Steen, 2016).

Table 3 – BluEye Explorer P1 specifications

Weight	kg	10
Length	mm	498
Height	mm	350
Width	mm	180
Width included thrusters	mm	329
Drag coefficient		0.1
Umbilical diameter	mm	2
Umbilical length	m	≤ 100

From Figure 15 it can be seen that there are an additional two thrusters embedded in the main body of the ROV. These two thrusters are built in to move the ROV in the other degrees of freedom. As such, the size of the thrusters must remain somewhat consistent in consideration of the design of a thruster to not implicate the original design of the Explorer P1.

4.1 Blue Robotics T200 Thruster

The current thruster-solution used by Blueye Robotics is the T200 manufactured by Blue Robotics, which has been tested and shipped since the end of 2014 (BlueRobotics, 2014). The thruster utilized on Explorer P1 and its predecessor consists of a propeller with nozzle, a motor installed in the hub and a speed controller. The T200, shown in Figure 16, has a starting price of $169 (as of May 2016), while an addition of their electronic speed controller (ESC) will add $25 to the price. Blue Robotics also has another option when it comes to speed controllers, namely their custom designed BlueESC which will add $80 to the starting price.

Some of the thruster properties such as the diameter and thrust are expressed in Table 4. Here it is important to notice that the design should be as compact as possible, and the T200 dimensions should be used as a guideline when it comes to the size of the thruster as to not affect the portability or design of the ROV. As important is it to inspect the performance of the thruster.

Figure 16 – T200 thruster

Table 4 – Properties of the T200 thruster

Physical Properties		
Total Diameter	mm	100
Propeller Diameter	mm	76
Length (without BlueESC)	mm	113
Length (with BlueESC)	mm	131
Weight (without BlueESC)	g	344
Weight (with BlueESC)	g	422
Electrical Properties		
Operating Voltage	V	6-20
Max Current	A	25
Max Power	W	350
Phase Resistance	Ohms	0.18
Performance Properties		
Maximum Forward Thrust @ 16V	N	50
Maximum Reverse Thrust @ 16V	N	40
Rotational Speed	RPM	300-3800

4.1.1 M200 Motor

The motor used in the T200 is a three-phase brushless DC motor developed by Blue Robotics. The M200 motor manufactured by Blue Robotics has slightly different parameters as the motor used in T200; it uses the same internal components, but other components such as the plastic nozzle are excluded in the M200. As proclaimed by Blue Robotics, the motor consists of a rugged design for use in the ocean and extreme environments, and high-performance plastic bearings that don't corrode. With standard mounting holes, the motor can easily be used to construct your own thruster or other underwater actuators. The M200 is shown in

Figure 17 and Figure 18.

Figure 17 – M200   **Figure 18 – M200 shaft end**

Figure 19 illustrates some of the differences from the standard M200 and the one installed in the T200. Most noticeable is that the shaft end is connected directly to the thruster base, while at the other end the protecting cap is removed. This is because the propeller in the T200 is mounted directly on the outside rotor of the M200.

Figure 19 – M200 installed on the T200

As previously noted, the T200 and its components should be used as a guideline. Thus, it is important to notice the specifications of the motor as well, as a means for comparison with other motors on the market. The specifications of the M200 motor can be seen in Table 5.

Currently, when in use on the ROV, the motor is running at 16.7 volts. Using the Kv-rating, calculation shows that the motor provides around 8000 RPM. From Table 4, the T200 has a rotational speed range of 300-3800 RPM, which is much lower than the counterpart.

Table 5 – M200 specifications

Physical Properties		
Overall length	mm	62
Diameter	mm	36
Shaft Diameter	mm	5
Electrical Properties		
Operating Voltage	V	6-20
Max Current	A	22
Max Power	W	350
Performance Properties		
Kv-rating	RPM/V	490

4.1.2 Speed Controller

An electronic speed control is an electronic circuit where its main purpose is to vary the speed of an electric motor. In addition, the ESC varies the direction of the rotational speed.

When in operation, the ESC will create a three-phase AC power output from the DC power input provided. With the AC output, of limited voltage, the ESC is sending a sequence of AC signals employing a very low impedance for rotation to run the motor.

Impedance is a measure of resistance from a circuit to a current when voltage is applied. In AC the impedance possesses magnitude and phase, while resistance only has magnitude. In a DC circuit however, there is no distinction between impedance and resistance, and the resistance can be thought of as impedance with a zero phase angle.

An ESC is necessary to run any three-phase brushless motors, like the one in the T200. As previously mentioned, Blue Robotics deliver two kinds of electronic speed controllers; the Basic ESC or BlueESC. The Basic ESC is a simple 30-amp ESC, which is sufficient for the T200. This electronic speed control runs on voltages between 6 and 17, and it is open-source, which makes it programmable to custom changes. The BlueESC on the other hand, is custom designed to mount directly on the thrusters. Furthermore, it is waterproof, water-cooled and pressure-resistant. This will alter some of the dimensions of the thruster, as noted in Table 4. Figure 20 shows how the ESC is mounted on the hub of the thruster.

Figure 20 – T200 with BlueESC mounted

The BlueESC runs on voltages between 6 and 22 with a max current of 35 amps, which is a bit higher than the Basic ESC. Other details, such as pulse width, I^{2}C protocol and more technical aspects when it comes to the coding and operation of the ESC, and thus the thruster, will not be discussed further.

BluEye's experience with the speed controller however, are very bad. It short circuits and burns after a short amount of time. It must be considered as an inadequately product where the protection against water is poor (Ludvigsen, 2016).

4.1.3 Propeller

The T200 is delivered with two different three-bladed propellers, one clockwise and one counterclockwise. As can be seen Figure 21, the propeller has a hollow boss, making room for the motor. Attached to the stator, the propeller will thusly spin with the motor's performance.
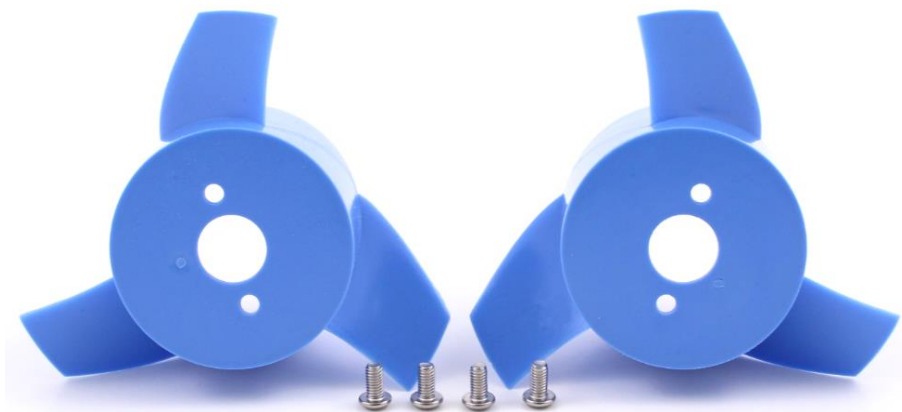
Figure 21 – Clockwise and Counterclockwise propeller parts for the T200

The boss diameter, measured to 40 mm, is quite high given the fact that the total propeller diameter is 76 mm as given in Table 4. Furthermore, we can see from the blade sections that the tips have been cut off, granting a bigger blade area compared to propellers that are more traditional with a rounded off tip. A reason for this might be to exploit the given diameter, giving the propellers the ability to provide more thrust with the same size, in exchange of lower propeller efficiency and higher torque requirements. This is discussed more in detail in section 5.2.

5 Design Process

There are many ways to approach the problem of designing a thruster. It is important to establish a method based on the design limitations the problem holds. Furthermore, it is easier to define a starting point for the process by beginning with looking at the boundaries. If a method or boundaries are not determined, the iteration process might be endless, and a result is unachievable. In our case, the limitations are defined by size, weight and voltage. Portability of the ROV must be upheld; as such, the size of the new thruster must be more or less the same size as the already implemented design. Of course, making the thruster as small as possible is preferable, but that might not be physically feasible. Furthermore, the operating voltage must be low enough to prevent any serious damage on the operator.

In chapter 2, motor alternatives are discussed while in chapter 4.1, the existing design and its limitations are covered. In chapter 3 propeller theory and estimation methods were established. With this in mind, a process can be initiated.

5.1 Motor Selection

The boundaries accounted over puts most constraints on the motor, as voltage, size and weight are important parameters. As deduced in chapter 2, a BLDC motor is most suitable in the thruster solution, both in regards to performance and reliability. Furthermore, inspecting the motor used in T200 in chapter 4.1.1, it is possible to compare specifications with other motors out in the market. The diameter of the M200 of 36 mm provides a limit when it comes to motor size. Moreover, the voltage and weight limitation set clear limitations on the choice of motor. Instead of considering millions of combinations, the search range is reduced due to the restrictions, and it is easier to find suitable alternatives.

Another important aspect of selecting the right motor, is the cost. It is essential to keep the costs as low as possible, considering the eventual profit when selling the ROVs, but also considering the asking price. Higher production costs might lead to a higher asking price for the final product, which in turn might affect the targeted consumer groups' willingness to buy. After talks with (Ludvigsen, 2016), to further minimize costs, it is desirable to talk to manufacturers for the production and deliverance of batches of motors. Hence, correspondence with several companies was initiated. The manufacturers were contacted using the specifications similar to those of the motor delivered by Blue Robotics; a low voltage motor, with a maximum diameter of 40 mm, maximum voltage of 50 V and a minimum thrust of 50 N. Several manufacturers were contacted, but only a handful responded positive. Nearly all of them could not deliver motors within the dimensional requirements. Those who did, had an

asking price ranging from 2 000 NOK to 40 000 NOK per motor, which is way more expensive than the original solution. A valid sales offer can be seen in Appendix D. In addition, the lead time on the motors varied from 8 to 22 weeks. As such, other solutions had to be found.

Radio-controlled cars, airplanes, quadcopters and drones are widely popular, thusly, the supply of parts has a great variety. This also includes electric motors, which is applicable to our design. Several marketplaces deliver thousands of alternatives for brushless DC motors, essentially targeted at modelers. While striking a deal with a manufacturer might provide high-end quality and reliability shaped after your requirements, the price is too high to even be considered. On the other hand, data provided when searching for electric motors on the marketplaces is less reliable. Performance charts of the motors are seldom shown, and it is close to impossible to decide the continued performance from the data. Thus, it is difficult to decide power and torque output of the motor for different RPM and voltage. Although this might be the case, the prices are nowhere near 2 000 NOK. Even though there are difficulties deciding the continuous performance of the motors, it is assumed that the specifications given for each motor can be seen as the continuous performance (Ludvigsen, 2016). Hence, the search for a suitable motor will be done in this segment of the market.

An important feature that is not listed in the specifications of these motors, is the thrust of the motor. To figure out how much thrust output it is possible to achieve from each motor, the torque output is a good indicator. By using OpenProp, a software developed for propeller design, to calculate the required torque for a given thrust output and blade profile, the performance of a motor and propeller combination can be found.

5.1.1 OpenProp

OpenProp is an open-source code suite written MATLAB with M-code. The free software can be used for the design, analysis and fabrication of optimized propellers and horizontal-axis turbines. The numerical model is based on propeller lifting line theory, as presented in previous sections. The software can be run using a simple graphical user interface or with a user-created script. From 2001, a team of researchers at MIT and Maine Maritime Academy has developed the OpenProp-code. As of 2012, the project has been moved from MIT to the Thayer School of Engineering at Dartmouth College.

Incorporated in the OpenProp software are graphical user interfaces for parametric design and preliminary bladerow design, geometry routines to generate a 3D printable propeller and a generalized propeller optimizer. Still under development, several other features have been added since 2001, such as an off-design analysis routine to predict the performance curve for

any given propeller, cavitation analysis capabilities and possibilities to handle the design of ducted propellers.

The software utilizes data structures to store the *input* parameters. Furthermore, *design*, *geometry* and operating *states* of a propeller are also stored within the data structures. The parameters can be used to perform either a parametric design study or a single propeller design (Epps, 2010). For the parametric design study, the data structure *parinput* is user-defined by running a short script. With the script, the operator gets the opportunity to define which ranges the parametric design software will scrutinize. Examples of the ranges are range of diameters, range of number of blades and range of rotational speed.

Combinations of the input parameters are run through a design optimization routine to determine the optimum propeller design. Eventually, these are returned in the *paroutput* data structure. After the parametric study, the data can be used to select the preferred combination of parameters for a detailed design and analysis of the desired propeller.

Figure 22 – OpenProp Parametric Study GUI

As can be seen from the GUI in Figure 22, the software demands certain input values such as required thrust, ship speed and propeller diameter. There are also optional variables,

such as the inflow profile values. It should be noted that when left blank, OpenProp uses the value 1 for the axial inflow velocity ratio *Va/Vs* and 0 for the tangential inflow velocity ratio *Vt/Vs*.

As mentioned, OpenProp can also handle single propeller design. By using the GUI, as can be seen in Figure 23, the *input* data are defined by the user. The code then determines the optimum propeller design for the given input. After OpenProp has processed the input data in the *optimizer* module, the propeller design can then be analyzed at off-design conditions to determine eventual other operating conditions. Furthermore, the program can determine a 3D geometry and prepare rapid prototyping files for production of the propeller.

OpenProp v3.3.4 — Single Design

Specifications

Number of blades:	3
Rotation speed (RPM):	200
Rotor diameter (m):	2
Required thrust (N):	25000
Ship speed (m/s):	5
Hub diameter (m):	0.4
Fluid density:	1000
# radial panels:	20
# chordwise panels:	20

Blade Design Values

r/R	c/D	Cd	t0/D	Skew	Xs/D
0.2	0.16	0.008	0.0329	0	0
0.3	0.1812	0.008	0.0281	0	0
0.4	0.2024	0.008	0.0239	0	0
0.5	0.2196	0.008	0.0198	0	0
0.6	0.2305	0.008	0.016	0	0
0.7	0.2311	0.008	0.0125	0	0
0.8	0.2173	0.008	0.0091	0	0
0.9	0.1807	0.008	0.006	0	0
0.95	0.1388	0.008	0.0045	0	0
1	0.001	0.008	0	0	0

Inflow Profile Values

r	Va/Vs	Vt/Vs

Options
- ◉ Propeller
- ○ Turbine
- ☑ Hub
- ☐ Chord optimiza...
- ☑ Viscous forces
- ☐ Optimization pl...
- ☑ Geometry plots
- ☐ Performance c...

Airfoil type

Meanline type:
NACA a=0.8

Thickness type:
NACA 65A010

...peller

Thrust Ratio:	1
Duct section drag (Cd):	0.008
duct D / prop D:	1

Non-dimensional Parameters

J = V/nD =	0.75
L = omega*R/V =	4.18879
CT =	0.63662
KT = T/(rho*n^2*D^4) =	0.140625

Tools

Filename: DefaultPropeller

Load   Save   Run OpenPr...

Figure 23 – OpenProp Single Design GUI

As can be seen by the illustration above, several design options are featured, ranging from ducts and airfoil types to whether or not a chord optimization should be done.

5.1.1.1 Formulation of the lifting line theory

As previously mentioned, OpenProp is based on lifting line theory. More specifically, moderately-loaded lifting line theory where trailing vorticity is aligned to the local flow velocity. In other words, the vector sum of the free-stream plus the induced vorticity (Epps & Kimball, 2013). OpenProp computes the induced velocities by utilizing a vortex lattice, which

is a numerical method used in computational fluid dynamics (CFD) to model lifting surfaces, in this case a propeller, as an infinitely thin sheet of discrete vortices to compute lift and induced drag. Thus, the software models helical trailing vortex filaments shed at separate stations along the blade. Furthermore, the blade is split into individual sections, which are represented with 2D properties, and loads on each section are computed by integrating over the span of the blade. An illustration of a 2D blade section is shown in Figure 24.
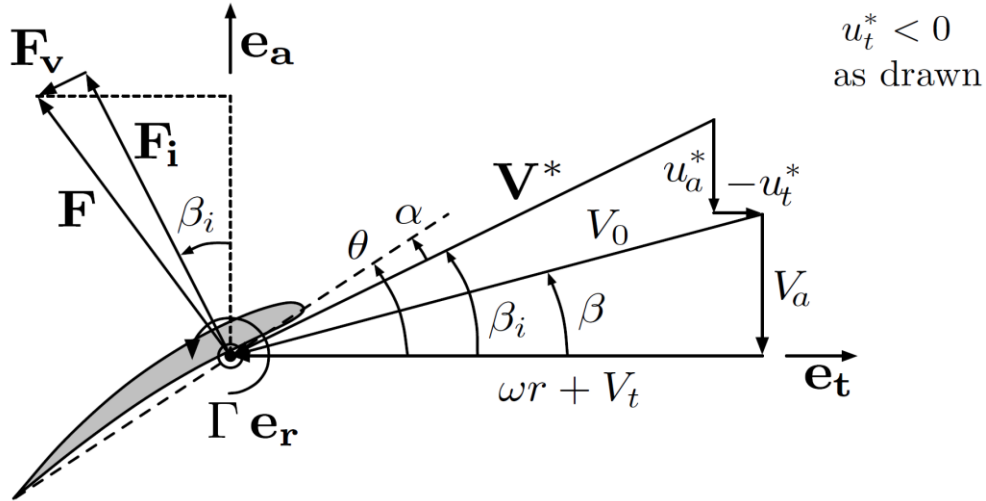
Figure 24 – Propeller velocity/force diagram

Figure 24 depicts the velocities and forces acting on the lifting line (per unit radius). Notice that the diagram is defined by the axial and tangential directions e_a and e_t with the rotational direction of the blade defined as e_r. By using the axial and tangential inflow velocities V_a and V_t, the induced velocities u_a* and u_t*, and the angular velocity ω, the total resultant inflow velocity is expressed as:

$$V^* = \sqrt{(V_a + u_a^*)^2 + (\omega r + V_t + u_t^*)^2} \qquad (5.1)$$

The inflow velocity is oriented at pitch angle β_i to the tangential direction e_t:

$$\beta_i = \arctan\left(\frac{V_a + u_a^*}{\omega r + V_t + u_t^*}\right) \qquad (5.2)$$

The forces acting on the blade section shown in Figure 24, are the inviscid lift F_i and the viscous drag F_v. Given a drag coefficient C_D, the section lift coefficient can be defined as:

$$C_L = \frac{F_i}{\frac{1}{2}\rho(V^*)^2 c} = \frac{2\Gamma}{V^* c} \tag{5.3}$$

where

$$F_i = \rho V^* \Gamma$$

$$F_v = \frac{1}{2}\rho(V^*)^2 C_D c$$

$$c = chord$$

Further, by assuming that the Z blades are identical, the total thrust and torque acting on the propeller are

$$T = Z \int_{r_h}^{R} [F_i \cos\beta_i - F_v \sin\beta_i] dr \tag{5.4}$$

$$Q = Z \int_{r_h}^{R} [F_i \sin\beta_i + F_v \cos\beta_i] r \, dr \tag{5.5}$$

where r_h and R are the hub and tip radii, respectively.

The power required to drive the propeller is the product of torque and angular velocity:

$$P = Q\omega \tag{5.6}$$

The efficiency of the propeller is described as:

$$\eta = \frac{TV_s}{Q\omega} \tag{5.7}$$

where TV_s is defined as the useful power produced by the propeller. Here, V_s is the free-stream speed, more commonly known as the ship speed.

With the use of (3.25), it is possible to connect the torque output from the motor and the required torque for a propeller at certain parameters.

5.1.2 Input Parameters

With the data collected, it is now possible to calculate the input parameters which the design of both the motor and propeller is based on.

To be able to perform whatever function is intended, the ROV needs some type of locomotion to move it around. Generated by a motor, thrust force moves an object through a fluid. To do so, the thrust must overcome the drag force, which is the resistance of an object in a fluid. In other words, excess thrust must be a positive vector quantity. Mathematically, excess thrust can be expressed by:

$$Excess\ thrust = Thrust - Drag \qquad \textbf{(5.8)}$$

To determine the thrust needed to move the ROV with the given velocity requirements, the first step is to calculate the drag forces on the vehicle.

5.1.2.1 The Drag Equation

In order to achieve movement, the vehicle must power itself and overcome the fluid drag of the vehicle and umbilical. The drag force, F_D, will increase proportionally to the density of the fluid and the surface area of the object, as well as the square of the vehicle's speed relative to the fluid. In other words, if the speed is doubled, the drag force is quadrupled. In addition, with a constant volume of the object, the shape will directly affect the force. This factor is referred to as the drag coefficient, C_D. Thus, the drag force can be expressed as:

$$F_D = \frac{1}{2}\rho C_D A U^2 \qquad \textbf{(5.9)}$$

where A is the reference area and U is the flow speed of the object relative to the fluid. ρ is the density of the fluid, which is 1025 kg/m^3 for seawater.

To determine the total drag of the system, both the vehicle and the umbilical must be accounted for. Total drag of the system is then equal to the vehicle drag plus the umbilical drag. Given the drag force equation, there are factors that will remain equal for both the vehicle and the umbilical, such as the density and the relative speed, while the drag coefficient and surface area are different. Caused by the length of the tether, the umbilical is the highest drag item on the ROV system. Hence, the total drag can be expressed as:

$$F_D = \frac{1}{2}\rho C_{D,v} A_v U^2 + \frac{1}{2}\rho C_{D,u} A_u U^2 \qquad \textbf{(5.10)}$$

5.1.2.2 Drag Coefficient

As previously mentioned, the drag coefficient is a factor defined by the shape of the object. This dimensionless quantity represents the resistance of an object in a fluid. Skin friction and form drag are the two basic effects that contributes to the coefficient. From data collected from a CFD analysis provided by Martin Ludvigsen, calculation of the drag coefficient for the ROV is possible. The data from the CFD is given in Appendix C. With a velocity of advance of 1 m/s, the drag working on the body is 24.34 N. The drag coefficient can be calculated as follows:

$$C_D = \frac{2F_D}{\rho U^2 A} \tag{5.11}$$

Hence, the drag coefficient for the vessel is 0.1, which is close to that of a streamlined body. It should be further noted that the CFD analysis is from a previous prototype and not the Explorer P1, but it is safe to assume that the new version holds at least the same standard. However, there are several ways to manipulate how the drag affects the vehicle and umbilical, which is discussed in the following subsections.

5.1.2.2.1 Skin Friction Drag

The first contributor to the coefficient is created by frictional forces between the skin and the fluid. The shear drag of fluid flowing tangentially over the surface area contributes to the resistance of the vehicle. Thus, minimizing the surface area for a given volume is beneficial. Furthermore, it is also important to maintain a smooth surface to avoid surface roughness and sharp discontinuities, which causes an increase in drag through separation of the flow from the vehicle's surface.

5.1.2.2.2 Reynolds Number

The Reynolds number is a dynamic factor for fluid flow, which determines the flow characteristics around and object. Naturally, this affects the drag equation directly. The flow around the vehicle can be divided into three different modes; laminar, transient and turbulent flow. Laminar flow means a smooth flow over the body, while turbulent flow is disorganized flow. Transient flow describes the region where the flow is approaching the critical Reynolds number where laminar flow transitions into turbulent. The ratio of inertial to viscous forces in the fluid flow can be expressed as:

$$Rn = \frac{Ud}{v} \tag{5.12}$$

where d is the diameter of the umbilical and v is the kinematic viscosity of the fluid. For seawater, the kinematic viscosity is $1.05 \cdot 10^6$ m^2/s for temperatures around 20 $^\circ$C.

5.1.2.2.3 Form Drag

The object creates form drag, as the fluid must move outwards to create room for the body. The general size and shape of the body are the most important factors; bodies with larger cross-section will have a higher drag than thinner, streamlined objects. Choice of body profile is essential for a low drag coefficient. Streamlines should be continuous, while attention to separation should be paid to avoid vortices.

5.1.2.2.4 Umbilical

The umbilical will also contribute to the drag equation, as mentioned. Because of the length of the cable, the reference area is much higher than that of the vehicle, which results in a big drag contribution.

There exist ways to lower the drag of the umbilical, more specifically by fairing. A faired cable is shown in Figure 25. Attachment of a cable fairing on the umbilical will streamline the flow around the cable.

Figure 25 – Fairing on a cable

An unfaired umbilical will have a drag coefficient around 1.2, while faired cables provide a drag coefficient in the range 0.1 - 0.6. This is a drastic reduction of the drag. On the other hand, fairing of the cable can increase the complexity of the handling system, which again makes it more complicated to operate. While an unfaired cable can be wrapped and stored easily, fairing might require the use of anti-stacking rings to not damage the cable fairing (Christ & Wernli, 2014). Hence, the drag coefficient of the umbilical is further assumed to be 1.2.

5.1.2.2.4.1 Vortex Shedding

Another important factor when it comes to drag is vortex shedding. In the starting process of separated flow around the umbilical, a symmetric wake picture develops, but due to instabilities, asymmetry will soon occur. The consequence is that low-pressure vortices are alternatively shed from each side of the umbilical. The umbilical will tend to move toward the low-pressure zones, forcing it to oscillate between the zones as the vortices get shed. The shedding of vortices will occur with Reynolds numbers in the region between 90 and 10^4. The oscillations caused by vortex shedding can damage the umbilical in terms of fatigue. Additionally, the unwanted movement of the cable can cause problems for the ROV positioning.

5.1.2.3 Thrust Power

The power required to move the ROV, is calculated by multiplying the drag and the velocity:

$$P = F_D \cdot U \tag{5.13}$$

Consequently, the power is proportional to the velocity cubed. To double the forward speed, the power increases eight times. As a result, speed requirements have a big impact on the vehicle design.

The ROV thrusters must produce enough thrust to exceed the drag produced by both the umbilical and the vehicle itself. Thus, when the thrust and the drag are of equal quantity, the thrust overcomes the drag. Hence, thrust power can be expressed through the thrust T:

$$P_T = T \cdot U \tag{5.14}$$

5.1.2.4 Calculation of Input Parameters

With the information provided in this chapter, it is now possible to calculate the total drag of the system and the necessary power to move the vessel forward in such conditions. The calculations have two variables; the relative forward speed and the operation depth of the ROV. With the data of BluEye Explorer P1 given in

Table 3, drag for different depth scenarios at variable speed are calculated. Using (5.9), an example is presented in Table 6.

Table 6 – Drag force for different scenarios

Velocity [knots]	1	
ROV Drag [N]	0.85	
Depth [m]	Umbilical Drag [N]	Total Drag [N]
20	6.51	7.36
40	13.02	13.88
60	19.53	20.39
80	26.04	26.90
100	32.55	33.41
Velocity [knots]	2	
ROV Drag [N]	3.42	
Depth [m]	Umbilical Drag [N]	Total Drag [N]
20	26.04	29.46
40	52.08	55.50
60	78.12	81.54
80	104.17	107.58
100	130.21	133.63
Velocity [knots]	3	
ROV Drag [N]	7.69	
Depth [m]	Umbilical Drag [N]	Total Drag [N]
20	58.59	66.28
40	117.19	124.88
60	175.78	183.47
80	234.37	242.06
100	292.97	300.66

From Table 6 it is clear that the umbilical will be the biggest contributor when it comes to drag. Because of the streamlined body of the ROV, the drag is almost negligible compared to that of the umbilical, especially with increasing depth. By implementing the required thrust, i.e. the total drag to overcome, as well as propeller dimensions and rotational speed into OpenProp, the software will return the torque and power values needed to achieve the thrust, as illustrated in Figure 26. Using the data from the T200, such as propeller and hub diameter and rotational speed, an equivalent propeller can be visualized through OpenProp. The propeller profile is optimized by the software, but the properties is put in by the user with the Wageningen B-3.80 as a base. Inserted are the blade design values for the B-3.80 such as thickness and chord length, as well as blade number. Figure 26 shows an iteration for the Explorer P1 at 100 m depth with a relative forward speed of 1 knot at 4000 RPM, which is within the operating conditions of the T200.
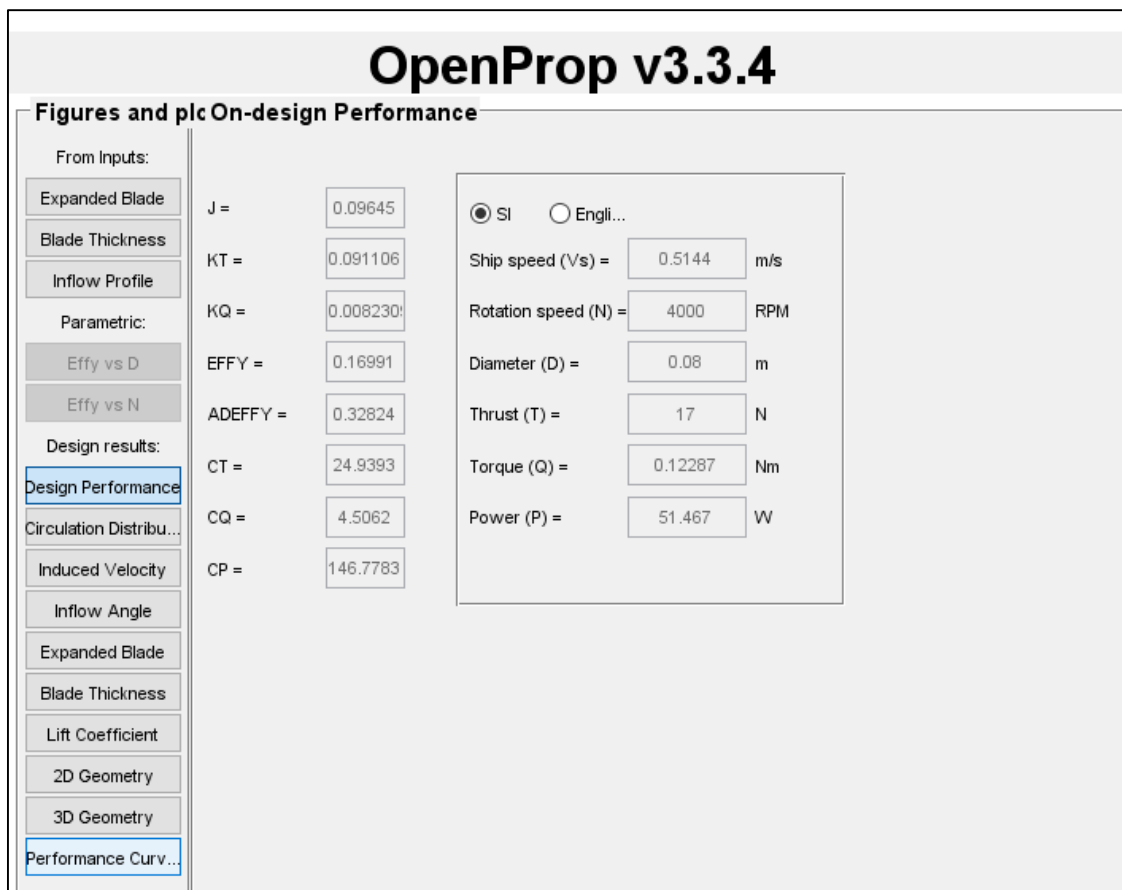
Figure 26 – OpenProp results for one thruster on an ROV with relative forward speed of 1 knot at a depth of 100 m

Lowering the RPM will raise the torque and vice versa. The propeller efficiency with these settings is very low. Usually, increasing the propeller diameter and decreasing the RPM leads to higher efficiency. In our case, the propeller diameter cannot be increased very much because of the portability of the ROV and the design. Disregarding this problem at this stage, the torque needed is ranging from 0.12 Nm to 2 Nm. This is the case for a propeller diameter of 80 mm running at 4000 RPM. The necessary power calculated with OpenProp for the same scenario is ranging from 50 W to 700 W. Hence, the chosen motor must perform within or better than these ranges, as well as being as compact as the M200.

It should be noted that the calculation is done with the operating speed of the T200 of around 4000 RPM. Changing the rotational speed will also alter torque and power following (5.6). Thus, there might be substantial differences between motors, but at this stage in the process, finding motors similar to the M200 in terms of physical dimensions is the important factor, and the contrast in operation can be taken into account thereafter.

5.1.3 Motor Alternatives

With the use of the estimation methods obtained in section 3.3, three motors were found that more or less met the conditions derived in section 5.1.2. Using the RPM of the motor, the computational script visualizes its thrust output with the torque as reference, which is derived from the generated power. For the computation, an arbitrary three-bladed propeller is chosen. Easy to modify, the MATLAB-script provides an approximation with low computational time compared with OpenProp which requires longer operational time to do the calculations.

The specifications of the three motors and the M200 are listed in Table 7. Here, the angular speed is calculated from RPM, and the torque is calculated by rewriting (5.6). As previously mentioned, it is difficult to know whether or not the given data is the continuous operating state or the maximum performance the motors can achieve over a short period of time.

The motor diameter of the three alternatives spans from 35 to 42 mm, where the upper limit is a bit bigger than the M200. However, what is most noticeable is the high RPM of the alternatives compared to the operating speed of 300 to 3800 RPM of the T200. Anyhow, the rotational speed of the M200 running at 16.7 V is 8183 RPM, calculated from the Kv-rating. The maximum torque is in this case 0.41 Nm. On the other hand, the performance charts of the T200 yields that the propeller will provide maximum power of 350 W at 3800 RPM. This equals a torque of 0.88 Nm with 50 N thrust forward.

60

Table 7 – Motor alternatives for the thruster in comparison with the M200

		Turnigy Multistar 2834	Turnigy AquaStar 4084	Turnigy Aerodrive SK3 4250	Blue Robotics M200
Kv-rating	RPM/V	800	620	350	490
RPM		12000	22940	6650	8183
Voltage	V	15	37	19	16.7
Max Power	W	660	3050	1190	350
Diameter	mm	35	39	42	36
Can Length	mm	37	79	33	
Total Length	mm	59	103	58	62
Max Current	A	45	105	53	22
Weight	g	195	508	266	
Angular Speed	rad/s	1257	2402	696	857
Torque	Nm	0.53	1.27	1.71	0.41

5.1.3.1 Calculating Motor Performance

By using OpenProp with the data in Table 7, several depth scenarios can be created by adjusting the required thrust and speed. Table 6 lists the different requirements for each case, and OpenProp is run to find the torque and power necessary to run the resulting propellers. The required torque and power is then again compared to that of the motor. This will give an idea of the performance of the chosen motor, when mounted on the ROV. The propeller used in T200 is difficult to model, as the dimensions of the blades are not listed or obtainable. Therefore, Wageningen B-3.80 is used as the reference propeller. As such, a direct comparison between the M200 and the motor alternatives in terms of thruster performance is impossible.

For the biggest motor, the Aerodrive SK3 from Turnigy, alterations on the hub diameter must be made. On the T200 thruster, the hub size is not much bigger than the motor diameter, as the propeller is connected directly to the rotor of the motor. However, the stator is connected to the thruster base, which expands the hub diameter to 40 mm. This coincides with the spacing between the rotor and the propeller base, as well as the thickness of 1 mm of the propeller which also equals 40 mm. Being a bit more conservative when modeling in OpenProp, 8 mm is added on top of the motor diameter. Taking this into account, 8 mm is added to the propeller diameter

as compensation for the expansion of the hub. The propeller diameter for the Aerodrive SK3 is then 81 mm opposed to the T200's 76 mm. For the Multistar 2834, the hub and propeller size are kept the same as for the T200, while for the AquaStar 4084 the diameter is expanded by 4 mm on both the hub and propeller.

Several depth and speed scenarios are run for the three motors, and the estimate when it comes to the motor performance are shown in Table 8. Using OpenProp, the scenarios are run to match the maximum torque and power the motors can provide. As such, the result is the maximum speed the motors can provide the ROV at different depth levels. More detailed results are shown in Appendix E.

Table 8 – Performance of the motor alternatives with a Wageningen B-3.80 propeller presented by achievable speed

		Turnigy Multistar 2834	Turnigy AquaStar 4084	Turnigy Aerodrive SK3 4250
Hub Diameter	mm	40	44	48
Propeller Diameter	mm	76	80	84
Max Rotational Speed	RPM	12000	22940	6650
Test Rotational Speed	RPM	9000	12500	6600
Depth [m]:		**Maximum Achievable Speed [m/s]:**		
5		3.5	5.3	5.2
10		2.9	4.3	4.2
20		2.2	3.2	3.3
30		1.9	2.8	2.7
40		1.7	2.5	2.4
50		1.5	2.3	2.2
60		1.4	2.1	2.0
70		1.3	2.0	1.9
80		1.2	1.8	1.8
90		1.2	1.8	1.7
100		1.1	1.7	1.6

The results in Table 8 should not be confused with continuous performance; the achievable maximum speed is the power the motors can provide over a short period of time.

Running the motors at these levels over longer periods, will eventually destroy them. Nonetheless, the results indicate that all of the three alternatives can operate within the speed range of 0.5 m/s to 1.5 m/s. The bollard pull force is around 97 percent of the total thrust, as discussed in section 3.3.3.1.

As can be seen from the aforementioned table, the RPM of the motors has been decreased during the analysis. This was done to obtain the highest possible forward speed, as the motors and associated propeller performed worse utilizing the max rotational speed. Usually, when the speed of a motor is decreased, the torque increases. Furthermore, the Figure 27 shows the main characteristics curves of a motor and an example of the relation between speed and torque. In the analysis previously performed, the speed was lowered while the torque was held constant. The torque was found from the maximum power in Table 7. From the example illustration presented in Figure 27, it is seen that the calculated torque is not the maximum torque achievable. Furthermore, the maximum power is seldom achieved at maximum rotational speed. As such, the calculated torque in Table 7 is lower than the torque provided at maximum power, and stall torque, which is the load that causes the output rotational speed to become zero, i.e. stalling. Thus, theoretically, it should be possible to attain even higher performance.
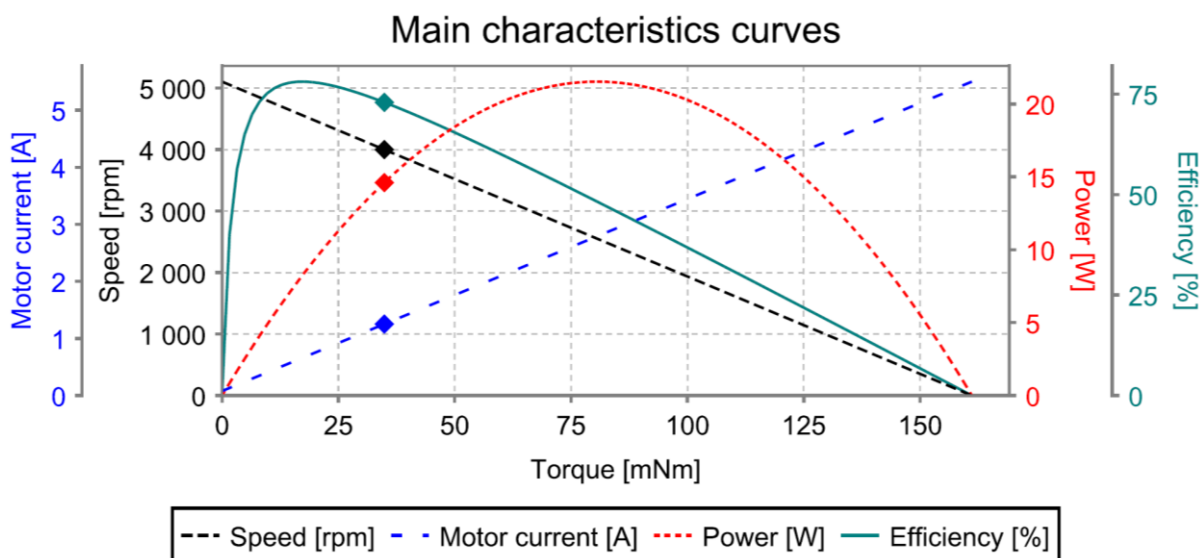
Figure 27 – **Main characteristics curves. An illustration of how the main characteristics of a motor advances in relation to each other**

5.2 Optimizing the Propeller

The motors and their performance have been mapped, and it is now possible to define the characteristics of the propeller associated with each motor. Due to size limitations, the propeller diameter will remain at the given size during the analysis in the previous section. As such, defining the blade number and EAR will be the focus of the optimization, as well as the efficiency. When calculating the maximum performance of the motors the efficiency was disregarded, and the power output was the vital point. Taking this into account, choosing the right propeller might enhance the overall performance of the thruster.

In general, for a specific pitch, diameter and thrust output on a well-designed propeller, the power and torque requirements are not expressively affected by other parameters such as number of blades, blade thickness and hub size (Sharkh, 2003). However, there are certain differences; adding a fourth blade on the propeller might increase acceleration, give better low-speed handling and cruise efficiency. Even so, a 4-bladed propeller will provide a lower top speed compared to a 3-bladed propeller. In addition, adding an extra blade will increase the amount of torque needed to run the propeller, as the EAR increases.

The reference propeller used in the analysis was the Wageningen B-3.80. Even though the series is not applicable for ducted propellers, the B-series is widely used for open propellers. Therefore, the blade design values of the B-series are used as a starting point in OpenProp. The specifications of the B-3.80 are expressed in Figure 28.

Blade Design Values

r/R	c/D	Cd	t0/D	Skew	Xs/D
0.2	0.43547	0.008	0.0329	0	0
0.3	0.48853	0.008	0.0281	0	0
0.4	0.53333	0.008	0.0239	0	0
0.5	0.56533	0.008	0.0198	0	0
0.6	0.58293	0.008	0.016	0	0
0.7	0.57813	0.008	0.0125	0	0
0.8	0.5672	0.008	0.0091	0	0
0.9	0.44187	0.008	0.006	0	0
0.95	0.3	0.008	0.0045	0	0
1	0	0.008	0	0	0

Figure 28 – Blade Design Values for the Wageningen B-3.80

The software will optimize the propeller dimensions, but the iterations are also very much based on the starting values. Thus, the difference in expanded blade area might lead to different results, and an indication of whether or not big or small EAR is the best solution will be evident. The Wageningen B-series exists of many propellers, and the combinations between blade number and the blade area ratio can be seen in Table 9.

Table 9 – Extent of the Wageningen B-series

Blade number (Z)	Blade area ratio A_E/A_O										
2	0.30										
3		0.35		0.50		0.65		0.80			
4			0.40		0.55		0.70		0.85	1.00	
5				0.45		0.60		0.75			1.05
6				0.50		0.65		0.80			
7					0.55		0.70		0.85		

As previously mentioned in chapter 4, skew is not a necessary factor on the propeller, as there is uniform inflow and there is no risk of neither cavitation nor vibration on the blades. Thus, a symmetric blade profile is simulated in OpenProp.

5.2.1 Number of Blades

Marine propellers usually have three, four or five blades, where three and four blades are most common. Generally, three-bladed propellers have proven to be the best combination between the expanded blade are and propeller efficiency. On the other hand, adding extra blades creates more total blade are with the same or less diameter, thus more thrust can be achieved with the same diameter. However, four-bladed propellers would rarely be as efficient as the opposing three-bladed propeller, because the closer the blades are, the more additional turbulence is created, disturbing the water flow on the other blades. Moreover, a higher motor torque is needed to spin the four-bladed propeller. Nonetheless, more blades can help reduce vibration, and give a smoother, uniform performance. In our case, vibrations will not be a problem (Steen, 2016). Other advantages of a four-bladed propeller versus a three-bladed one, are faster acceleration and better low-speed handling.

The motor alternatives in Table 8 are constructed with a relatively high RPM. For the given power output, this means that the torque is likewise relatively low. It is evident from the simulations of the motors that there is more leftover power than there is torque, because of the reduction in motor speed. Taking propeller efficiency into account, lowering the RPM even further proves to give a higher efficiency, which again yields a higher torque requirement at the given thrust and forward speed output.

Seeing that the T200 utilizes a three-bladed propeller, and adding a fourth blade will entail more torque, sticking with a three-bladed propeller seems sensible.

5.2.2 Expanded Blade Area Ratio

As previously mentioned, adding an extra blade on the propeller will increase the required torque, but also give a higher thrust and acceleration for the same diameter. In other words, increasing the expanded blade area ratio will lead to these changes. As such, experimenting with the blade area can alter, albeit minimal, the output. A smaller ratio tends to give a higher propeller efficiency, but on the other hand less thrust. Finding the right compromise can result in a significant improvement in performance. Already covered earlier in the chapter, the Wageningen B-series is used for the analysis. Investigating the different combinations between blade area ratio and three blades with OpenProp will define the contrasts between them.

Analyzing the three motor alternatives with Wageningen B-3.80, B-3.65, B-3.50 and B-3.35, there are certain differences between the propeller and motor combinations. Firstly, as already pointed out, the propeller efficiency increases with decreasing EAR, i.e. B-3.35 has the highest propeller efficiency. Secondly, the required torque decreases with decreasing EAR. Detailed calculations can be seen in Appendix E.

The efficiency of the Multistar 2834 and the Aquastar 4084 increases with roughly 10 percent when switching from B-3.80 to B-3.35 with a five meter long umbilical. The Aerodrive SK3 4250 has an increase of around 3 percent in the same scenario. In addition, the propeller efficiency with the B-3.80 is approximately 14 percent higher than the other two. The longer the cable gets, the more even the propeller efficiency becomes. Although there are slight differences here, these numbers represent only the given scenario. What is more important is how the performance curves develop for the designed propeller. However, with an efficiency difference of 14 percent, the Aerodrive is the most reasonable choice, even with the increase in size.

5.2.3 Performance Curves

Figure 29 shows the performance curves of the Aerodrive SK3 and the different propeller combinations. As is evident, there are slight differences between the propeller designs. The smaller blades give the highest efficiency, but in return a small drawback in acceleration. Furthermore, with a high advance ratio, i.e. when the forward speed increases and rotational speed decreases, the needed torque surpass the requirements of the bigger blades.

66

The slightly lower efficiency on the bigger blades can be justified with the increase in low-speed handling and acceleration. Even though forward speed is important for the usage of this ROV, the exploration feature on the Explorer P1 requires good low-speed handling, as consumers will use the vessel to investigate several different places with the onboard camera. As such, the bigger blades are preferred.
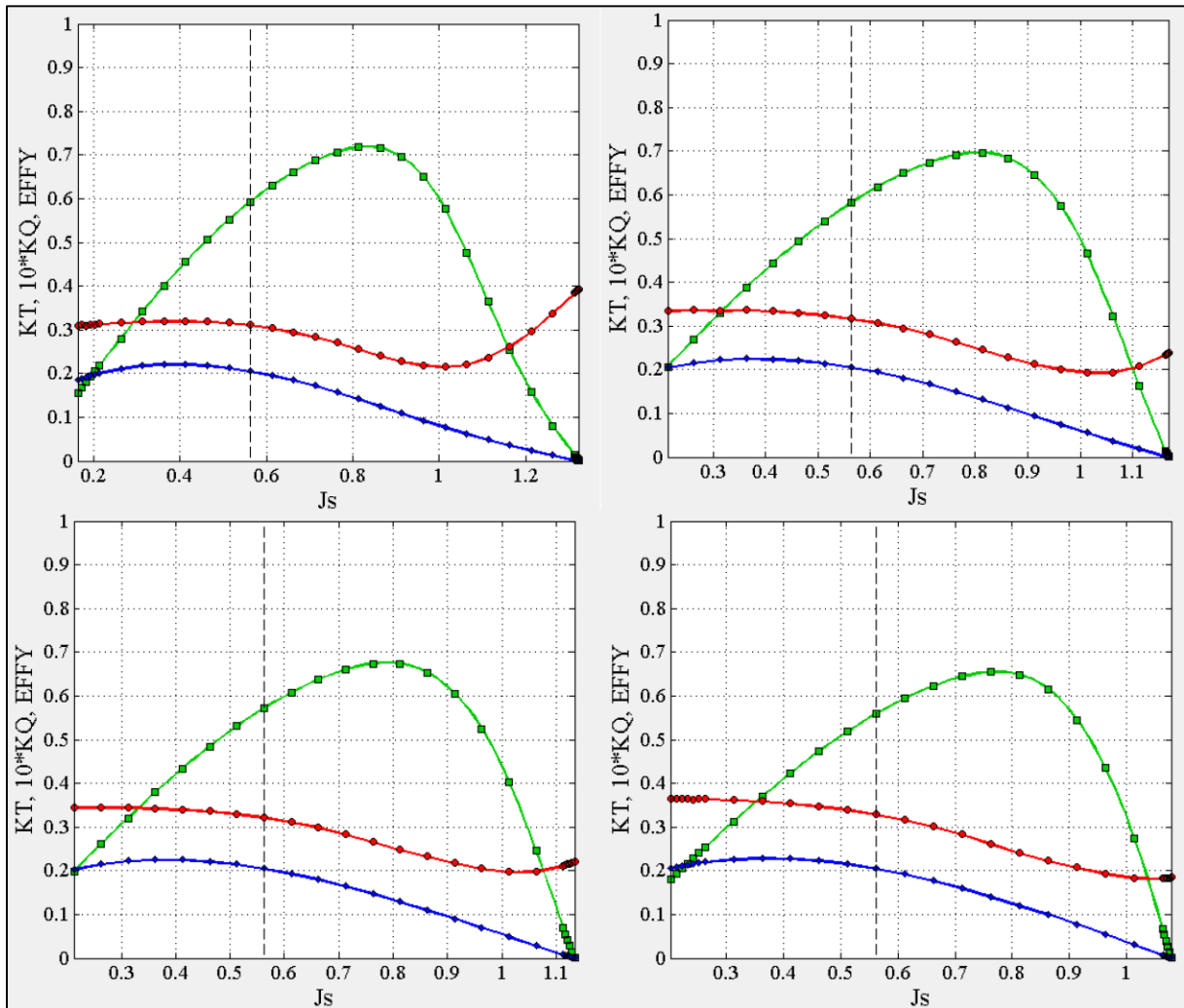
Figure 29 – Performance curves for the Turnigy Aerodrive SK3 4250 with (a) Wageningen B-3.35, (b) Wageningen B-3.50, (c) Wageningen B-3.65 and (d) Wageningen B-3.80

5.2.4 Foils and Thickness Types

Foils comes in different shapes, and a standard that is commonly used are NACA foil shapes developed by the National Advisory Committee for Aeronautics (NACA). OpenProp operates with NACA a=0.8, a modified NACA a=0.8 and a parabolic meanline type. The NACA a=0.8 or its modified version is the mostly used profile, due to the fact that 100 percent lift is obtained. In comparison, a NACA a=1.0 profile obtains only 74 percent lift. The NACA a=0.8 provides a circulation that is constant from the leading edge up to 80 percent of the chord

which declines linearly to zero up to the trailing edge, whereas on the NACA a=1.0, the circulation is constant from the leading edge to the trailing edge. Even though the NACA a=1.0 theoretically is the preferable profile, the risk of separation and reduced lift leads to seldom usage of the profile (Steen, 2014).

In addition to the meanline types, there are several thickness types to choose from. The different thickness profiles show little to no modification in the final product. As such, the NACA 65A010 is chosen.

5.3   Umbilical

Up to this point, the umbilical has been considered as a vertical straight line. In practice, this is not the case. The umbilical might drift with the water current, and even though the ROV is operating in shallower water, the length of the umbilical might still be 100 meters. Operators might also want to explore the area surrounding them even more, using the range of the umbilical even though the diving depth is shallow. These factors affect the drag force on the vessel, which yields higher resistance and lower forward speed than calculated in Table 8. Despite the fact that this has adverse impact on the system, the thrusters are still able to provide a forward relative speed of up to 1.6 m/s in any scenario.

5.4   Final Design of the Thruster
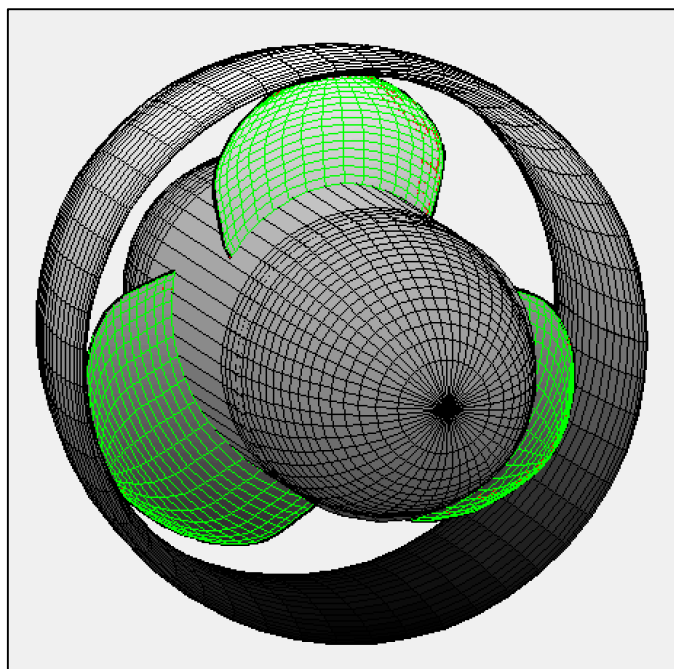
Figure 30 – Visualization of the thruster

Running the data through OpenProp, the software adds a nozzle to the propeller as well. A standard duct is issued, with a thrust ratio of 1. The thruster is illustrated in Figure 30, and

the dimensions of the thruster are following Table 8. Located in the center, the hub will contain the motor, and a solution regarding power supply should be in the same manner as the T200. As mentioned in section 5.1.1, OpenProp generates a file which contains a 3D printable geometry ready to print. As such, the design of the thruster is uncomplicated and not very time consuming. Prototype production is also cheap and effective, as the equipment needed is basically a 3D-printer. Although, the design is kept simple, and differs from the T200 thruster, where the propeller is mounted directly on the rotor. From Figure 30, it can be seen that this is the case. Even so, the design is of a high standard, efficient system, with an optimized propeller. Comparing the newly designed thruster with the T200, it is outperforming the currently used solution. The T200 provides a maximum forward thrust of 50 N, while the Aerodrive SK3 in combination with the propeller produce up to 160 N. A testing phase should definitely be incorporated, but the initial data and design show great promise.

5.4.1 Cost Estimation

The Turnigy Aerodrive SK3 is priced at €33.12 as of July 2016 (Hobbyking, n.d.). In dollars, this equals $36.4 (exchange rate of 1.1 as of July 2016). The disassembly and stripping of the motor to better fit the hub and thruster solution might add some additional expenses. The design of the propeller with OpenProp is free, as the program is an open-source, free to download software. Thus, what remains is coating of the motor and printing of the thruster.

Testing of different coating types must be performed to decide which provides the best reliability as well as longevity. Additionally, cost is also a factor in this process. As an estimate, resin and hardener from West System Epoxy are evaluated (West System, n.d.). Their 105-A resin of almost one liter and 205-A hardener of 0.20 liters give a mixed quantity of 1.15 liters. According to West System, this is enough to cover 8.5 to 12.5 square meters of surface, more than enough for the motors on one ROV. The cost for these products is a total of $66.18. Procurement of bigger quantities usually grants a lower price, and it is possible to do arrangements with manufacturers which lower the price even more. A conservative estimate of 2000 motors covered with epoxy is assumed, supposing that the resin and hardener cover 8.5 square meters of surface. Hence, epoxy coating for a single motor will cost $0.033.

Investing in a 3D-printer for development of prototypes and other parts can pay off in the long run. Industrial printers are preferred, as the quality are superior to consumer-grade 3D-printers. The price of such printers ranges from $6,000 for the smallest printers to $35,000 for the bigger ones, where the small printers can print a maximum size of 15 x 15 x 15 centimeters while the bigger printers can print up to 250 x 250 x 260 centimeters (Stratasys, n.d.). As the

build size of the thrusters are relatively small, the smaller printers work just as good as the bigger ones. As such, the $6,000 printer is suitable for the production of prototypes.

The asking price for the material has not been accounted for. Acrylonitrile butadiene styrene (ABS) and polylactic acid (PLA) plastics are the most commonly used materials in 3D-printing. ABS is sturdy, hard and suitable for machine parts while PLA has a higher printing speed and is more environmental friendly. Either way, the price for the material per kg varies between $19 and $175 for both plastics, depending on diameter, color and length.

For the production of the final product, higher quality is sought and thus by using molding to shape the frame the thruster achieves a better finish. Investing in molding tools is costly, but as a longtime investment it will pay off over time. It is difficult to estimate the cost of each thruster, as the cost of the tools varies with complexity, quality and brand. Additionally, there are expenses related to the used material. On the other hand, when starting production on the Explorer P1, the entire ROV-system must be molded with molding tools. As such, the production of the thrusters can utilize the same equipment. With some alterations and extra tools for the complexity of the thruster, in-house production of the entire system pays off over time.

The T200 weighs 344 g including the M200 motor. The weight of the motor is not specified by Blue Robotics. The Turnigy Multistar 2834, which is a smaller motor than the M200, weighs 195 g. Suppose that the M200 weighs the same as the Multistar, the rest of the T200 is 149 g. The newly designed thruster is bigger in size than the T200, and a reasonable weight estimate is 200 g. With a material price of $100 per kg, each thruster uses $20 worth of plastic.

With the data deduced in this section, the cost estimate for producing one thruster is around $58, excluding the disassembly and stripping of the motor. Any other expenses, such as administration, work force etc. are not included. The cost estimation is summarized in Table 10.

Table 10 – Cost estimation for the thruster

	Cost [USD]	Unit Cost [USD]
Motor	36.4	36.4
Epoxy Coating	66.18	0.033
Thruster Design	0	0
Printer Material	100	20
Total Unit Cost		56

Compared with the asking price of the T200 of $169, the production costs of the newly designed thruster is significantly less. It should be noted that a speed controller has not been accounted for, as it is assumed that the price for the ESC is more or less equal for the T200 as for the designed thruster. Additionally, the molding cost has not been included in the cost estimate, as it is very difficult to estimate the price and longevity of the equipment. Even so, it seems improbable that the total costs will exceed the asking price of the T200. Some alterations to the Explorer P1 might be required, as the thruster size is different than the T200, but the low cost in addition to the enhanced performance makes the thruster highly attractive.

6 Results

The final thruster solution consists of several parts, which fundamentally can be divided into motor and propeller. Through the design process, covered in chapter 5, motor and propeller are chosen and optimized to comply with the demands set by the boundaries of the objective and the already installed T200 thruster by Blue Robotics. The chosen motor is the Turnigy Aerodrive SK3 4250 with a Kv-rating of 350. The specifications, along with the motor utilized in the T200, are shown in Table 11. The angular speed and torque are deduced from the given RPM and power.

Table 11 – Motor specifications for the Turnigy Aerodrive SK3 4250 in comparison with the Blue Robotics M200

		Turnigy Aerodrive SK3 4250	Blue Robotics M200
Kv-rating	RPM/V	350	490
Rotational Speed	RPM	6650	8183
Voltage	V	19	16.7
Max Power	W	1190	350
Diameter	mm	42	36
Can Length	mm	33	
Total Length	mm	58	62
Max Current	A	53	22
Weight	g	266	
Angular Speed	rad/s	696	857
Torque	Nm	1.71	0.41

The size of the Aerodrive is a bit bigger than the M200. In fact, there is a 17 percent expansion of diameter, as well as an increase in voltage. In return, the power output is substantially higher. Utilizing the estimation methods derived in section 3.3, achievable thrust output and relative forward speed are approximated, resulting in a thrust of up to 160 N. Compared to the T200 with a thrust output of 50 N, the Turnigy motor is significantly stronger.

To compensate for the bigger motor, both the hub of the thruster and propeller diameter are widened by 8 mm in comparison with the T200, resulting in diameters of 48 mm and 84

mm respectively. Using OpenProp with the specifications in Table 11, the thruster is modeled and optimized. It was further decided that the propeller should consists of three blades with a big blade area ratio, yielding high propeller efficiency as well as good low-speed handling. More specifically, the Wageningen B-series was used as initial values for the propeller design, resulting in the B-3.80 as the starting point for the optimization. Calculations on three-bladed propellers and their performance can be seen in Appendix E. The inserted design values from the B-3.80 is shown in Figure 31. Furthermore, no skew on the blade profile is added, as there is no risk of cavitation and vibration with the uniform inflow.

r/R	c/D	Cd	t0/D	Skew	Xs/D
0.2	0.43547	0.008	0.0329	0	0
0.3	0.48853	0.008	0.0281	0	0
0.4	0.53333	0.008	0.0239	0	0
0.5	0.56533	0.008	0.0198	0	0
0.6	0.58293	0.008	0.016	0	0
0.7	0.57813	0.008	0.0125	0	0
0.8	0.5672	0.008	0.0091	0	0
0.9	0.44187	0.008	0.006	0	0
0.95	0.3	0.008	0.0045	0	0
1	0	0.008	0	0	0

Figure 31 – Blade design values for the Wageningen B-3.80 propeller

The input data is optimized by OpenProp, and the details of the resulting design are shown in figures Figure 32, Figure 33, Figure 34, Figure 35, Figure 36, Figure 37, Figure 38, Figure 39. Comparing the On-design performance data with the motor performance in Table 11, the power and torque needed to move the propeller is within the limits of operation for the Aerodrive SK3. As such, two thrusters running will overcome the total drag of 254 N with a relative forward speed of 5.2 m/s at a depth of 5 m. Even though this is the maximum achievable speed, it does not by no means signify that running at these speeds are practical for the operation of the vessel. The drag contributors are the body of the Explorer P1 and the umbilical. The umbilical is assumed as a vertical straight line during the calculations. This will not be the case in practice, as current will make the umbilical drift. Furthermore, operators might use the umbilical range to explore horizontally as well, affecting the drag at shallow depth. As such, high speeds of 5 m/s is not achievable in practice.

The streamlined body of the ROV has a drag coefficient of only 0.1, while for the umbilical the standard value of 1.2 is applied, which is common for unfaired umbilical cables. Caused by the length of the umbilical, the drag contribution of the ROV is almost negligible, standing for only 2.4 percent of the total drag at an umbilical length 100 meters and a forward speed of 1 m/s. Calculation of the drag coefficient can be found in section 5.1.2.2.
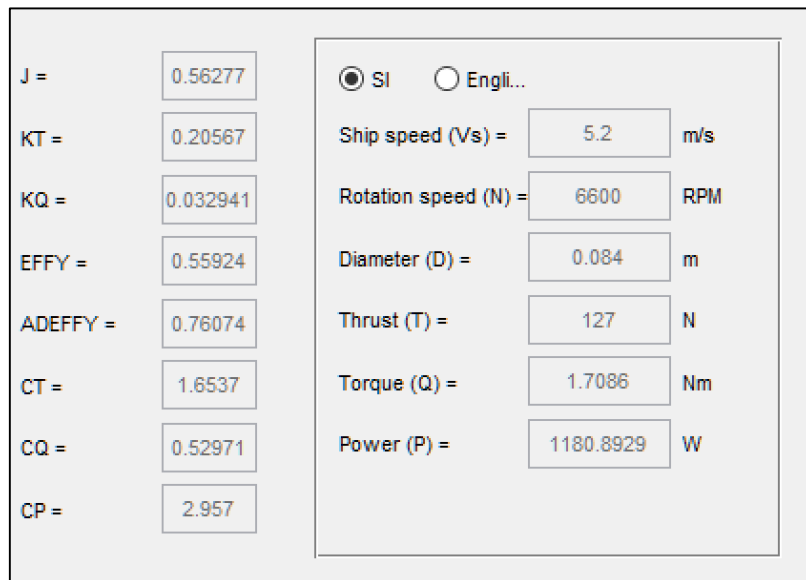
Figure 32 – On-design performance
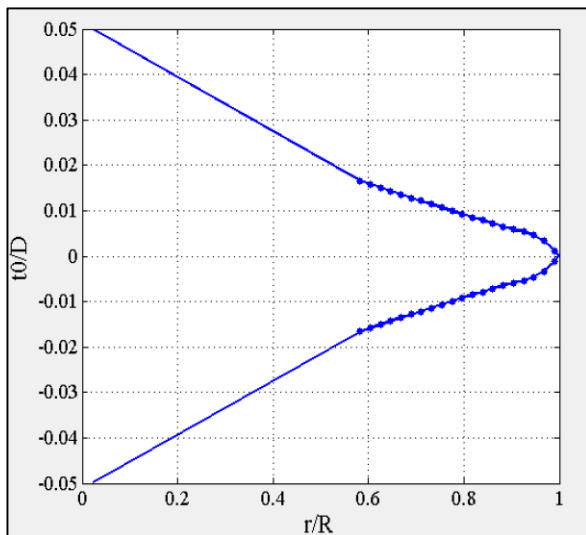
Figure 33 – Blade thickness
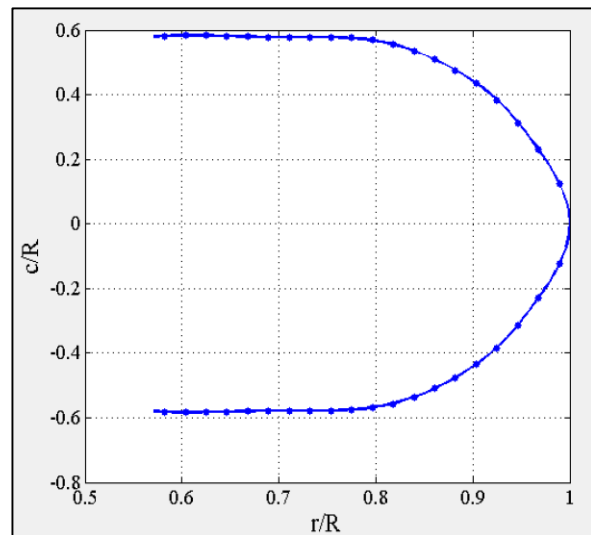
Figure 34 – Expanded blade
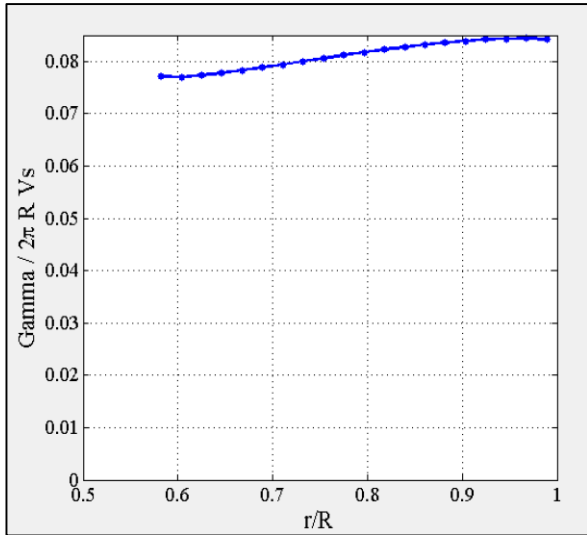
Figure 35 – Circulation distribution
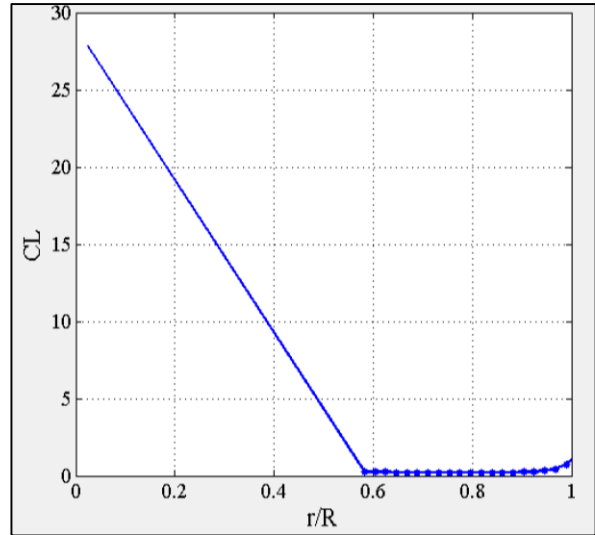
Figure 36 – Lift coefficient
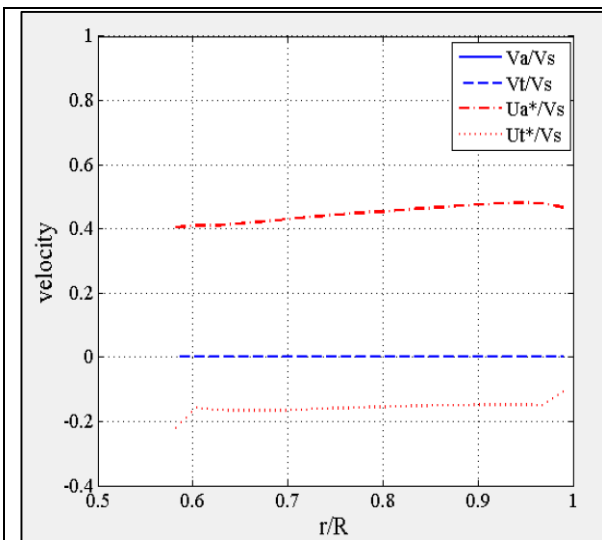
Figure 37 – Induced velocity
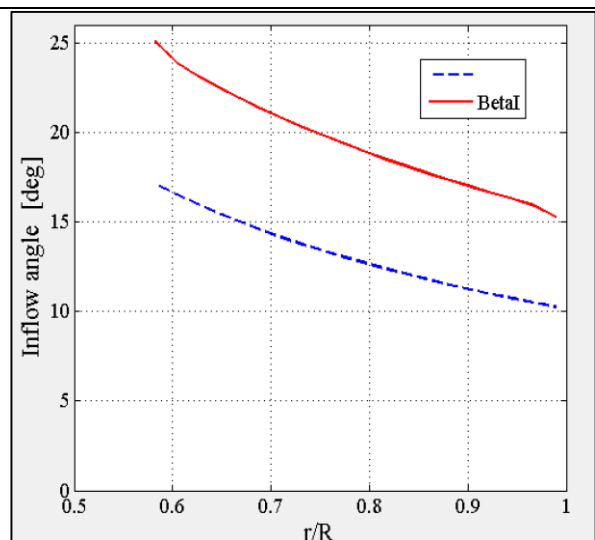
Figure 38 – Inflow angle
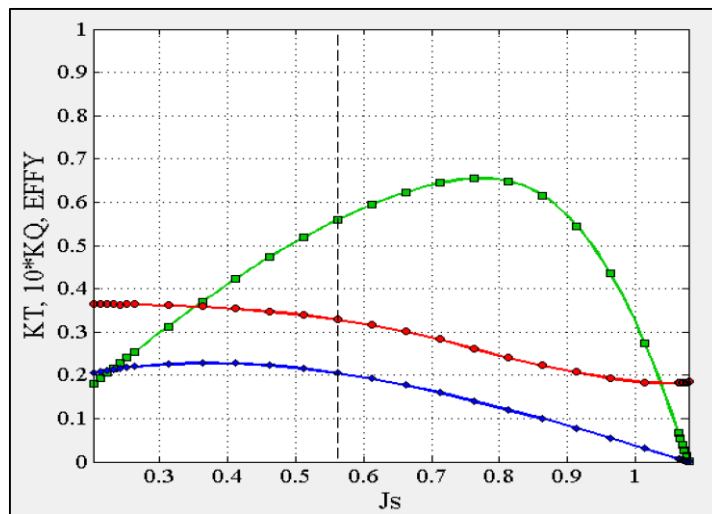
Figure 39 – Performance curves

The performance curves in Figure 39 shows a propeller efficiency of up to 65 percent. Albeit a bit low, this solution was chosen over the more effective smaller blades because of the better low-speed handling and faster acceleration.

There are difficulties finding the continuous performance of the motor. Assumptions were made concerning the overall output of the motor, as stated in section 5.1. With these in mind, the designed thruster outperforms the T200 in terms of power and torque output. In Table 11 and in the motor documentation for the M200 (BlueRobotics, n.d.), the rotational speed is set to around 8000 RPM calculated with the Kv-rating of 490 and the operating voltage of the T200 of 16.7 V. The thruster documentation for the T200 (BlueRobotics, n.d.) specifies a rotational speed range of 300 – 3800 RPM, lower than what is stated for the M200. Even so, the torque output of the T200 running at 3800 RPM with a maximal power output of 350 is 0.88 Nm, almost half of what the Aerodrive SK3 generates. Moreover, the SK3 has a maximal power output of 1190 W, more than three times more than the M200. On the other hand, the operating voltage is 19 V, a bit higher than the T200.

Considering that the battery supplies up to four T200 thrusters with 16.7 V, it is sensible to assume that this solution will suffice for the Turnigy as well.
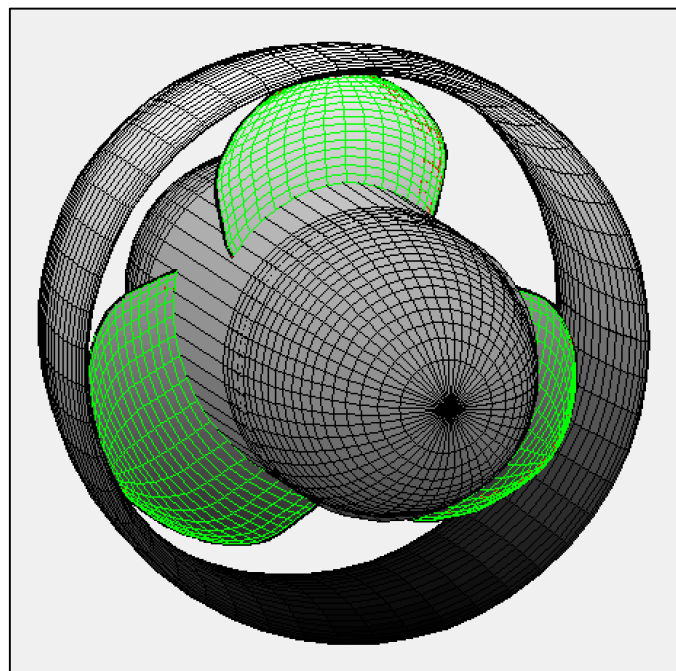
Figure 40 – Visualization of the final thruster design

Figure 40 illustrates the final design of the thruster. The motor will be located within the streamlined hub with a power supply similar to that of the T200. Furthermore, OpenProp

generates files that can be taken straight to 3D-printing. As such, the design can be taken straight to prototype development.

The cost estimate for the design is presented in Table 12. Compared with the asking price of the T200 of $169, the production costs of the thruster are notably lower. A more detailed deduction is found in section 5.4.

Table 12 – Estimation of production costs

	Cost [USD]	Unit Cost [USD]
Motor	36.4	36.4
Epoxy Coating	66.18	0.033
Thruster Design	0	0
Printer Material	100	20
Total Unit Cost		56

7 Discussion

During the design process, several complications occurred. For instance, talking to motor manufacturers, the asking price was not acceptable in addition to the long lead time. This resulted in searching in other segments of the market. Arranging deals with manufacturers are preferable, as it is easier to order batches of the wanted product with a given deliverance time. Moreover, the product can be altered and customized to do a specific job. In the marketplaces, the motors must be taken as is. Even though there is a price difference between these two options, opting for manufacturers will usually result in better production flow and less problems with the final ROV product. Manufacturers also have complete overview of how their motors perform for different input variables, thusly several alternatives for the choice of motor can considered for different scenarios. With motors acquired from the hobby segment, three are no overview of motor performance with the exception of list values. Furthermore, test results and performance charts are seldom easy to obtain. Even so, the listed specifications might not even be correct, and the lead time on these motors is unknown.

Through the design process, it is proven that these motors are much cheaper than the motors suggested by manufacturers. Nonetheless, there are uncertainty when it comes to the motor performance, and more energy must be put into testing of these, unlike the high-end motors as they are delivered with performance charts and test results. In addition, the lead time is an important aspect considering planning of production. However, the delivery time of the manufacturers spans from eight weeks and up, but long-term planning yields better production flow and continuity than for the other alternative. As such, striking a deal with a manufacturer that can deliver the wanted product for a reasonable price should be priority. Besides, custom production of a motor can be arranged with a manufacturer, shaping the performance to meet the needed output.

However, the current design is indeed low-cost, as specified in the objective. On the other hand, the lack of certainty when it comes to performance is troublesome. As OpenProp is based on lifting line theory, optimizes the thruster solution and presents performance curves close to actual values, it is mainly the motor that should undergo a thorough testing phase. With the long lead time of the manufacturers and the uncertain delivery time from sellers on different marketplaces, it was difficult to allocate time for testing of the motor. Nonetheless, this should definitely be conducted to assure that the design fulfills the demands set.

Except the testing of the motor, the size brings up other problems. With a diameter of 42 mm, it is 6 mm wider than the original solution. As a consequence, both the hub and the

propeller diameter are expanded. This affects the overall thruster size, making it almost 1 cm wider than the T200. Although this is not very much, the main body of the ROV might undergo some changes as there are two thrusters embedded in the Explorer P1. The bigger size can lead to changes of the ROV width, which again leads to alterations to the drag of the vessel. However, if modifications cannot be avoided, widening the body by 1 cm will not have a massive impact on the drag force. Besides, the thrusters provide more power than the T200. The two thrusters outside of the main body will not influence the overall design, but the portability of the ROV might be affected slightly. Despite the fact that the new design is bigger than the T200, one centimeter on each thruster is miniscule compared to the overall width. Installation of the thrusters will give a total overall width of 339 mm compared to the original 329 mm if the positions are kept the same. If the decision is to move the thrusters one centimeter out to the side, the total width becomes 349 mm.

Also affecting the size, a speed controller has not been considered. The ESC is needed to operate the motor, and the T200 utilizes special designed speed controllers made exclusively for the thruster. This is mounted directly on the hub, extending the length of the hub while upholding its diameter, giving it a smooth surface. A solution for a speed controller for a new thruster must be designed in the same matter, or in another way that does not influence the performance of the thruster.

The diameter of the propeller has also been changed, more specifically extended with 8 mm to weigh up for the bigger hub. Testing of the new solution has not been executed, but the performance curves from OpenProp more or less conforms with tests. However, the motor-propeller combination has not been tested, and acceleration, bollard pull and so on should be sorted out. Even though analytical and design tools have improved and are quite reliable, there are still some deviation from the final product. Moreover, with the lack of reliable data accumulated during this thesis, testing is even more important.

Important to keep in mind when testing the thruster, is the effect of the umbilical. With the highest contribution to drag, the length and thickness plays a major role. When operating the ROV, the total range of the vessel is 100 m, limited by the length of the umbilical. As such, high drag contributions can occur at shallow depth. With the design deduced in this thesis, the performance of the thrusters should be enough to operate the Explorer P1 with 1 m/s relative forward speed in any scenario. Even so, improvement of the umbilical, whether it be thickness, fairing or other solutions, can account for drastic changes to the design of the vessel, especially size of the body and thrusters, and its portability. The thickness of the umbilical also limits the amount of voltage and current to be sent through the wire to the ROV. As of now, the T200

runs on 16.7 V, and in the thesis it was assumed that the power supply could provide the Turnigy Aerodrive SK3 with 19 V using the same umbilical. If it should turn out that this is not the case, delivering 16.7 V to the motors will reduce the output, but it is realistic to presume that the performance is still adequate.

It is evident through this chapter that thorough testing of equipment is necessary to determine the performance of the final product. This is also the case for the protection of corrodible materials, such as the motor parts. Coated with epoxy, the rotor and stator is protected against the corrosive seawater. What is worrisome is the longevity of the coating. With the high rotational speeds of the motor parts, galling on the epoxy can occur, and eventually peel off the layer of protection. There exist different types of epoxy with different abilities. Testing and research on applicable epoxies should be executed to ensure the longevity of the system. Other options should also be explored, such as superhydrophobic materials. However, the epoxy layer will eventually disappear due to galling and wear, and easy access to the motor core must be made available so consumers can apply epoxy themselves.

The cost estimation of each thruster is $56 compared to the asking price of $169 for the T200. Even though the total price is lower, expenses such as salary to the staff during production, speed controller and other variables that can affect the total cost are not included in the estimate. Nonetheless, developing and producing in-house products proves to be less expensive than outsourcing. With the development in technology, prototype production is made easy through 3D-printing. A more comprehensive product might be achieved if both the motor and thruster are produced in-house, or given to the same manufacturer.

8 Conclusion

For the detailed design of a thruster-solution for a mass-market ROV, the BLDC motor, a Turnigy Aerodrive SK3 4250, is 6 mm bigger than the motor employed in the Explorer P1 Prototype 2.0. However, the motor outperforms the M200 with a power output of 1190 W at 6650 RPM opposed to the M200's 350 W at 3800 RPM. To protect the motor against damage, e.g. corrosion, barriers are installed; epoxy is applied to the motor core and plastic ball bearings are utilized for the shaft. Moreover, this is encapsulated in a motor case. Additionally, the plastic ball bearings remove the need for lubrication, which further reduces the maintainability and increases the reliability of the motor.

Defining for the propeller dimensions, and also for the choice of motor, is the total drag of the system. The umbilical, with a 2 mm thickness and a length of 100 m, gives the biggest contribution to the drag force. The ROV dimensions are 498 mm x 350 mm x 180 mm, and with data from a CFD analysis, the calculated drag coefficient is 0.1. Taking the drag from the umbilical into account, the contribution from the ROV is almost negligible. With 1 m/s relative forward speed, the drag of the Explorer P1 is 3.23 N, while the 100 m umbilical has a drag of 123 N.

Even though the energy requirement is higher for the Aerodrive, it is realistic to presume that the battery supply can deliver 19 V to each motor. If not, the performance of the Aerodrive will not be much affected if clocked down to 16.7 V, which the M200 utilize.

Utilizing two thrusters for the forward motion, the thrust output of the motors amount to 320 N compared to 100 N with two T200 thrusters. The designed thruster is based on the Wageningen B-series, more specifically a 3-bladed propeller with an expanded blade-area ratio of 0.80. Computed with OpenProp in MATLAB, the software optimizes the input values of the B-3.80, altering them to best fit the propeller specifications. With a rotational speed up to 6650 RPM, the efficiency of the propellers reaches the peak of 0.65. In return, the thrusters have good low-speed handling and bollard pull. The resulting propeller diameter is 84 mm, while the hub is 42 mm, which is an 8 mm extension of the T200's measurements.

8.1 Further Work

Looking at the project description, development of a prototype and testing remains. Talks with Protolab and Trollabs in Trondheim concerning printing was initiated, but since there was not found time for testing, production was discarded. In addition to testing of the thruster design as a whole, performance tests on the motor should commence. As stated in

chapter 7, the specifications are somewhat unreliable, and to assure adequate quality, verification of the motor's performance should be conducted.

Production-wise, arrangements with motor manufacturers is important to provide an even production flow as well as reliability when it comes to quality. With the ability to custom design motors, a product shaped for the specific thruster and specific behavior will result in a more complete package. This will be a more expensive solution than buying hobby motors, but the quality is superior as well as dependable lead and delivery times. Investing in 3D-printers and molding tools for in-house production of the thrusters is cheaper than outsourcing and gives more control over the design process, making it easier to do eventual necessary adjustments.

Testing is the main focus moving ahead. This is also the case for the protection of the motor. Whether it be epoxy solutions or superhydrophobics, assuring the longevity of the corrosive parts of the thruster is vital.

Working on the design and looking for other solutions to the problem is as important. To be able to move forward, and perhaps outperform the competition, new and thoughtful interpretations might give an advantage. For instance, eliminating the hub results in a bigger propeller area which leads to more thrust. Installing a rim-drive thruster might be the solution to give the Explorer P1 the extra edge in performance, quality and aesthetic design. Furthermore, this will lead to possibilities to shrink the thrusters and ROV, resulting in lower weight and better portability abilities.

9 Bibliography

BlueRobotics, 2014. *Blue Robotics Blog.* [Online]
Available at: https://www.bluerobotics.com/t-shirts-stickers-shipped-updates/
[Accessed 23 March 2016].

BlueRobotics, n.d. *M200 Motor Documentation.* [Online]
Available at: http://docs.bluerobotics.com/thrusters/motors/m200
[Accessed 2015].

BlueRobotics, n.d. *T200 Thruster Documentation.* [Online]
Available at: http://docs.bluerobotics.com/thrusters/t200/
[Accessed 25 October 2015].

Carlton FREng, J. S., 2012. *Marine Propellers and Propulsion.* 3rd ed. Oxford: Butterworth-Heinemann.

Christ, R. D. & Wernli, R. L., 2014. *The ROV Manual; A User Guide for Remotely Operated Vehicles.* 2nd ed. Waltham(Massachusetts): Butterworth-Heinemann.

Epps, B., 2010. *OpenProp v2.4 Theory Document.* Cambridge: Department of Mechanical Engineering, Massachusetts Institute of Technology.

Epps, B. & Kimball, R., 2013. Unified Rotor Lifting Line Theory. *Journal of Ship Research,* 57(4).

Epps, B. P. & Kimball, R. W., 2013. *OpenProp v3: Open-source software for the design and analysis of marine propellers and horizontal-axis turbines.* [Online]
Available at: http://engineering.dartmouth.edu/epps/openprop/
[Accessed 2016].

Faltinsen, O. M., 1990. *Sea Loads on Ships and Offshore Structures.* Camgbridge: Cambridge University Press.

84

Hobbyking, n.d. *Turnigy Aerodrive SK3 - 4250-350kv Brushless Outrunner Motor.* [Online]
Available at:
http://www.hobbyking.com/hobbyking/store/__18170__Turnigy_Aerodrive_SK3_4250_350k
v_Brushless_Outrunner_Motor.html
[Accessed 2016].

Kerwin, J. E., 2001. *Hydrofoils and Propellers.* Massachusetts: MIT.

Lerbs, H. W., 1952. *Moderately Loaded Propellers with a Finite Number of Blades and an Arbitrary Distribution of Circulation.* s.l.:SNAME.

Lewis, E. V., 1988. *Principles of Naval Architecture.* Jersey City(New Jersey): The Society of Naval Architects and Marine Engineers.

Ludvigsen, M., 2016. [Interview] 2016.

Marzocca, P., n.d. *The NACA Airfoil Series.* Potsdam, New York: Clarkson University.

MEPS LTD, 2015. *World Stainlees Steel Prices.* [Online]
Available at: http://www.meps.co.uk/Stainless%20Prices.htm

Nissan, 2014. *Nissan Develops the First Self-Cleaning Car | Nissan USA.* [Online]
Available at: http://www.nissanusa.com/blog/self-cleaning-car-paint
[Accessed 11 November 2015].

Oosterveld, M. W. C. & Oossanen, P. v., 1975. *Further computer-analyzed data of the Wageningen B-screw series.* Wageningen: Netherlands Ship Model Basin.

Pettersen, B., 2007. *Hydrodynamikk.* Trondheim: NTNU.

Robotics, B., n.d. *Blueye Robotics.* [Online]
Available at: http://www.blueye.no

Sharkh, S. M. A., 2003. Propulsion Systems for AUVs. In: G. Griffiths, ed. *Technology and Applications of Autonomous Underwater Vehicles.* London: Taylor & Francis, pp. 109-125.

Steen, S., 2007. *Motstand og Propulsjon, Propell- og Foilteori.* 2nd red. Trondheim: NTNU.

Steen, S., 2014. *Foil and Propeller Theory.* 2nd ed. Trondheim: NTNU.

Steen, S., 2016. [Interview] 2016.

Stratasys, n.d. *3D Printers for Professional Applications.* [Online]
Available at: http://www.stratasys.com/3d-printers
[Accessed 2016].

Tipler, P. A. & Mosca, G., 2008. *Physics For Scientists and Engineers.* 6th ed. New York: W. H. Freeman and Company.

Ultratech International, I., n.d. *Ultra-Ever Dry.* [Online]
Available at: http://spillcontainment.com/ever-dry
[Accessed 10 November 2015].

West System, n.d. *WEST SYSTEM | Epoxy Resins and Hardeners.* [Online]
Available at: http://www.westsystem.com/ss/epoxy-resins-and-hardeners
[Accessed 2016].

White, M., 2008. *Marine Engineering Systems.* 4th ed. Trondheim: NTNU.

Appendix A Wageningen B-series Polynomial Coefficients

$$K_T = \sum A_{abcd} \cdot J^a \left(\frac{P}{D}\right)^b \left(\frac{A_E}{A_0}\right)^c Z^d;$$

A_{abcd}	a — J	b — $\frac{P}{D}$	c — $\frac{A_E}{A_0}$	d — Z
+0.00880496	0	0	0	0
−0.204554	1	0	0	0
+0.166351	0	1	0	0
+0.158114	0	2	0	0
−0.147581	2	0	1	0
−0.481497	1	1	1	0
+0.415437	0	2	1	0
−0.0144043	0	0	0	1
−0.0050054	2	0	0	1
+0.0143481	0	1	0	1
+0.0606826	1	1	0	1
−0.0125894	0	0	1	1
+0.0109689	1	0	1	1
−0.133698	0	3	0	0
+0.000638407	0	6	0	0
−0.00132718	2	6	0	0
+0.168496	3	0	1	0
−0.0507214	0	0	2	0
+0.0854559	2	0	2	0
−0.0504475	3	0	2	0
+0.010465	1	6	2	0
−0.00648272	2	6	2	0
−0.00841728	0	3	0	1
+0.0168424	1	3	0	1
−0.00102296	3	3	0	1
−0.0317791	0	3	1	1
+0.018604	1	0	2	1
−0.00410798	0	2	2	1
−0.000606848	0	0	0	2
−0.0049819	1	0	0	2
+0.0025983	2	0	0	2
−0.000560528	3	0	0	2
−0.00163652	1	2	0	2
−0.000328787	1	6	0	2
+0.000116502	2	6	0	2
+0.000690904	0	0	1	2
+0.00421749	0	3	1	2
+0.0000565229	3	6	1	2
−0.00146564	0	3	2	2

$$K_Q = \sum B_{abcd} J^a \left(\frac{P}{D}\right)^b \left(\frac{A_E}{A_0}\right)^c Z^d$$

B_{abcd}	a — J	b — $\frac{P}{D}$	c — $\frac{A_E}{A_0}$	d — Z
+0.00379368	0	0	0	0
+0.00886523	2	0	0	0
−0.032241	1	1	0	0
+0.00344778	0	2	0	0
−0.0408811	0	1	1	0
−0.108009	1	1	1	0
−0.0885381	2	1	1	0
+0.188561	0	2	1	0
−0.00370871	1	0	0	1
+0.00513696	0	1	0	1
+0.0209449	1	1	0	1
+0.00474319	2	1	0	1
−0.00723408	2	0	1	1
+0.00438388	1	1	1	1
−0.0269403	0	2	1	1
+0.0558082	3	0	1	0
+0.0161886	0	3	1	0
+0.00318086	1	3	1	0
+0.015896	0	0	2	0
+0.0471729	1	0	2	0
+0.0196283	3	0	2	0
−0.0502782	0	1	2	0
−0.030055	3	1	2	0
+0.0417122	2	2	2	0
−0.0397722	0	3	2	0
−0.00350024	0	6	2	0
−0.0106854	3	0	0	1
+0.00110903	3	3	0	1
−0.000313912	0	6	0	1
+0.0035985	3	0	1	1
−0.00142121	0	6	1	1
−0.00383637	1	0	2	1
+0.0126803	0	2	2	1
−0.00318278	2	3	2	1
+0.00334268	0	6	2	1
−0.00183491	1	1	0	2
+0.000112451	3	2	0	2
−0.0000297228	3	6	0	2
+0.000269551	1	0	1	2
+0.00083265	2	0	1	2
+0.00155334	0	2	1	2
+0.000302683	0	6	1	2
−0.0001843	0	0	2	2
−0.000425399	0	3	2	2
+0.0000869243	3	3	2	2
−0.0004659	0	6	2	2
+0.0000554194	1	6	2	2

B

A.1 Wageningen B-series Scale Effects Coefficients

$$\Delta K_T = \sum C_{abcd} \left(\frac{A_E}{A_0}\right)^a \left(\frac{P}{D}\right)^b z^c J^d$$

C_{abcd}	a $\left(\frac{A_E}{A_0}\right)$	b $\left(\frac{P}{D}\right)$	c z	d J
0.000353485	0	0	0	0
-0.00333758	1	0	0	2
-0.00478125	1	1	0	1
$+0.000257792 \, (\lg R_n - 0.301)^2$	1	0	0	2
$+0.0000643192 \, (\lg R_n - 0.301)$	0	6	0	2
$-0.0000110636 \, (\lg R_n - 0.301)^2$	0	6	0	2
$-0.0000276305 \, (\lg R_n - 0.301)^2$	1	0	1	2
$+0.0000954 \, (\lg R_n - 0.301)$	1	1	1	1
$+0.0000032049 \, (\lg R_n - 0.301)$	1	3	2	1

$$\Delta K_Q = \sum C_{abcd} \left(\frac{A_E}{A_0}\right)^a \left(\frac{P}{D}\right)^b z^c J^d$$

C_{abcd}	a $\left(\frac{A_E}{A_0}\right)$	b $\left(\frac{P}{D}\right)$	c z	d J
0.000591412	0	0	0	0
-0.00696898	0	1	0	0
$+0.0000666654$	0	6	1	0
-0.0160818	2	0	0	0
$+0.000938091 \, (\lg R_n - 0.301)$	0	1	0	0
$-0.00059593 \, (\lg R_n - 0.301)$	0	2	0	0
$-0.0000782099 \, (\lg R_n - 0.301)^2$	0	2	0	0
$+0.0000052199 \, (\lg R_n - 0.301)$	1	0	1	2
$+0.00000088528 \, (\lg R_n - 0.301)^2$	1	1	1	1
$-0.0000230171 \, (\lg R_n - 0.301)$	0	6	1	0
$+0.00000184341 \, (\lg R_n - 0.301)^2$	0	6	1	0
$-0.00400252 \, (\lg R_n - 0.301)$	2	0	0	0
$+0.000220915 \, (\lg R_n - 0.301)^2$	2	0	0	0

$$\begin{Bmatrix} K_T(R_n) \\ K_Q(R_n) \end{Bmatrix} = \begin{Bmatrix} K_T(R_n = 2 \times 10^6) \\ K_Q(R_n = 2 \times 10^6) \end{Bmatrix} + \begin{Bmatrix} \Delta K_T(R_n) \\ \Delta K_Q(R_n) \end{Bmatrix}$$

A.2 Wageningen Ka-Series Polynomial Coefficients

	x	y	Nozzle No. 19A			Nozzle No. 37		
			Axy	Bxy	Cxy	Axy	Bxy	Cxy
0	0	0	+ 0.030550	+ 0.076594	+ 0.006735	−0.0162557	−0.016806	+ 0.016729
1		1	−0.148687	+ 0.075223				
2		2		−0.061881	−0.016306			
3		3	−0.391137	−0.138094				
4		4			−0.007244	−0.077387		
5		5		−0.370620				
6		6		+ 0.323447			−0.099544	+ 0.030559
7	1	0		−0.271337		+ 0.598107		+ 0.048424
8		1	−0.432612	−0.687921		−1.009030	−0.548253	−0.011118
9		2		+ 0.225189	−0.024012		+ 0.230675	−0.056199
10		3						
11		4						
12		5						
13		6		−0.081101				
14	2	0	+ 0.667657	+ 0.666028		+ 0.085087	+ 0.460206	+ 0.084376
15		1				+0.425585		
16		2	+ 0.285076	+ 0.734285	+ 0.005193			+ 0.045637
17		3						−0.042003
18		4						
19		5						
20		6						
21	3	0	−0.172529	−0.202467	+ 0.046605		−0.215246	−0.008652
22		1						
23		2		−0.542490				
24		3						
25		4						
26		5				−0.021044		
27		6		−0.016149				
28	4	0			−0.007366		+ 0.042997	
29		1						
30		2						
31		3		+ 0.099819				
32		4						
33		5						
34		6						
35	5	0						
36		1		+ 0.030084		−0.038383		
37		2						
38		3						
39		4						
40		5						
41		6						
42	6	0			−0.001730			
43		1	−0.017283		−0.000337			−0.001176
44		2		−0.001876	+ 0.000861	+ 0.014992		+ 0.002441
45		3						
46		4						
47		5						
48		6						
49	0	7				+ 0.036998	+ 0.051753	−0.012160

D

Appendix B Computational Program for Deciding Propeller Characteristics with The Wageningen B-series

```matlab
function B_series(Z, EAR, nstart, nstop, V_a, D, P_D)
%This function calculates thrust and torque coefficients (Kto,
Kqo) from
%Wageningen B-series of user specified input. The routine uses
axial
%advance number J, adjusted for oblique inflow. Polynomial
coefficients
%used in the calulations are given in separate file.
%Furthermore, this function calculates thrust and torque (T,
Q) from the
%coefficients.

%% Definitions
%EAR is the expanded blade area ratio, restricted to values
between
%0.3 and 1.05 by the propeller series.
%Z is the blade number ranging from 2 to 7.
%nstart and nstop indicate the range of revolutions/sec to be
utilized.
%V_a is the advance speed of the screw.
%D is the propeller diameter in meters.
%P_D is the pitch ratio restricted to values between 0.50 and
1.40 by the
%propeller series.
%ct, itt, iut, ivt, cq, itq, iuq, ivq, exp_Kt0 and exp_Kqo are
polynomial
%coefficients used in the calculations of Kto and Kqo.

%% Including polynomial coefficients
format long
[ct,itt,iut,ivt,cq,itq,iuq,ivq,exp_Kto,exp_Kqo] =
B_series_polycoefs();

%% Calculating Kto, Kqo, J, T, Q and efficiency
nL = nstop - nstart;
X = zeros(nL,7);
teller = 1;
close all;
for n = nstart:nstop
Kt_help = ct.*(P_D.^itt).*(EAR.^iut).*(Z.^ivt); %temporary
function
Kq_help = cq.*(P_D.^itq).*(EAR.^iuq).*(Z.^ivq); %temporary
function

[~, exp_length] = size(exp_Kto);
```

F

```matlab
J = V_a/(n*D);

tmp_Kto = 0; tmp_Kqo = 0;
for i = 1:exp_length
    tmp_Kto = tmp_Kto + (J^exp_Kto(i))*Kt_help(i);
    tmp_Kqo = tmp_Kqo + (J^exp_Kqo(i))*Kq_help(i);
end

if tmp_Kto < -0.03
    tmp_Kto = 0;
    tmp_Kqo = 0;
end

Kto = tmp_Kto;
Kqo = tmp_Kqo;

rho = 1025; %water density, 1025 kg/m^3 for seawater
T = Kto*rho*n^2*D^4;
Q = Kqo*rho*n^2*D^5;
eta_prop = (J/(2*pi))*(Kto/Kqo);

X(teller,3) = T;
X(teller,4) = Q;
X(teller,2) = eta_prop;
X(teller,1) = n;
X(teller,5) = J;
X(teller,6) = Kto;
X(teller,7) = Kqo;
teller = teller + 1;
end
%% Calculating pitch angle
P = P_D*D;
P_anglerad = atan(P/(2*pi*0.7*(D/2)));
P_angledeg = 180*P_anglerad/pi;

%% Plotting
fig1 = figure;
movegui(fig1,'northeast')
plot(X(:,5),X(:,6),'r',X(:,5),X(:,7)*10,'g', X(:,5),X(:,2),'-
.b');
grid on
legend('K_T', '10*K_Q', '\eta','Location','NorthWest');
xlabel('Advance ratio J');
ylabel('K_T, 10*K_Q, \eta');
title('Thrust and torque coefficients');

fig2 = figure;
movegui(fig2,'northwest')
plot(X(:,1),X(:,3),'r',X(:,1),X(:,4)*10^2,'g');
grid on
legend('T', '10^2*Q','Location','NorthWest');
```

```matlab
xlabel('Revolutions per second');
ylabel('Newton');
title('Thrust and Torque');


format short g;

disp('         rev/s   Efficiency      Thrust          Torque
Advance ratio    Kt         Kq');
disp('-----------------------------------------------------------
----------------------------------------');
disp(X);
disp('         rev/s   Efficiency      Thrust          Torque
Advance ratio    Kt         Kq');
disp('-----------------------------------------------------------
----------------------------------------');

disp('Pitch angle in degrees:'); disp(P_angledeg);
end


function [ct, itt, iut, ivt, cq, itq, iuq, ivq,...
         exp_Kto, exp_Kqo] = B_series_polycoefs()
%This function stores the polynomial coefficients which are
used in the
%calculation of Kt and Kq for given J and P/D with the
B_series function.
%These coefficients are not depending on the chosen propeller
%characteristics, and shall therefore remain unchanged. The
coefficients
%are listed in a separate function to make the calculation
%steps in the B_series function more easy-to-follow.

%% Polynomial coefficients for Kt
ct = [0.00880496, -0.204554, 0.166351, 0.158114, -0.147581, -
0.481497,...
    0.415437, 0.0144043, -0.0530054, 0.0143481, 0.0606826, -
0.0125894,...
    0.0109689, -0.133698, 0.00638407, -0.00132718, 0.168496, -
0.0507214,...
    0.0854559, -0.0504475, 0.010465, -0.00648272, -
0.00841728,...
    0.0168424, -0.00102296, -0.0317791, 0.018604, -
0.00410798,...
    -0.000606848, -0.0049819, 0.0025983, -0.000560528, -
0.00163652,...
    -0.000328787, 0.000116502, 0.000690904, 0.00421749,
5.65229E-05,...
    -0.00146564, 0, 0, 0, 0, 0, 0, 0, 0];

itt = [0, 0, 1, 2, 0, 1, 2, 0, 0, 1, 1, 0, 0, 3,...
```

H

```matlab
    6, 6, 0, 0, 0, 0, 6, 6, 3, 3, 3, 3, 0, 2, 0, 0,...
    0, 0, 2, 6, 6, 0, 3, 6, 3, 0, 0, 0, 0, 0, 0, 0, 0];

iut = [0, 0, 0, 0, 1, 1, 1, 0, 0, 0, 0, 1, 1, 0,...
    0, 0, 1, 2, 2, 2, 2, 2, 0, 0, 0, 1, 2, 2, 0, 0,...
    0, 0, 0, 0, 0, 1, 1, 1, 2, 0, 0, 0, 0, 0, 0, 0, 0];

ivt = [0, 0, 0, 0, 0, 0, 0, 1, 1, 1, 1, 1, 1, 0,...
    0, 0, 0, 0, 0, 0, 0, 0, 1, 1, 1, 1, 1, 1, 2, 2,...
    2, 2, 2, 2, 2, 2, 2, 2, 2, 0, 0, 0, 0, 0, 0, 0, 0];

exp_Kto = [0, 1, 0, 0, 2, 1, 0, 0, 2, 0, 1, 0, 1, 0,...
    0, 2, 3, 0, 2, 3, 1, 2, 0, 1, 3, 0, 1, 0, 0, 1, 2,...
    3, 1, 1, 2, 0, 0, 3, 0, 0, 0, 0, 0, 0, 0, 0, 0];

%% Polynomial coefficients for Kq
cq = [0.00379368, 0.00886523, -0.032241, 0.00344778, -
0.0408811,...
    -0.108009, -0.0885381, 0.188561, -0.00370871, 0.00513696,
0.0209449,...
    0.00474319, -0.00723408, 0.00438388, -0.0269403,
0.0558082,...
    0.0161886, 0.00318086, 0.015896, 0.0471729, 0.0196283, -
0.0502782,...
    -0.030055, 0.0417122, -0.0397722, -0.00350024, -
0.0106854,...
    0.00110903, -0.000313912, 0.0035985, -0.00142121, -
0.00383637,...
    0.0126803, -0.00318278, 0.00334268, -0.00183491,
0.000112451,...
    -2.97228E-05, 0.000269551, 0.00083265, 0.00155334,
0.000302683,...
    -0.0001843, -0.000425399, 8.69243E-05, -0.0004659,
5.54194E-05];

itq = [0, 0, 1, 2, 1, 1, 1, 2, 0, 1, 1, 1, 0, 1,...
    2, 0, 3, 3, 0, 0, 0, 1, 1, 2, 3, 6, 0, 3, 6, 0,...
    6, 0, 2, 3, 6, 1, 2, 6, 0, 0, 2, 6, 0, 3, 3, 6, 6];

iuq = [0, 0, 0, 0, 1, 1, 1, 1, 0, 0, 0, 0, 1, 1,...
    1, 1, 1, 1, 2, 2, 2, 2, 2, 2, 2, 2, 0, 0, 0, 1,...
    1, 2, 2, 2, 2, 0, 0, 0, 1, 1, 1, 1, 2, 2, 2, 2, 2];

ivq = [0, 0, 0, 0, 0, 0, 0, 0, 1, 1, 1, 1, 1, 1,...
    1, 0, 0, 0, 0, 0, 0, 0, 0, 0, 0, 0, 1, 1, 1, 1,...
    1, 1, 1, 1, 1, 2, 2, 2, 2, 2, 2, 2, 2, 2, 2, 2, 2];

exp_Kqo = [0, 2, 1, 0, 0, 1, 2, 0, 1, 0, 1, 2, 2, 1,...
    0, 3, 0, 1, 0, 1, 3, 0, 3, 2, 0, 0, 3, 3, 0, 3, 0,...
    1, 0, 2, 0, 1, 3, 3, 1, 2, 0, 0, 0, 0, 3, 0, 1];
End
```

B.1 Computational Program for Deciding Propeller Characteristics with the Ducted Propeller Ka-4.70/19A

```matlab
function Ka19A_series(nstart, nstop, V_a, D, P_D)
%This function calculates thrust and torque coefficients from
%Wageningen propeller 4.70 with nozzle 19A of user specified
input.
%The routine uses axial advance number J, adjusted for oblique
inflow.
%Polynomial coefficients used in the calulations are given in
separate file.
%Furthermore, this function calculates thrust and torque (T,
Q) from the
%coefficients.

%% Definitions
%EAR is the expanded blade area ratio, restricted to 0.70 for
the
%Ka-4.70/19A.
%Blade number restricted to 4 for the Ka-4.70/19A.
%nstart and nstop indicate the range of revolutions/sec to be
utilized.
%V_a is the advance speed of the screw.
%D is the propeller diameter in meters.
%P_D is the pitch ratio restricted to values between 0.50 and
1.40 by the
%propeller series.
%ct, itt, iut, ivt, cq, itq, iuq, ivq, exp_Kt0 and exp_Kqo are
polynomial
%coefficients used in the calculations of Kto and Kqo.

%% Including polynomial coefficients
format long
[A0y, A1y, A2y, A3y, A4y, A5y, A6y, B0y, B1y, B2y, B3y,
B4y,...
   B5y, B6y, C0y, C1y, C2y, C3y, C4y, C5y, C6y] =
Ka19A_series_polycoefs();

A = [A0y; A1y; A2y; A3y; A4y; A5y; A6y];
B = [B0y; B1y; B2y; B3y; B4y; B5y; B6y];
C = [C0y; C1y; C2y; C3y; C4y; C5y; C6y];

%% Calculating Kto, Kqo, Ktn, J, T, Tn, Q and efficiency
nL = nstop - nstart;
X = zeros(nL,9);
teller = 1;
close all;
for n = nstart:nstop
    Kto = 0; Ktno = 0; Kqo = 0;
```

J

```matlab
    for x = 1:7
        for y =1:7

        J = V_a/(n*D);

        tmp_Kto = A(x,y)*(P_D.^(x-1))*J^(y-1);
        tmp_Ktno = B(x,y)*(P_D.^(x-1))*J^(y-1);
        tmp_Kqo = C(x,y)*(P_D.^(x-1))*J^(y-1);

Kto = Kto + tmp_Kto;
Ktno = Ktno + tmp_Ktno;
Kqo = Kqo + tmp_Kqo;

        end
    end
rho = 1025;%water density, 1025 kg/m^3 for seawater
T = Kto*rho*n^2*D^4;
Tn = Ktno*rho*n^2*D^4;
Q = Kqo*rho*n^2*D^5;
eta_d = J*(1/(2*pi))*(Kto/Kqo);
%eta_d = ((Kto/pi)^(3/2))/Kqo;
%eta_d = (V_a*(T+Tn))/(2*pi*n*Q);


X(teller,1) = n;
X(teller,2) = eta_d;
X(teller,3) = T;
X(teller,4) = Tn;
X(teller,5) = Q;
X(teller,6) = J;
X(teller,7) = Kto;
X(teller,8) = Ktno;
X(teller,9) = Kqo;
teller = teller + 1;
end
%% Calculating pitch angle
P = P_D*D;
P_anglerad = atan(P/(2*pi*0.7*(D/2)));
P_angledeg = 180*P_anglerad/pi;

%% Plotting
fig1 = figure;
movegui(fig1,'northeast')
plot(X(:,6),X(:,7),'r',X(:,6),X(:,8),':m',X(:,6),X(:,9)*10,'g'
,...
    X(:,6),X(:,2),'-.b');
grid on
legend('K_T', 'K_{TN}', '10*K_Q', '\eta','Location','West');
xlabel('Advance ratio J');
ylabel('K_T, 10*K_Q, K_{TN}, \eta');
title('Thrust and torque coefficients');
```

```matlab
fig2 = figure;
movegui(fig2,'northwest')
plot(X(:,1),X(:,3),'r',X(:,1),X(:,4),':m',
X(:,1),X(:,5)*10^2,'g');
grid on
legend('T', 'T_N', '10^2*Q','Location','NorthWest');
xlabel('Revolutions per second');
ylabel('Newton');
title('Thrust and Torque');

format short g;

disp('            rev/s   Efficiency      Thrust     Nozzle thrust
Torque     Advance ratio      Kt          Ktno           Kq');
disp('-------------------------------------------------------
-------------------------------------------------------
');
disp(X);
disp('            rev/s   Efficiency      Thrust     Nozzle thrust
Torque     Advance ratio      Kt          Ktno           Kq');
disp('-------------------------------------------------------
-------------------------------------------------------
');

disp('Pitch angle in degrees:'); disp(P_angledeg);
end




function [A0y, A1y, A2y, A3y, A4y, A5y, A6y, B0y, B1y, B2y,
B3y, B4y,...
    B5y, B6y, C0y, C1y, C2y, C3y, C4y, C5y, C6y] =
Ka19A_series_polycoefs()

%This function stores the polynomial coefficients which are
used in the
%calculation of Kt and Kq for given J and P/D with the
Ka_series function.
%These coefficients are not depending on the chosen propeller
%characteristics, and shall therefore remain unchanged. The
coefficients
%are listed in a separate function to make the calculation
%steps in the B_series function more easy-to-follow.

%% Polynomials for Kt
A0y = [0.030550, -0.148687, 0, -0.391137, 0, 0, 0];
A1y = [0, -0.432612, 0, 0, 0, 0, 0];
A2y = [0.667657, 0, 0.285076, 0, 0, 0, 0];
A3y = [-0.172529, 0, 0, 0, 0, 0, 0];
```

L

```matlab
A4y = [0, 0, 0, 0, 0, 0, 0];
A5y = [0, 0, 0, 0, 0, 0, 0];
A6y = [0, -0.017283, 0, 0, 0, 0, 0];

%% Polynomials for Ktn
B0y = [0.076594, 0.075223, -0.061881, -0.138094, 0, -0.370620,
0.323447];
B1y = [-0.271337, -0.687921, 0.225189, 0, 0, 0, -0.081101];
B2y = [0.666028, 0, 0.734285, 0, 0, 0, 0];
B3y = [-0.202467, 0, -0.542490, 0, 0, 0, -0.016149];
B4y = [0, 0, 0, 0.099819, 0, 0, 0];
B5y = [0, 0.030084, 0, 0, 0, 0, 0];
B6y = [0, 0, -0.001876, 0, 0, 0, 0];

%% Polynomials for Kq
C0y = [0.006735, 0, -0.016306, 0, -0.007244, 0, 0];
C1y = [0, 0, -0.024012, 0, 0, 0, 0];
C2y = [0, 0, 0.005193, 0, 0, 0, 0];
C3y = [0.046605, 0, 0, 0, 0, 0, 0];
C4y = [-0.007366, 0, 0, 0, 0, 0, 0];
C5y = [0, 0, 0, 0, 0, 0, 0];
C6y = [-0.001730, -0.000337, 0.000861, 0, 0, 0, 0];
end
```

B.2 Computational Program for Deciding Propeller Characteristics with The Ducted Propeller Ka-4.70/37

```matlab
function Ka37_series(nstart, nstop, V_a, D, P_D)
%This function calculates thrust and torque coefficients from
%Wageningen propeller 4.70 with nozzle 37 of user specified
input.
%The routine uses axial advance number J, adjusted for oblique
inflow.
%Polynomial coefficients used in the calulations are given in
separate file.
%Furthermore, this function calculates thrust and torque (T,
Q) from the
%coefficients.

%% Definitions
%EAR is the expanded blade area ratio, restricted to 0.70 for
the
%Ka-4.70/37.
%Blade number restricted to 4 for the Ka-4.70/37.
%nstart and nstop indicate the range of revolutions/sec to be
utilized.
%V_a is the advance speed of the screw.
%D is the propeller diameter in meters.
```

```matlab
%P_D is the pitch ratio restricted to values between 0.50 and
1.40 by the
%propeller series.
%ct, itt, iut, ivt, cq, itq, iuq, ivq, exp_Kt0 and exp_Kqo are
polynomial
%coefficients used in the calculations of Kto and Kqo.

%% Including polynomial coefficients
format long
[A0y, A1y, A2y, A3y, A4y, A5y, A6y, B0y, B1y, B2y, B3y,
B4y,...
    B5y, B6y, C0y, C1y, C2y, C3y, C4y, C5y, C6y] =
Ka37_series_polycoefs();

A = [A0y; A1y; A2y; A3y; A4y; A5y; A6y];
B = [B0y; B1y; B2y; B3y; B4y; B5y; B6y];
C = [C0y; C1y; C2y; C3y; C4y; C5y; C6y];

%% Calculating Kto, Kqo, Ktn, J, T, Tn, Q and efficiency
nL = nstop - nstart;
X = zeros(nL,9);
teller = 1;
close all;
for n = nstart:nstop
    Kto = 0; Ktno = 0; Kqo = 0;
    for x = 1:7
        for y =1:7

        J = V_a/(n*D);

        tmp_Kto = A(x,y)*(P_D.^(x-1))*J^(y-1);
        tmp_Ktno = B(x,y)*(P_D.^(x-1))*J^(y-1);
        tmp_Kqo = C(x,y)*(P_D.^(x-1))*J^(y-1);

Kto = Kto + tmp_Kto;
Ktno = Ktno + tmp_Ktno;
Kqo = Kqo + tmp_Kqo;

        end
    end
Kto = Kto + 0.036998*(P_D.^(1-1))*J^(8-1);
Ktno = Ktno + 0.051753*(P_D.^(1-1))*J^(8-1);
Kqo = Kqo + (-0.012160)*(P_D.^(1-1))*J^(8-1);

rho = 1025;%water density, 1025 kg/m^3 for seawater
T = Kto*rho*n^2*D^4;
Tn = Ktno*rho*n^2*D^4;
Q = Kqo*rho*n^2*D^5;
eta_d = J*(1/(2*pi))*(Kto/Kqo);
%eta_d = ((Kto/pi)^(3/2))/Kqo;
%eta_d = (V_a*(T+Tn))/(2*pi*n*Q);
```

```matlab
    X(teller,1) = n;
    X(teller,2) = eta_d;
    X(teller,3) = T;
    X(teller,4) = Tn;
    X(teller,5) = Q;
    X(teller,6) = J;
    X(teller,7) = Kto;
    X(teller,8) = Ktno;
    X(teller,9) = Kqo;
    teller = teller + 1;
end
%% Calculating pitch angle
P = P_D*D;
P_anglerad = atan(P/(2*pi*0.7*(D/2)));
P_angledeg = 180*P_anglerad/pi;

%% Plotting
fig1 = figure;
movegui(fig1,'northeast')
plot(X(:,6),X(:,7),'r',X(:,6),X(:,8),':m',X(:,6),X(:,9)*10,'g'
,...
    X(:,6),X(:,2),'-.b');
grid on
legend('K_T', 'K_{TN}', '10*K_Q', '\eta','Location','West');
xlabel('Advance ratio J');
ylabel('K_T, 10*K_Q, K_{TN}, \eta');
title('Thrust and torque coefficients');

fig2 = figure;
movegui(fig2,'northwest')
plot(X(:,1),X(:,3),'r',X(:,1),X(:,4),':m',
X(:,1),X(:,5)*10^2,'g');
grid on
legend('T', 'T_N', '10^2*Q','Location','NorthWest');
xlabel('Revolutions per second');
ylabel('Newton');
title('Thrust and Torque');

format short g;

disp('         rev/s   Efficiency    Thrust    Nozzle thrust
Torque    Advance ratio     Kt         Ktno          Kq');
disp('------------------------------------------------------
------------------------------------------------------------
');
disp(X);
disp('         rev/s   Efficiency    Thrust    Nozzle thrust
Torque    Advance ratio     Kt         Ktno          Kq');
```

```matlab
disp('------------------------------------------------------
------------------------------------------------------
');

disp('Pitch angle in degrees:'); disp(P_angledeg);
end



function [A0y, A1y, A2y, A3y, A4y, A5y, A6y, B0y, B1y, B2y,
B3y, B4y,...
    B5y, B6y, C0y, C1y, C2y, C3y, C4y, C5y, C6y] =
Ka37_series_polycoefs()

%This function stores the polynomial coefficients which are
used in the
%calculation of Kt and Kq for given J and P/D with the
Ka_series function.
%These coefficients are not depending on the chosen propeller
%characteristics, and shall therefore remain unchanged. The
coefficients
%are listed in a separate function to make the calculation
%steps in the B_series function more easy-to-follow.

%% Polynomials for Kt
A0y = [-0.162557, 0, 0, 0, -0.077387, 0, 0];
A1y = [0.598107, -1.009030, 0, 0, 0, 0, 0];
A2y = [0.085087, 0.425585, 0, 0, 0, 0, 0];
A3y = [0, 0, 0, 0, 0, -0.021044, 0];
A4y = [0.042997, 0, 0, 0, 0, 0, 0];
A5y = [0, -0.038383, 0, 0, 0, 0, 0];
A6y = [0, 0, 0.014992, 0, 0, 0, 0];

%% Polynomials for Ktn
B0y = [-0.016806, 0, 0, 0, 0, 0, -0.099544];
B1y = [0, -0.548253, 0.230675, 0, 0, 0, 0];
B2y = [0.460206, 0, 0, 0, 0, 0, 0];
B3y = [-0.215246, 0, 0, 0, 0, 0, 0];
B4y = [0, 0, 0, 0, 0, 0, 0];
B5y = [0, 0, 0, 0, 0, 0, 0];
B6y = [0, 0, 0, 0, 0, 0, 0];

%% Polynomials for Kq
C0y = [0.016729, 0, 0, 0, 0, 0, 0.030559];
C1y = [-0.048424, -0.011118, -0.056199, 0, 0, 0, 0];
C2y = [0.084376, 0, 0.045637, -0.042003, 0, 0, 0];
C3y = [-0.008652, 0, 0, 0, 0, 0, 0];
C4y = [0, 0, 0, 0, 0, 0, 0];
C5y = [0, 0, 0, 0, 0, 0, 0];
C6y = [0, -0.001176, 0.002441, 0, 0, 0, 0];
end
```

P

Appendix C CFD Analysis of ROV
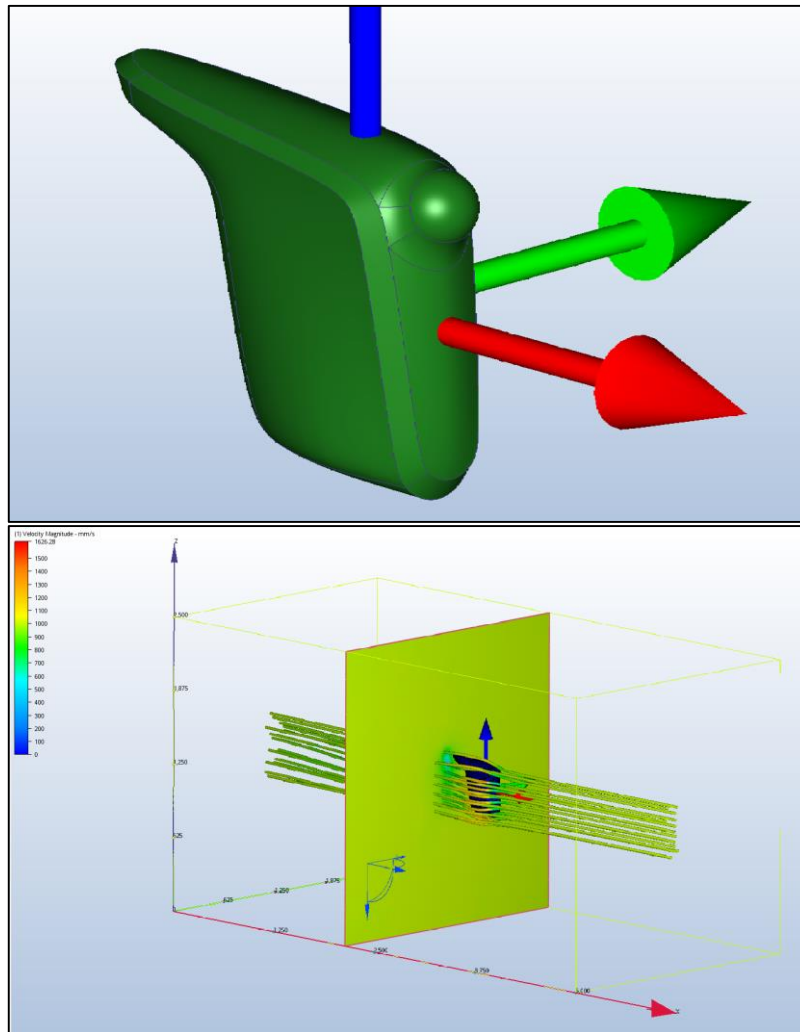
Summary: u = -1 m/s, v = w = 0

Total area	476321	mm^2
TOTAL FX	-24.3421	Newton
TOTAL FY	3.14998	Newton
TOTAL FZ	-6.80237	Newton
Center of Force about X-Axis (Y-Z)	1.03589	34.6857
Center of Force about Y-Axis (X-Z)	7.75201	-13.9847
Center of Force about Z-Axis (X-Y)	-71.6657	0.514199
TOTAL MX	-0.116306	N-m
TOTAL MY	0.393148	N-m
TOTAL MZ	-0.213229	N-m
Torque	0.148225	N-m

R

Appendix D Sales Offer From Staubo

Staubo Elektro-Maskin AS Bjørnerudveien
12 C | 1266 Oslo | Norway
Tel.: +47 22 75 35 00 | E-mail: post@staubo.no
Web: www.staubo.no | NO 916 201 796 VAT

Our ref.: PEDRAM AYOUBI
E-mail: pedram.ayoubi@Staubo.no
Your ref.: JOHNNY QUANG TUAN HUYNH
Revision: 01
Currency: NOK

Customer No.: 13500
BLUEYE ROBOTICS AS
RICHARD BIRKELANDS VEI 2 B
7034 TRONDHEIM

Delivery address:
BLUEYE ROBOTICS AS
RICHARD BIRKELANDS VEI 2
B 7034 TRONDHEIM

Pos.	Item	Description	Unit Price	Qty.	Total
1	3564K036B	Motor Ø35 36V (@ 1-4 stk.)	4238,00	1	4238,00
2	3564K036B	Motor Ø35 36V (@ 5-19 stk.)	3661,00	1	3661,00
3	3564K036B	Motor Ø35 36V (@ 20-99 stk.)	3314,00	1	3314,00
4	3564K036B	Motor Ø35 36V (@ 100-249 stk.)	2780,00	1	2780,00
5	3564K036B	Motor Ø35 36V (@ 250-499 stk.)	2551,00	1	2551,00
6	3564K036B	Motor Ø35 36V (@ 500-999 stk.)	2480,00	1	2480,00
7	3564K036B	Motor Ø35 36V (@ 1000 stk.)	2265,00	1	2265,00
Alternative Solution:					
8	3056K024B	Motor Ø30 24V (@ 1-4 stk.)	3637,00	1	3637,00
9	3056K024B	Motor Ø30 24V (@ 5-19 stk.)	3141,00	1	3141,00
10	3056K024B	Motor Ø30 24V (@ 20-99 stk.)	2843,00	1	2843,00
11	3056K024B	Motor Ø30 24V (@ 100-249 stk.)	2385,00	1	2385,00
12	3056K024B	Motor Ø30 24V (@ 250-499 stk.)	2189,00	1	2189,00
13	3056K024B	Motor Ø30 24V (@ 500-999 stk.)	2128,00	1	2128,00
14	3056K024B	Motor Ø30 24V (@ 1000 stk.)	1943,00	1	1943,00

LEAD TIME:

AT THE MOMENT, 12 PCS. 3564K ARE AT FAULHABER'S STOCK. THE NUMBERS CAN BE CHANGED EVERY SINGLE MINUTE. OTHERWISE, STANDARD LEAD-TIME IS 6 WORKING WEEKS.

NO 3056K IN STOCK. STANDARD LEAD-TIME IS 6 WORKING WEEKS.

NB! LEAD-TIME TO BE CONFIRMED BY MANUFACTURER. WAITING FOR FEEDBACK.

PRICES ARE BASED ON EXCHANGE RATE EUR/NOK= 9.3475 PER 11.05.2016, NORGES-BANK.

PRICES ARE IN NORWEGIAN KRONER (NOK), EXCL. VAT, EXWORKS OUR WAREHOUSE (OSLO). OTHER CONDITIONS ACC. TO STAUBO ELEKTRO-MASKIN'S GENERAL SALES AND DELIVERY CONDITIONS.

T

Appendix E Calculations at Several Depth Scenarios for the Turnigy Aerodrive SK3 4250 With A 3-bladed Propeller

Model	Parameter	5	10	20	30	40	50	60	70	80	90	100
Wageningen-3.80	Speed	5.2	4.2	3.25	2.74	2.43	2.21	2.04	1.9	1.77	1.7	1.61
	Thrust	127	137	147	151	155	158	160	162	160	160	163.5
	Torque	1278	1.7022	1.7001	1.677	1.6868	1.6959	1.6982	1.7055	1.6543	1.6432	1.6804
	Power	1180.8929	1176.4636	1175.023	1159.0829	1165.8314	1172.1209	1173.694	1178.7398	1143.3562	1135.7277	1161.4382
	Efficiency	0.5592	0.4891	0.4066		0.3231		0.2781		0.2477		0.2266
Wageningen-3.65	Speed	5.2	4.2	3.25		2.43		2.04		1.77		1.61
	Thrust	127	137	147		155		160		160		163.5
	Torque	1.6717	1.6663	1.6651		1.6525		1.6642		1.6205		1.6467
	Power	1155.385	1151.6877	1150.8495		1142.1261		1150.1834		1120.0032		1138.1484
	Efficiency	0.57158	0.49961	0.41513		0.32978		0.28378		0.25286		0.23128
Wageningen-3.50	Speed	5.2	4.2	3.25		2.43		2.04		1.77		1.61
	Thrust	127	137	147		155		160		160		163.5
	Torque	1.6438	1.6393	1.6388		1.6267		1.6386		1.5952		1.6215
	Power	1136.106	1133.0111	1132.6673		1124.3272		1132.5432		1102.4921		1120.6882
	Efficiency	0.58128	0.50785	0.42179		0.335		0.2882		0.25687		0.23489
Wageningen-3.35	Speed	5.2	4.2	3.25		2.43		2.04		1.77		1.61
	Thrust	127	137	147		155		160		160		163.5
	Torque	1.6114	1.6079	1.6082		1.5968		1.6089		1.5656		1.592
	Power	1113.7489	1111.3194	1111.5225		1103.6071		1111.9992		1082.0911		1100.344
	Efficiency	0.59295	0.51776	0.42982		0.34129		0.29353		0.26172		0.23923

E.1 Calculations at Several Depth Scenarios for the Turnigy Multistar 2834 With A 3-bladed Propeller

		5	10	20	30	40	50	60	70	80	90	100
Wageningen-3.80	Speed	3.53	2.86	2.22	1.88	1.66	1.51	1.39	1.29	1.22	1.15	1.1
	Thrust	58.5	63.5	68.5	71	72	74	74.5	74.5	75.5	75	76
	Torque	0.52337	0.52379	0.52466	0.52375	0.51896	0.52451	0.52155	0.51887	0.52201	0.5148	0.51899
	Power	493.2619	493.6585	494.4804	493.6213	489.1121	494.3436	491.5517	461.8549	464.6523	458.2334	461.9626
	Efficiency	0.41865	0.36789	0.30754		0.24436		0.22612		0.19823		0.18097
Wageningen-3.65	Speed	3.53	2.86	2.22		1.66		1.39		1.22		1.1
	Thrust	58.5	63.5	68.5		72		74.5		75.5		76
	Torque	0.48414	0.48493	0.4861		0.48065		0.48334		0.48122		0.47839
	Power	456.292	457.0312	458.141		453.0029		455.5418		453.5381		450.8755
	Efficiency	0.45257	0.39737	0.33193		0.26384		0.22732		0.20309		0.18542
Wageningen-3.50	Speed	3.53	2.86	2.22		1.66		1.39		1.22		1.1
	Thrust	58.5	63.5	68.5		72		74.5		75.5		76
	Torque	0.45443	0.45552	0.45695		0.4517		0.45449		0.45246		0.44963
	Power	428.2911	429.3165	430.6668		425.7212		428.3428		426.4352		423.765
	Efficiency	0.48216	0.42302	0.3531		0.28075		0.24176		0.216		0.19728
Wageningen-3.35	Speed	3.53	2.86	2.22		1.66		1.39		1.22		1.1
	Thrust	58.5	63.5	68.5		72		74.5		75.5		76
	Torque	0.42001	0.42143	0.42315		0.41812		0.42104		0.41904		0.41625
	Power	395.8534	398.1922	398.806		394.0711		396.8177		394.934		392.3026
	Efficiency	0.52167	0.45723	0.38131		0.3033		0.26096		0.23323		0.2131

E.2 Calculations at Several Depth Scenarios for the Turnigy Aquastar 4084 With A 3-bladed Propeller

		5	10	20	30	40	50	60	70	80	90	100
Wageningen-3.80	Speed	5.3	4.3	3.24	2.83	2.51	2.28	2.1	1.95	1.84	1.75	1.66
	Thrust	132	143.5	155	161	165	168	170	170	172	174.5	174
	Torque	1.2651	1.2654	1.268	1.2652	1.2674	1.2674	1.2659	1.2532	1.2577	1.2675	1.2563
	Power	1656.0075	1656.3745	1726.1449	1656.121	1725.3581	1659.0235	1657.0705	1640.4794	1646.2886	1659.1032	1644.4489
	Efficiency	0.42246	0.37253	0.30507		0.2499		0.21544		0.20207		0.17565
Wageningen-3.65	Speed	5.3	4.3	3.24	2.83	2.51	2.28	2.1	1.95	1.84	1.75	1.66
	Thrust	132	143.5	155	161	165	168	170	170	172	174.5	174
	Torque	1.1691	1.1703	1.1633		1.172		1.1724		1.1643		1.163
	Power	1530.3076	1531.86	1522.7602		13534.499		1534.6791		1524.1189		1522.4249
	Efficiency	0.45716	0.40281	0.3298		0.26989		0.23262		0.20765		0.18972
Wageningen-3.50	Speed	5.3	4.3	3.24	2.83	2.51	2.28	2.1	1.95	1.84	1.75	1.66
	Thrust	132	143.5	155	161	165	168	170	170	172	174.5	174
	Torque	1.0967	1.0987	1.0924		1.1018		1.1022		1.0943		0.91537
	Power	1435.6399	1438.1757	1429.9929		1442.2829		1442.7544		1432.378		1198.2227
	Efficiency	0.48731	0.42905	0.35119		0.28715		0.24744		0.22095		0.20365
Wageningen-3.35	Speed	5.3	4.3	3.24	2.83	2.51	2.28	2.1	1.95	1.84	1.75	1.66
	Thrust	132	143.5	155	161	165	168	170	170	172	174.5	174
	Torque	1.0127	1.0155	1.01		1.0198		1.0204		1.0127		1.0116
	Power	1325.6203	1329.2375	1322.0629		1334.8771		1335.7517		1325.5773		1324.1367
	Efficiency	0.52775	0.46421	0.37986		0.31025		0.26727		0.23875		0.21813